UNIVERSIDADE DE SÃO PAULO

FACULDADE DE CIÊNCIAS FARMACÊUTICAS DE RIBEIRÃO PRETO

Repurposing of antimalarial drugs in the treatment of schistosomiasis based on the selective inhibition of the enzyme dihydroorotate dehydrogenase

Reposicionamento de drogas antimaláricas no tratamento da esquistossomose baseado na inibição seletiva da enzima diidroorotato desidrogenase

Felipe Antunes Calil

Ribeirão Preto
2018

UNIVERSIDADE DE SÃO PAULO

FACULDADE DE CIÊNCIAS FARMACÊUTICAS DE RIBEIRÃO PRETO

Felipe Antunes Calil

Repurposing of antimalarial drugs in the treatment of schistosomiasis based on the selective inhibition of the enzyme dihydroorotate dehydrogenase

Reposicionamento de drogas antimaláricas no tratamento da esquistossomose baseado na inibição seletiva da enzima diidroorotato desidrogenase

Doctoral thesis presented to the Graduate Program of School of Pharmaceutical Sciences of Ribeirão Preto/USP for the degree of Doctor in Sciences.

Concentration Area: Chemistry and Biological Physics

Supervisor: Prof. Dr. Maria Cristina Nonato

Versão corrigida da Tese de Doutorado apresentada ao Programa de Pós-Graduação em Ciências Farmacêuticas em 08/02/2019. A versão original encontra-se disponível na Faculdade de Ciências Farmacêuticas de Ribeirão Preto/USP.

Ribeirão Preto
2018

Calil, Felipe Antunes

Repurposing of antimalarial drugs in the treatment of schistosomiasis based on the selective inhibition of the enzyme dihydroorotate dehydrogenase. Ribeirão Preto, 2018.
135 p.; 30 cm.

Doctoral thesis presented to the Graduate Program of School of Pharmaceutical Sciences of Ribeirão Preto/USP for the degree of Doctor in Sciences. Concentration Area: Chemistry and Biological Physics.

Supervisor: Nonato, Maria Cristina

1. Schistosomiasis 2. Dihydroorotate dehydrogenase 3. Drug repositioning 4. Neglected tropical diseases 5. Malaria

APPROVAL PAGE

Felipe Antunes Calil

Repurposing of antimalarial drugs in the treatment of schistosomiasis based on the selective inhibition of the enzyme dihydroorotate dehydrogenase

Doctoral thesis presented to the Graduate Program of School of Pharmaceutical Sciences of Ribeirão Preto/USP for the degree of Doctor in Sciences.

Concentration Area: Chemistry and Biological Physics

Supervisor: Prof. Dr. Maria Cristina Nonato

Approved on:

Examiners

Prof. Dr. _____

Institution: _____ Signature:_____

Prof. Dr. _____

Institution: _____ Signature:_____

Prof. Dr. _____

Institution: _____ Signature:_____

Prof. Dr. _____

Institution: _____ Signature:_____

Prof. Dr. _____

Institution: _____ Signature:_____

Prof. Dr. _____

Institution: _____ Signature:_____

Inscription

A minha esposa, Anelize, que com seu carinho e intenso incentivo, acreditou na minha capacidade e me ensinou a amar a pesquisa. Sem você este trabalho não existiria.

Acknowledgements

I would like to thank my parents, Fátima e Flávio, who have created the pillars for my professional growth and as a person; and for all the support in my scientific career. To my entire family, for accepting my choices and my absence.

To my wife, Anelize, for being the best companion anyone could ever dream of; for being so loyal, faithful and sincere; and for being by my side every moment. In addition, I thank her family, my new family, for all the support.

To my supervisor, Cristina Nonato, for all the opportunities, guidance and continuous encouragement throughout the development of this project. And for never refusing to teach with enthusiasm whenever requested.

To the entire LCP group, for all the helps and discussions. I would like to specially thank Márcia, Victor, Valquíria, Iara, and Juliana, for the important contributions to this work and/or the friendship.

To Prof. Flavio Emery and Fernando Fumagalli (QHeteM group), for providing synthetic compounds used in this work and for the valuable discussions.

To Prof. Fernanda Anibal's group, especially Ricardo Correia, for all the effort with the in vitro experiments.

To the Broad Institute, for providing synthetic compounds used in this work.

To Prof. Marcelo Castilho, for the pharmacophore study and discussions.

To Professors Marcelo Baruffi, Renata Fonseca, Eliane Candiani, Vanderlei Rodrigues, Richard Ward and Antonio Jose da Costa Filho, for kindly allowing the use of their labs/equipments.

To Synchrotron SOLEIL, used for data collection and to Beatriz Guimarães.

To the School of Pharmaceutical Sciences of Ribeirão Preto and to the Pharmaceutical Sciences Graduate Program. Especial thanks to Eleni and Rafael.

To São Paulo Research Foundation (FAPESP, grant number 2015/25099-5) and National Council for Scientific and Technological Development (CNPq, grant number 140445/2016-1) for financial support.

This study was also financed in part by the Coordenação de Aperfeiçoamento de Pessoal de Nível Superior - Brasil (CAPES) – Finance Code 001.

“Science, my lad, is made up of mistakes, but they are mistakes which it is useful to make, because they lead little by little to the truth”

Jules Verne, A Journey to the Center of the Earth

“Words are, in my not-so-humble opinion, our most inexhaustible source of magic, capable of both influencing injury, and remedying it.”

J.K. Rowling, Harry Potter and the Deathly Hallows

RESUMO

CALIL, FELIPE. A. **Reposicionamento de drogas antimaláricas no tratamento da esquistossomose baseado na inibição seletiva da enzima diidroorotato desidrogenase**. 2018. 135f. Tese de Doutorado. Faculdade de Ciências Farmacêuticas de Ribeirão Preto – Universidade de São Paulo, Ribeirão Preto, 2018.

Reposicionamento de fármacos, a aplicação de um tratamento existente a uma nova doença, promete um rápido impacto clínico a um custo menor do que o desenvolvimento de novos fármacos. Essa estratégia é de particular interesse para o desenvolvimento de novos fármacos para o tratamento de doenças negligenciadas, devido à escassez de investimento e ao elevado número de indivíduos afetados. A esquistossomose é uma doença crônica debilitante causada por trematódeos do gênero *Schistosoma* que afeta mais de 200 milhões de pessoas no mundo. Apesar de ser um grave problema de saúde, o único medicamento disponível, Praziquantel, está se tornando um grave problema devido à resistência parasitária. Neste contexto, este trabalho teve como objetivo avaliar compostos sintéticos que apresentam atividade antimalárica para potencial descoberta de novas drogas contra a esquistossomose. Os compostos foram selecionados com base em sua capacidade de inibir a enzima diidroorotato desidrogenase (DHODH). A enzima DHODH participa da síntese de novo dos nucleotídeos de pirimidina e é um alvo terapêutico validado para muitas doenças. Nossos estudos identificaram vários compostos como potentes inibidores da diidroorotato desidrogenase (*Sm*DHODH) do *S. mansoni*. Um total de 34 compostos foram identificados como inibidores e estudos mecanísticos permitiram agrupá-los em três classes: inibidores competitivos, não competitivos e misto. Os estudos inibitórios, juntamente com ensaios de estabilidade térmica, sugerem que não apenas a distribuição química e estérica do sítio de ligação é importante, mas a dinâmica do domínio N-terminal desempenha um papel importante na interação do ligante. O índice de seletividade (SI) foi estimado pela avaliação dos melhores acertos contra a enzima homóloga humana (*Hs*DHODH). Os resultados identificaram o composto 17 (2-hidroxi-3-isopentilnaftaleno-1,4-diona) como o melhor composto para a inibição seletiva de *Sm*DHODH (IC_{50} = 23 ± 4 nM, SI 30,83). Estudos *in vitro* utilizando vermes adultos de *S. mansoni* foram usados para identificar o impacto de compostos selecionados na morfologia e atividade esquistossomicida. Os resultados mostram uma atividade potente contra os parasitas, especialmente para o composto atovaquona, um antimalárico.
O *Plasmodium falciparum* DHODH (*Pf*DHODH), um alvo validado contra a malária, também foi foco do presente trabalho. Desenvolvemos um pipeline para avaliar a potência, seletividade e mecanismo de inibição. Em nosso trabalho, diferentes classes de compostos foram testadas e os ligantes identificados tiveram seu mecanismo de inibição determinado. A cristalização de *Pf*DHODHΔloop (onde o loop flexível de Gly^{285} até Lys^{294} foi removido) foi alcançada com sucesso e fornecerá a base estrutural para entender a potência e seletividade de ligantes. Nossos resultados apoiam nossa proposta original de reaproveitar compostos e/ou seus análogos, originalmente desenvolvidos contra o *Pf*DHODH, para buscar estratégias alternativas para o tratamento da esquistossomose.

Palavras-chave: Esquistossomose, diidroorotato desidrogenase, reposicionamento de drogas, doenças tropicais negligenciadas, malária

ABSTRACT

CALIL, FELIPE. A. **Repurposing of antimalarial drugs in the treatment of schistosomiasis based on the selective inhibition of the enzyme dihydroorotate dehydrogenase**. 2018. 135f. Doctoral Thesis. Faculdade de Ciências Farmacêuticas de Ribeirão Preto – Universidade de São Paulo, Ribeirão Preto, 2018.

Drug repurposing, the application of an existing therapeutic to a new disease indication, holds the promise of rapid clinical impact at a lower cost than *de novo* drug development. This strategy is of particular interest for the development of new drugs for the treatment of neglected diseases, due to the scarcity of investment and the high number of individuals affected. Schistosomiasis is a chronic, debilitating disease caused by trematodes of the genus *Schistosoma* affecting over 200 million people worldwide. Despite being a serious health burden, the only drug available, Praziquantel, is becoming a significant issue due to parasite resistance. In this context, this work aimed to evaluate synthetic compounds which display antimalarial activity as potential leads for the discovery of new therapeutics for schistosomiasis. The compounds were selected based on their ability to inhibit the enzyme dihydroorotate dehydrogenase (DHODH). DHODH enzyme participates in the *de novo* synthesis of pyrimidine nucleotides and it is a validated therapeutic target for many diseases. Our studies identified several compounds as potent inhibitors of *Schistosoma mansoni* dihydroorotate dehydrogenase (*Sm*DHODH). A total of 34 compounds were identified as inhibitors and mechanistic studies allowed us to sort them into three classes: competitive, non-competitive and mixed-type inhibitors. The inhibitory studies together with thermal stability assays suggest that not only chemical and steric distribution of the binding pocket is important but dynamics of the N-terminal helical domain plays an important role in ligand binding. The selectivity index (SI) was estimated by evaluating the best hits against the human homologue enzyme (*Hs*DHODH). The results identified compound 17 (2-hydroxy-3-isopentylnaphthalene-1,4-dione) as the best compound for *Sm*DHODH selective inhibition (IC_{50} = 23 ± 4 nM, SI 30.83). *In vitro* studies using adult *S. mansoni* worms were used to identify the impact of selected compounds on the morphology and schistosomicidal activity. Results show a potent activity against the parasites, especially for the compound atovaquone, an antimalarial drug.
Plasmodium falciparum DHODH (*Pf*DHODH), a validated target against malaria, was also focus of the present work. We developed a pipeline to evaluate potency, selectivity and mechanism of inhibition. In our work, different classes of compounds were assayed and identified ligands had their mechanism of inhibition determined. Crystallization of *Pf*DHODHΔloop (where the flexible loop from Gly^{285} to Lys^{294} was removed) was successfully achieved and will provide the structural basis to understand potency and selectivity of ligands. Our results support our original proposal of repurposing compounds and/or its analogues, originally developed against *Pf*DHODH, to search for alternative strategies to treat schistosomiasis.

Keywords: Schistosomiasis, dihydroorotate dehydrogenase, drug repositioning, neglected tropical diseases, malaria

LIST OF FIGURES

LIST OF TABLES

LIST OF ABBREVIATIONS

A771726	Teriflunomide
ADMET	Absorption, distribution, metabolism, excretion, toxicity
AIDS	Acquired immunodeficiency syndrome
bp	Base pair
C8E5	Pentaethylene glycol ether
CD	Circular dichroism
CDC	Centers for disease control and prevention
CoQ	Coenzyme Q
$CoQH_2$	Reduced coenzyme Q
CQ	Chloroquine
DCIP	2,6-Dichlorophenolindophenol
DHF	Dihydrofolate
DHO	Dihydroorotate
DHODH	Dihydroorotate dehydrogenase
DMSO	Dimethyl sulfoxide
DNA	Deoxyribonucleic acid
DSF	Differential scanning fluorimetry
DTT	Dithiothreitol
EC	Enzyme commission number
*Ec*DHODH	*Escherichia coli* dihydroorotate dehydrogenase
EDTA	Ethylenediamine tetraacetic acid
FAD	Flavin adenine dinucleotide
FLINT	Fluorescence intensity
FMN	Flavin mononucleotide
$FMNH_2$	Reduced flavin mononucleotide

*Hs*DHODH	human dihydroorotate dehydrogenase
IC_{50}	Half maximal inhibitory concentration
IPTG	Isopropyl β-D-1-thiogalactopyranoside
k_{cat}	Enzyme turnover
K_M	Michaelis-Menten constant
k_{obs}	Apparent first order rate constant
LDAO	Lauryldimethylamine N-oxide
LNLS	Laboratório Nacional de Luz Síncrotron
MES	2-(N-Morpholino)ethanesulfonic acid
MIT	Massachusetts institute of technology
MMV	Medicines for malaria venture
MRW	Mean molecular weight
NAD^+	Nicotinamide adenine dinucleotide
NTD	Neglected tropical diseases
ORO	Orotate
OSDD	Open source drug discovery
PCR	Polymerase chain reaction
PDB	Protein data bank
PEG	Polyethylene glycol
*Pf*DHODH	*Plasmodium falciparum* dihydroorotate dehydrogenase
PK/PD	Pharmacokinetics/pharmacodynamics
PMSF	Phenylmethylsulfonyl fluoride
PZQ	Praziquantel
Q_0	2,3-dimethoxy-5-methyl-1,4-benzoquinone
Q_{10}	Ubiquinone 10
Q_D	Decylubiquinone
*Rn*DHODH	*Rattus norvegicus* dihydroorotate dehydrogenase

SDS-PAGE	Polyacrylamide gel electrophoresis
SI	Selectivity index
*Sm*DHODH	*Schistosoma mansoni* dihydroorotate dehydrogenase
SOLEIL	Synchrotron facility near Paris, France
SUMO	Small ubiquitin-like modifier protein
TB	Tuberculosis
T_m	Melting temperature
ULP1	Ubiquitin-like-specific protease 1
V_{max}	Maximum velocity
WHO	World health organization

SUMMARY

CHAPTER 1. INITIAL CONSIDERATIONS

1.1 General Introduction

On the bright side, globalization can be considered a set of processes that afford easy access to knowledge, economic stability and social equality.[1] However, it has also helped to spread some of the deadliest infectious diseases across wide geographic areas. Malaria has crossed the African borders and became global as humans migrated to other continents and parasites got adapted to different mosquito species that were evolutionarily distant from African vectors.[2] Ebola virus outbreak, which killed more than 11,000 people and infected at least 28,000, is a stark reminder of the world fragility in health security.[3] A recent example of the negative impact of globalization is the spread of Zika virus from Uganda in 1947,[4, 5] to other African countries within a few years, and then to the Micronesia, to finally arrive at Americas late December 2015, where 440,000–1,300,000 suspected cases have occurred.[6] Despite the fact that Zika has drawn attention to flavivirus infections which remained largely forgotten by the pharmaceutical industry, the scenario for other neglected diseases remains unchanged.

The Neglected Tropical Diseases (NTDs) consist of a large number of diseases (e.g. Chagas disease, dengue, leishmaniasis, malaria, leprosy, schistosomiasis, among others) caused by several pathogens such as viruses, bacteria, protozoa and helminths. These diseases together affect more than 1 billion people, including half a billion children, especially in poor and marginalized areas, representing a serious burden to public health.[7, 8] To make matters worse, NTDs, previously found in developing countries, are also becoming widespread posing a serious challenge to the health systems of developed countries that receive immigrants and refugees from endemic areas.[9, 10]

Although the tropical diseases are a major cause of morbidity and mortality in the world, the lack of investment in research and development of new therapies is still a striking feature, as well as the resistance of pathogens to the already existing drugs.[11] Thus, NTDs are a global public health problem, and new policies for control, prevention and investment in research and development, both by the public and private sectors, are essential for the implementation of new diagnostic strategies and effective therapeutic modalities.

Many steps are necessary to ensure efficacy and safety of a drug before being approved to patient's uses. In the best case scenario, the average cost to introduce a drug in the market is about U$ 800,000,000, that in a period of 12 to 15 years. In average, out of ten thousand compounds identified and submitted to pre-clinical assays, only five are approved to clinical trials, from which only one is approved to clinical use (**Figure 1**).[12]

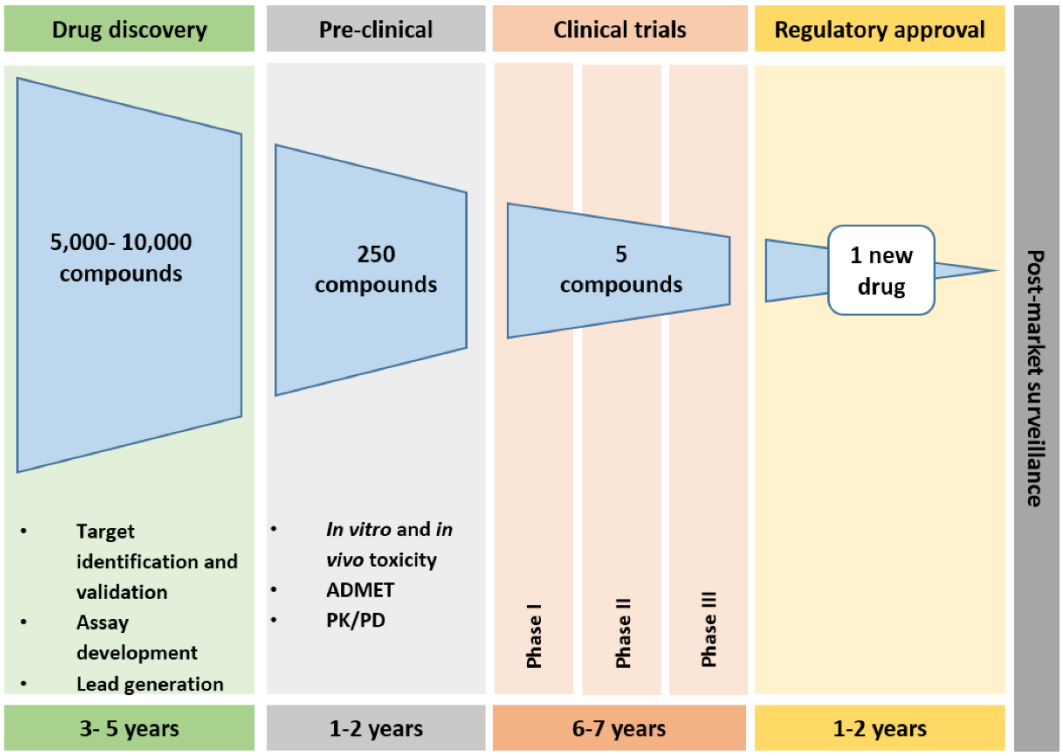

Figure 1. Drug discovery and development timeline. The current drug approval pipeline can take up to 15 years. It is estimated that from 5,000–10,000 compounds only one new drug reaches the market (extracted from Matthews, Hanison and Nirmalan, 2016 [12]).

The gap between compound discovery and its use in clinical trials is called the "Valley of Death" and represents a major barrier to the development of new drugs. Among several, one of the major limitations to decrease this gap is the high cost associated with this step during the translational process.

One way to accelerate the pharmaceutical research process is through the use of a strategy called drug repositioning (or repurposing of drugs). This strategy consists on

the evaluation and/or use of existing drugs for the treatment of diseases other than those for which they were originally developed.[13] Through repositioning of drugs, it is expected that bioactive molecules will be identified within shorter development periods, besides the risk reduction with compounds that have already undergone regulatory clinical trials.[14] Previous pharmacokinetic and toxicological data provide estimates of therapeutic concentrations in the new application. In addition, regulatory procedures can be expedited, in which the applicant can rely on data from previous studies. This has worked as a stimulus to identify new activities for already known molecules.[13] All these factors contribute to significant cost savings - important in the context of diseases that afflict the less favored, such NTDs, where return on investment is marginal.[14-16]

Many drugs have already been successfully repurposed and many projects using this strategy are currently under development (**Table 1**),[17] including ongoing repurposing programs (Medicines for Malaria Venture, the Global Alliance for TB Drug Development, Drugs for Neglected Diseases, and the OSDD initiative) and completely repurposed drugs that target NTDs.[18]

Table 1. Examples of repurposed or candidate drugs for many diseases, including NTDs.[17, 18]

Drug	Originally Developed	Repurposed
All-Trans Retinoic Acid (ATRA)	Severe Acne	Leukemia
Amphotericin B	Antifungal	Leishmaniasis
Astemizole	Antihistamine	Malaria
Avermectin	River blindness and Elephantiasis	Tuberculosis
Chloroquine	Malaria	Lung Cancer
Eflornithine	Anticancer	African Sleeping Sickness
Methotrexate	Anticancer	Rheumatoid Arthritis
Miltefosine	Antineoplastic	Leishmaniasis
Phosphodiesterase-inhibitor analogues	Erectile dysfunction	African Sleeping Sickness; Chagas Disease
Ropinirole	Parkinson's Disease	Restless Leg Syndrome
Tamoxifen	Anticancer	Leishmaniasis
Thalidomide	Morning Sickness	Multiple Myeloma; Leprosy

Cases of malaria in developed countries combined to worldwide investments from some of these programs are supporting the development of new strategies to treat this parasitic disease and helped malaria to be removed from the current list of NTDs. One approach was based on the selective inhibition of the enzyme dihydroorotate dehydrogenase (DHODH) from *Plasmodium sp*., parasites responsible for human malaria.[19, 20] In fact, over the last several years several molecules have been identified as selective inhibitors of *Plasmodium falciparum* DHODH (*Pf*DHODH),[21] some receiving the investment needed to overcome the "Valley of Death" and reaching the clinical trial stages.

DHODH (EC 1.3.1.14, 1.3.1.15, 1.3.5.2 or 1.3.98.1, depending on the type) is the fourth enzyme that acts in the *de novo* biosynthesis of uridylate, the precursor of all pyrimidine nucleotides (**Figure 2**); it catalyzes the oxidation of dihydroorotate to orotate according to a ping-pong-type enzymatic mechanism.[22-24]

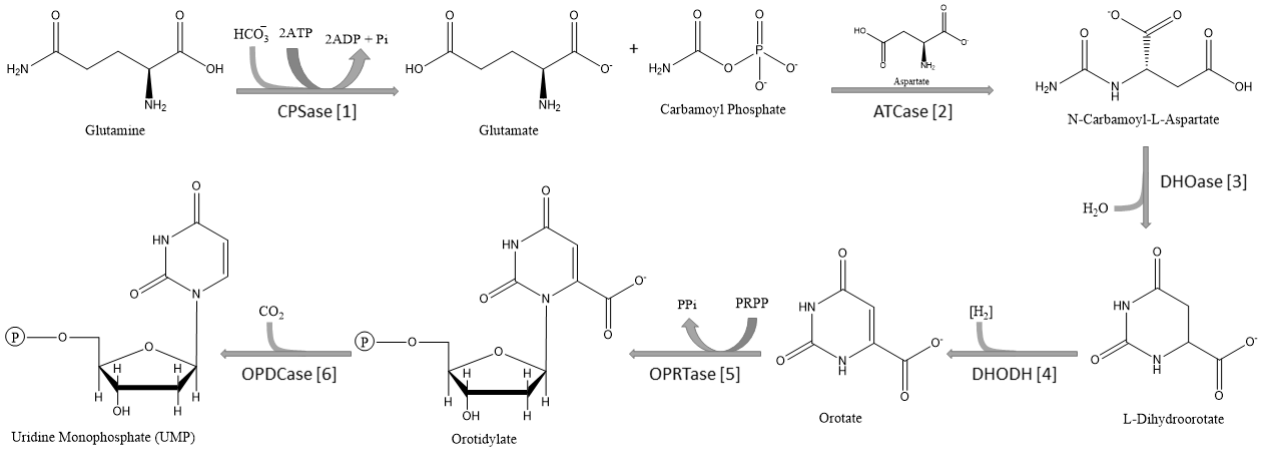

Figure 2. Schematic illustration of the pyrimidine de novo synthesis pathway.

DHODH was first detected in 1953 by Lieberman and Kornberg in extracts of the anaerobic bacterium *Zymobacterium oroticum* (now known as *Clostridium oroticum*).[25] Over the last 30 years, DHODH has been identified as the pharmacological target of a number of chemical and natural compounds such as Arava® (leflunomide, which is approved for the treatment of rheumatoid arthritis in humans), isoxazole, triazine, bicinchoninic acid and quinone derivatives.[26-28] These compounds interfere in uncontrolled reactions of the immune system, assist in fighting parasitic infections such as malaria and boost antiviral therapies by decreasing the intracellular concentration of pyrimidine nucleotides.[29] Currently, interest has arisen in exploiting DHODH inhibition as a strategy to combat a broad range of diseases,[30-37] including for malaria where the triazolopyrimidine DSM265 has progressed to clinical development.[34-38]

In the performance of its biological functions, DHODH uses flavin mononucleotide (FMN) as a cofactor. In the initial phase of the enzymatic reaction, FMN is reduced and the dihydroorotate substrate is oxidized, to orotate. In the second half of the reaction, FMN is reoxidized ($FMNH_2$ is converted to FMN) with the aid of a third molecule that acts as an electron acceptor (**Figure 3**).[33, 39]

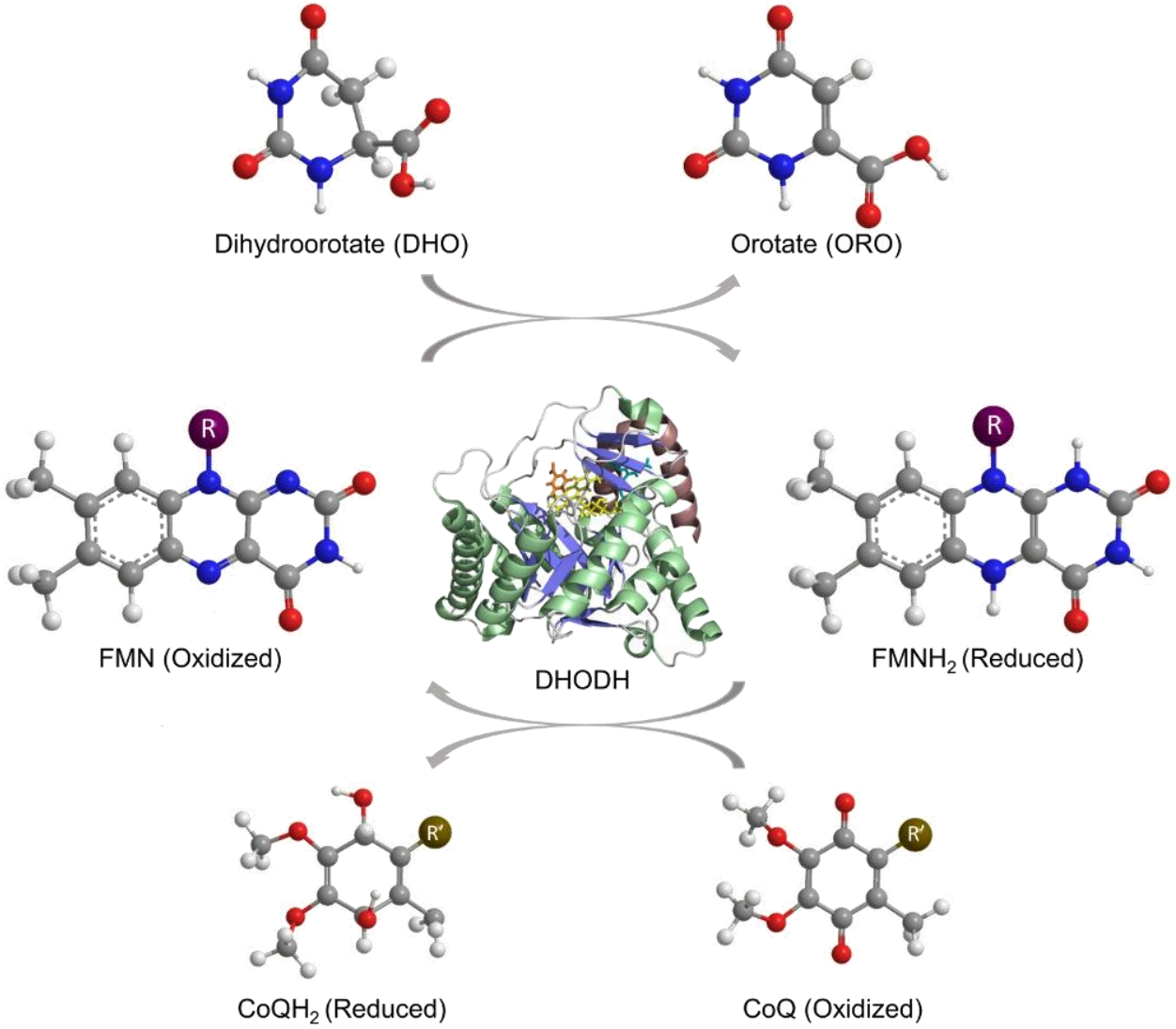

Figure 3. Enzymatic reaction catalyzed by dihydroorotate dehydrogenases (DHODHs). In this particular case, the oxidizing agent showed, CoQ, is used by Class 2 DHODHs.

According to their primary structures and cellular locations, the DHODH enzymes of various organisms can be divided into two classes, Class 1 and Class 2.[40] Class 1 enzymes can be subdivided into Classes 1A, 1B and a new class (1S) that was found in *Sulfolobus solfataricus*.[41] The Class 1 enzymes are found in the cytosol, whereas enzymes belonging to Class 2 are associated with cytosolic or mitochondrial membranes.[42, 43] Due to their association with membranes, all members of Class 2 possess an extension in the N-terminal region known as the membrane domain; this

extension allows interaction of the enzymes with the membrane.[44, 45] Enzymes belonging to Class 1 are found in Gram-positive bacteria, anaerobic fungi and in eukaryotes such as trypanosomatids. In contrast, enzymes belonging to Class 2 are found in eukaryotes and in certain prokaryotes such as Gram-negative bacteria. The division of DHODHs into two classes also correlates with the preferences of the enzymes for different electron acceptors and with their oligomeric states. The enzymes of Class 1A are homodimeric; as oxidizing agents, they use oxygen molecules or molecules that are soluble in water, such as fumarate, which oxidizes $FMNH_2$ for the regeneration of FMN. DHODHs of Class 1B are heterotetrameric enzymes that use NAD^+ as an oxidizing agent and contain not only FMN but also a flavin adenine dinucleotide molecule (FAD), besides a [2Fe-2S] cluster.[46, 47] Class 1B enzymes appear to prevail in Gram-positive bacteria, some of which express forms 1A and 1B. In contrast, the 1A form appears as a single form in selected eukaryotes, for example, in species of the genera *Leishmania* and *Trypanosoma*. Class 2 enzymes are monomeric proteins that use hydrophobic molecules (e.g., ubiquinone, CoQ_n) as oxidizing agents (**Figure 3**).[43, 48]

Another important difference between the two classes is regarding the catalytic residue, which is a cysteine for class 1, whereas a serine residue is found in members of class 2. These residues act as catalytic bases in the first step of the reaction (the reductive half-reaction), deprotonating C5 of DHO. DHO then transfer a hydride from C6 to N5 of the isoalloxazine moiety of FMN. In the second step of the reaction (the oxidative half-reaction), FMN transfer a hydride to the fumarate or the quinone, through either a direct hydride transfer, or two single-electron transfers. The mechanism for the second-half reaction is not yet fully elucidated.[24, 49]

In order to study the global reaction described above, many assays have been developed. They can be used to probe the enzymatic activity, ligand binding, and inhibition mechanisms of dihydroorotate dehydrogenase. DHODH activity can be assayed by monitoring the direct orotate formation at 300 nm ($\varepsilon = 2650\ M^{-1}\ cm^{-1}$) in a reaction mixture containing 50 mM Tris, pH 8.0, 150 mM KCl, and both substrates, dihydroorotate and oxidant agent.[22] The kinetic parameters, V_{max} and K_M, can be determined by varying the steady-state concentrations of both substrates. The reaction is initiated by the addition of

DHODH enzyme and the rate of orotate production is determined over time. Kinetic constants are estimated from the fit of the data to the equation that describes the ping-pong mechanism.[24]

With the purpose of performing the orotate formation assay described above, Triton X-100 may be used.[42, 43] Triton X-100 is typically used for screening libraries of potential inhibitors, helping solubilizing the compounds, and avoiding false positives induced by aggregate enzyme interactions, or to solubilize and stabilize class 2 DHODH enzymes. However, Triton X-100 absorbs in the near ultraviolet, interfering with the monitoring of orotate formation at 300 nm. In this situation, an indirect assay that monitors the activity of the enzyme through the use of the 2,6-dichlorophenolindophenol (DCIP) has been developed. DCIP is a colorimetric agent commonly used as the final electron acceptor in the enzymatic studies of DHODHs because the reduction of DCIP can be identified by a color change and monitored spectrophotometrically at 600-610 nm.[50-52] The reduction of DCIP is stoichiometrically equivalent to reoxidation of reduced quinone (**Figure S1A**, in appendices). This colorimetric method has been the most common assay used to monitor DHODH enzymatic reactions. It has been widely used for evaluating enzymatic activity and inhibition studies, including high throughput screening assays.[53-56]

A fluorescence intensity (FLINT) high-throughput assay to monitor the oxidation of L-DHO to orotate was also recently developed.[57] The assay was originally developed for *Pf*DHODH, but can be applied to other class 2 DHODHs. This assay uses the oxidizing agent resazurin as a second substrate. Resazurin is a redox-sensitive fluorogenic dye that varies from a blue non-fluorescent state to a pink, highly fluorescent state upon reduction to resorufin, monitored at 590 nm (**Figure S1B**, in appendices).[57]

Considering this global introduction regarding DHODHs, we will describe subsequently, divided in chapters, a deeper introduction, methods and the results obtained on the two target enzymes studied in this work, DHODH from *Schistosoma mansoni* (Chapter 2) and DHODH from *Plasmodium falciparum* (Chapter 3).

CHAPTER 2. *SCHISTOSOMA MANSONI* DHODH

2.1 Introduction

Schistosomiasis, is a chronic, debilitating disease caused by blood-dwelling trematodes of the genus *Schistosoma* capable of infecting mammals, birds and reptiles.[58] Five species are capable of infecting humans: *S. mekongi, S. intercalatum, S. mansoni, S. haematobium* and *S. japonicum*. Of these, the last three are more important in public health, being responsible for most cases of schistosomiasis. Only the etiological agent *S. mansoni* is found in Brazil.[59] **Figure 4** illustrates the distribution of these species worldwide.[60] This disease affects over 206 million people (3.3 million DALYs) in more than 70 countries, including sub-Saharan Africa, the Middle East, Southwest Asia and parts of South America.[61, 62] Although this disease is not endemic in other regions, cases have already been reported in Scotland,[63] France, Germany, Italy[64, 65] and China.[66]

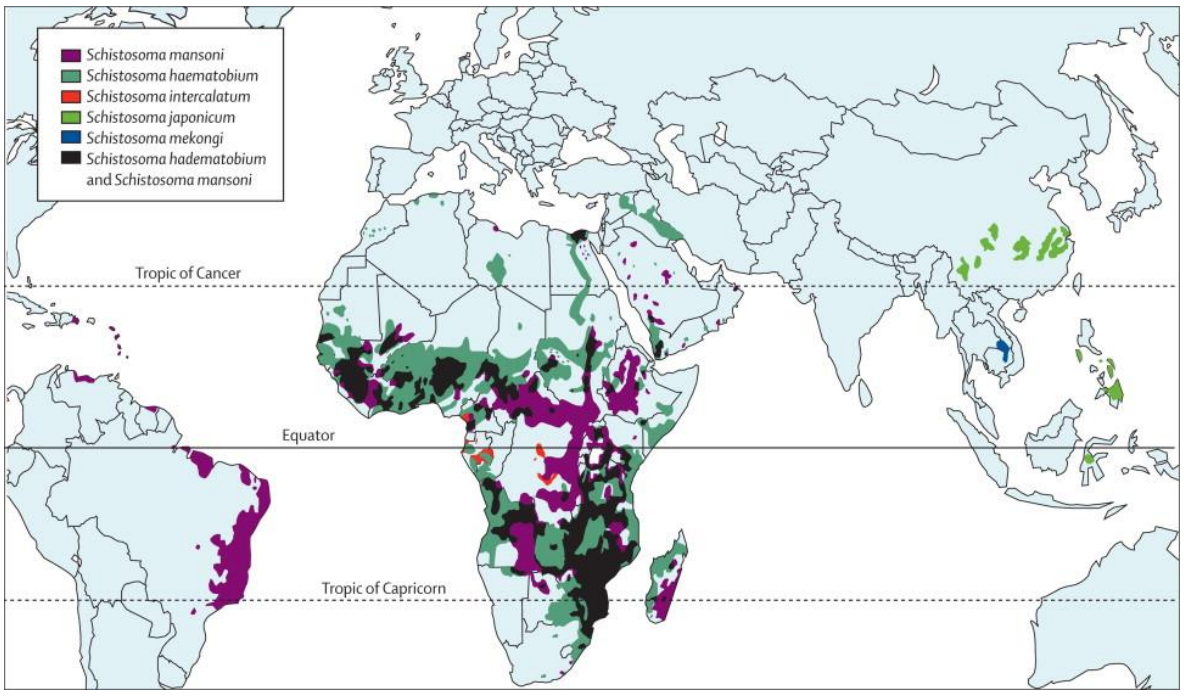

Figure 4. Global distribution of schistosomiasis (extracted from Ferrari and Moreira, 2011 [60]).

The evolutionary cycle of *Schistosoma mansoni* (**Figure 5**)[67] involves an asexual reproduction phase in the intermediate host, a freshwater snail of the genus *Biomphalaria*; a sex-specific phase in the definitive host, the human; and two infective larval stages, cercariae and miracidia, both adapted to favor transmission between hosts.[68, 69]

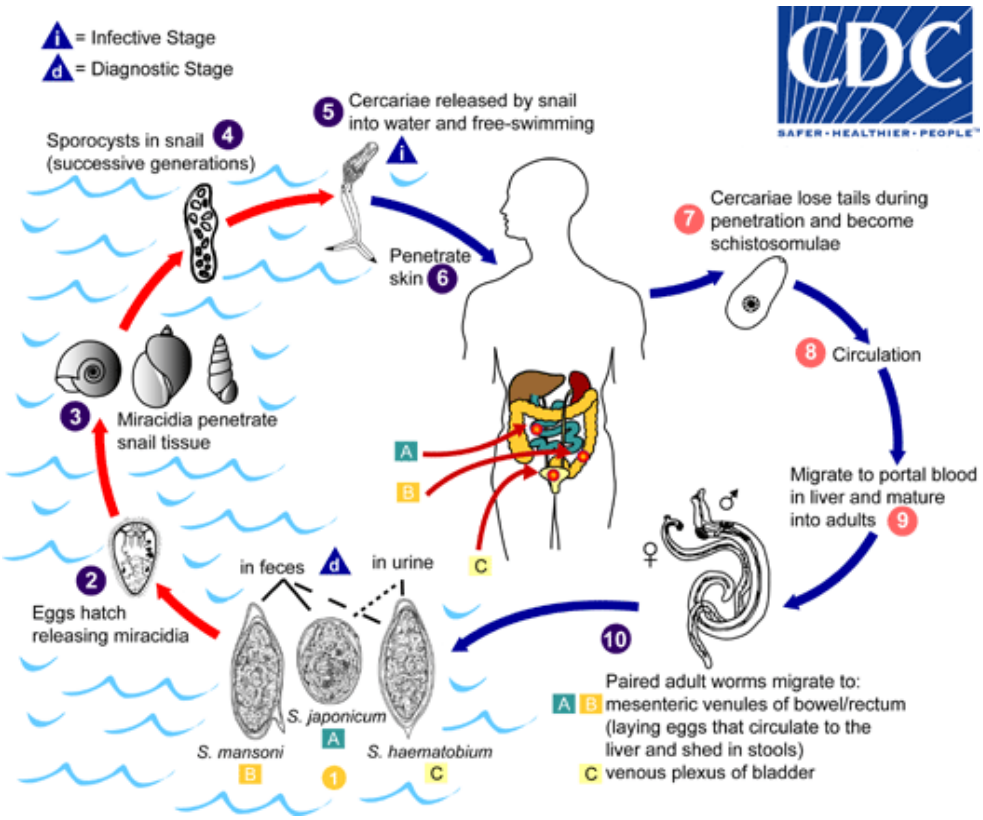

Figure 5. Schistosomiasis parasites life cycle involves two hosts. Eggs are eliminated with feces or urine (1). Under optimal conditions the eggs hatch and release miracidia (2), which swim and penetrate specific snail intermediate hosts (3). The stages in the snail include 2 generations of sporocysts (4) and the production of cercariae (4). Upon release from the snail, the infective cercariae swim, penetrate the skin of the human host (6), and shed their forked tail, becoming schistosomulae (7). The schistosomulae migrate through several tissues and stages to their residence in the veins (8,9). Adult worms in humans reside in the mesenteric venules in various locations, which at times seem to be specific for each species (10). For instance, *S. japonicum* is more frequently found in the superior mesenteric veins draining the small intestine (A), and *S. mansoni* occurs more often in the superior mesenteric veins draining the large intestine (B). However, both species can occupy either location, and they are capable of moving between sites, so it is not possible to state unequivocally that one species only occurs in one location. *S. haematobium* most often occurs in the venous plexus of bladder (C), but it can also be found in the rectal venules. The females deposit eggs in the small venules of the portal and perivesical systems. The eggs are moved progressively toward the lumen of the intestine (*S. mansoni* and *S. japonicum*) and of the bladder and ureters (*S. haematobium*), and are eliminated with feces or urine (1), respectively (extracted from CDC, 2018 [67]).

The parasites have separate sexes and accentuated sexual dimorphism. Adult males measure about 1 centimeter in length and present a foeaceous form, while adult females measure 1.2 to 1.6 centimeters in length, exhibit cylindrical shape, and when they reach one to two years, they can produce up to 400 eggs per day. Infected individuals are

able to eliminate viable *Schistosoma* eggs for 5 years on average. However, some individuals eliminate them for even more than 20 years.[68, 69]

In the chronic phase, the clinical condition of the patient is variable and the disease can evolve into several clinical forms. The intestinal form may be asymptomatic or characterized by diarrhea and abdominal pain. During the hepatointestinal form, there are signs of diarrhea and epigastralgia, with hepatomegaly and characteristic nodules of fibrosis of the hepatic tissue. It is important to mention that the parasite and/or its eggs can still lodge outside the hepatic portal system, generating the ectopic, neurological, vasculopulmonary and renal forms of the disease. Neuroschistosomiasis, for example, is the most severe disabling form of this disease.[60, 69]

The only drug available to treat the patients (Praziquantel) has been on the market for over 50 years and parasite resistance is becoming a significant issue in some areas.[11, 70] Thus, the development of novel drugs to fight schistosomiasis is of utmost importance. One well-established strategy to accomplish this goal is through repurposing of drugs. Herein we propose to take a similar approach by repositioning knowledge and results towards enzymes considered potential drug-targets.

The metabolic pathways responsible for pyrimidine biosynthesis (*de novo* pathway, the salvage pathway[71-73] and thymidylate cycle[74, 75]) are functional in *S. mansoni*. Among the enzymes involved in the *de novo* biosynthesis of pyrimidine nucleotides, *S. mansoni* expresses the flavoenzyme dihydroorotate dehydrogenase (DHODH).[76-78] As described before, this enzyme can be categorized into 2 classes according to their structural features and cellular location.[31] DHODH from humans, *S. mansoni*, *P. falciparum* and *Escherichia coli* pertain to class 2 (**Figure 6**) and, with exception to *Sm*DHODH, they have been extensively studied, and used as a drug target.[41]

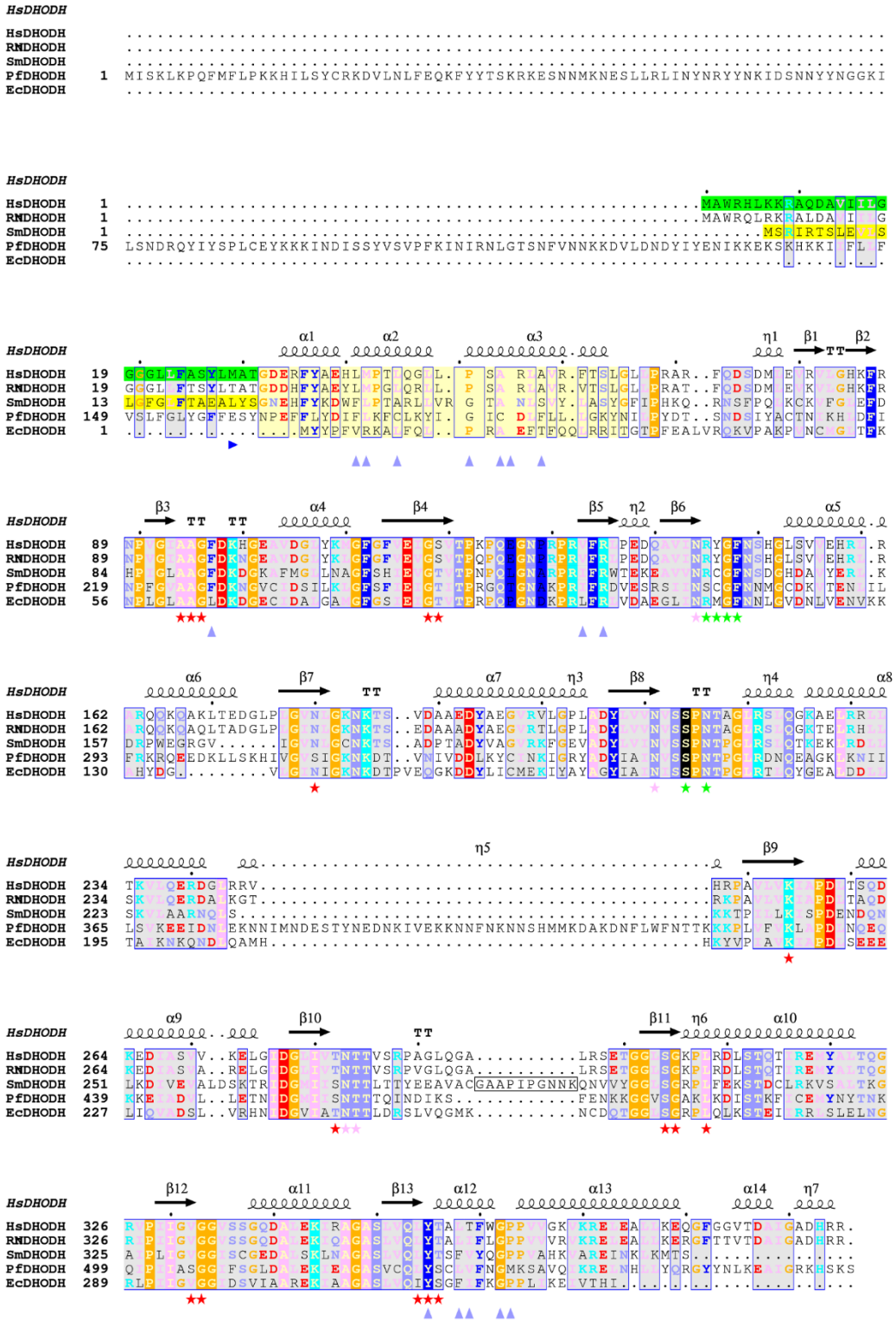

Figure 6. Sequence alignment of selected class 2 DHODHs: *Hs*DHODH (Human DHODH), *Rn*DHODH (*Rattus norvergicus* DHODH), *Sm*DHODH (*Schistosoma mansoni* DHODH), *Pf*DHODH (*Plasmodium falcipurum* DHODH) and *Ec*DHODH (*Escherichia coli* DHODH). Similar residues are colored based on their physical-chemistry properties: polar neutral amino acids (S, T, Q, N) are brown, polar basic residues (K, R,

H) are cyan, polar acidic (D, E) are red, non-polar aromatic (F, Y) are blue, and non-polar aliphatic (A, V, L, I, M) amino acids are pink. G and P are colored in brown. Signal peptide and transmenbrane domain predicted for *Hs*DHODH are highlighted in green. Signal peptide predicted for *Sm*DHODH is highlighted in yellow. Starting point for truncated *Sm*DHODH and *Hs*DHODH constructs is indicated by a blue arrow. N-terminal microdomain responsible to allow protein anchoring to the membrane, harboring the respiratory quinones for FMN reoxidation is highlighted in pale yellow. The serine catalytic residue of class 2 DHODH is highlighted in black. The residues significant for FMN binding, orotate binding, or both FMN and orotate binding are indicated by red, green and pink stars, respectively. Residues recognized as involved in inhibitor binding are indicated by grey arrows. Residue numbering for each sequence is shown at the left. The alignment was performed using MULTALIN[79] and graphically displayed using ESPript 3.0.[80]

Class 2 DHODHs are inhibited by quinone derivatives.[29, 81] Interestingly, chemically similar compounds also display cercaricidal activity:[82] Plumbagin, a naphthoquinone isolated from *Plumbago scandens*;[61] norobtusifolin and kwanzoquinone E, anthraquinones isolated from *Hemerocallis fulva*,[83, 84] resulted in either the mortality or the immobilization of *S. mansoni* cercariae. Derivatives of lapachol and isolapachol have shown activity against different life cycle stages of *S. mansoni*.[85] The relevance of nucleotides production, along with our extensive knowledge regarding class 2 DHODH inhibition by quinone derivatives points out to this enzyme as a druggable target for development of new therapies against schistosomiasis.

The goal of the present project was to perform inhibitory studies against *Sm*DHODH by testing libraries of compounds originally developed as *Pf*DHODH inhibitors. Protein-ligand interaction characterization was initiated by a multi-approach strategy using a combination of structural, biophysical and biochemical techniques.

It is important to mention that previous work has been done regarding *Sm*DHODH and *Hs*DHODH by our laboratory (former master student Juliana S. David).[86, 87] Data previously obtained (initial expression and purification protocols and biochemical characterization of the enzyme) has helped the development of this work. Kinetic parameters, previously determined (**Table 2**) were used to set parameters for activity and inhibitory assays applied and also for the mechanism of inhibition.

Table 2. Kinetic parameters for the steady-state kinetics for the two reactions catalyzed by the enzymes *Sm*DHODH and *Hs*DHODH.

Kinetic Parameters	*Sm*DHODH	*Hs*DHODH
k_{cat} (s^{-1})	31 ± 2	78 ± 4
$K_{M\ DHO}$ (μM)	228 ± 26	286 ± 31
$K_{M\ Q0}$ (μM)	167 ± 21	354 ± 38

Two different constructs were used as models for our studies, named *Sm*DHODH and *Sm*DHODHΔloop. *Sm*DHODH comprises residues Leu[23] to Ser[379], where the predicted mitochondrial targeting peptide and transmembrane region (Met[1] to Ala[22]) has been omitted. *Sm*DHODHΔloop comprises the same fragment as *Sm*DHODH, but a flexible loop (Gly[285] to Lys[294]), not present in other class 2 DHODH, was removed to favor crystallization studies (shown in slate blue in **Figure 7**).

Figure 7 is a homology model built (Modeller)[88] using class 2 DHODH structures previously elucidated from other organisms. Apart from the additional extended loop described before, the figure also shows the α/β barrel catalytic central barrel composed of eight parallel β strands and surrounded by eight α-helices, illustrated in pink, present in both classes 1 and 2. At the top of the barrel, antiparallel β-strands form a domain covering the redox site, likewise at the bottom of the barrel is formed by a pair of antiparallel β-strands. The orotate binding site is located at the top of the barrel, where several strands form the substrate and FMN binding pocket. It is also indicated in the figure, the N-terminal domain in yellow, present only in class 2. The residue highlighted in green is the catalytic residue, Ser[203].

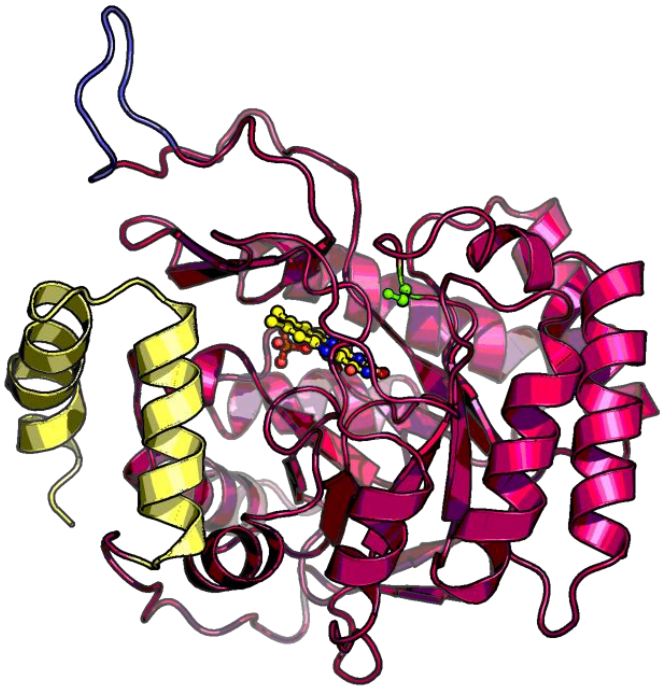

Figure 7. Cartoon representation of *Sm*DHODH homology model.[87] The hydrophobic N-terminal domain composed by two helices is illustrated in yellow. The catalytic central barrel composed of eight parallel β strands and surrounded by eight α-helices is illustrated in pink. The FMN group is located at the top of the barrel and is illustrated as a ball-and-stick model. The catalytic residue Ser^{203} is shown in green. The main structural difference between *Sm*DHODH and other class 2 DHODHs is the presence of a ten-residue peptide that folds as a protuberant subdomain and is illustrated in slate blue.

The studies described next shows the biochemical and biophysical characterization of the enzymes *Sm*DHODH and *Hs*DHODH, as well as the search for ligands, as a first step to evaluate the potential of the selective inhibition of the enzyme *Sm*DHODH. The best inhibitors identified also had their efficacy assessed through *in vitro* assays in the presence of adult *S. mansoni* parasites. The study described in this Chapter can be helpful, in the future, as a therapeutic strategy in the fight against schistosomiasis.

2.2 Objectives

The general goal of this work was to evaluate the therapeutic potential of antimalarial drugs based on the selective inhibition of the enzyme dihydroorotate dehydrogenase as a strategy for the development of new therapies for the treatment of schistosomiasis.

The specific steps can be summarized in:

- Heterologous expression in *E. coli* and purification for the enzymes *Sm*DHODH, *Sm*DHODHΔloop and *Hs*DHODH;
- Cloning of a new construct, named *Sm*DHODHΔloop where the protruding loop is removed;
- Biophysical and biochemical characterization, crystallization assays and structural elucidation of *Sm*DHODHΔloop by X-ray diffraction techniques;
- Inhibitory assays for *Sm*DHODH in the presence of antimalarials and determination of inhibition mechanisms;
- Evaluation of compounds activities using *in vitro* assays (adult *Schistosoma mansoni* worms).

2.3 Materials and Methods

2.3.1 Cloning of SmDHODH, HsDHODH and SmDHODHΔloop

The gene encoding active *Sm*DHODH enzyme (Leu^{23} to Ser^{379}) and *Hs*DHODH enzyme (Met^{29} to Arg^{395}) had been previously cloned in our laboratory using the pET-SUMO expression vector.

In order to favor crystallization in a reproducible manner, a novel construct, named *Sm*DHODHΔloop, was prepared where the flexible region (Gly^{285} to Lys^{294}) was removed from the target protein. *Sm*DHODH enzyme gene code was used as template for carrying out gene amplification.

Using the overlap extension technique (**Figure 8**), the fragment of interest was deleted through a sequence of three polymerase chain reactions (PCR). In the first two PCR reactions, two external oligonucleotides (A and D) were used together with two internal oligonucleotides (B and C) to create two fragments (**Table 3**). Amplifications of both fragments (AB and CD) were performed according to the specifications indicated in the manual of the polymerase enzyme used Phusion DNA Polymerase (Thermo Scientific). The third step was divided into two PCRs, the first for the extension of incomplete fragments (AB and CD) and the second for amplification, through the external oligonucleotides, of the complete fragment (AD). The fragments obtained in the PCR reactions were purified from the 0.8% agarose gel using the QIAquick Gel Extraction Kit (QIAGEN) and then cloned into the pET-SUMO vector.

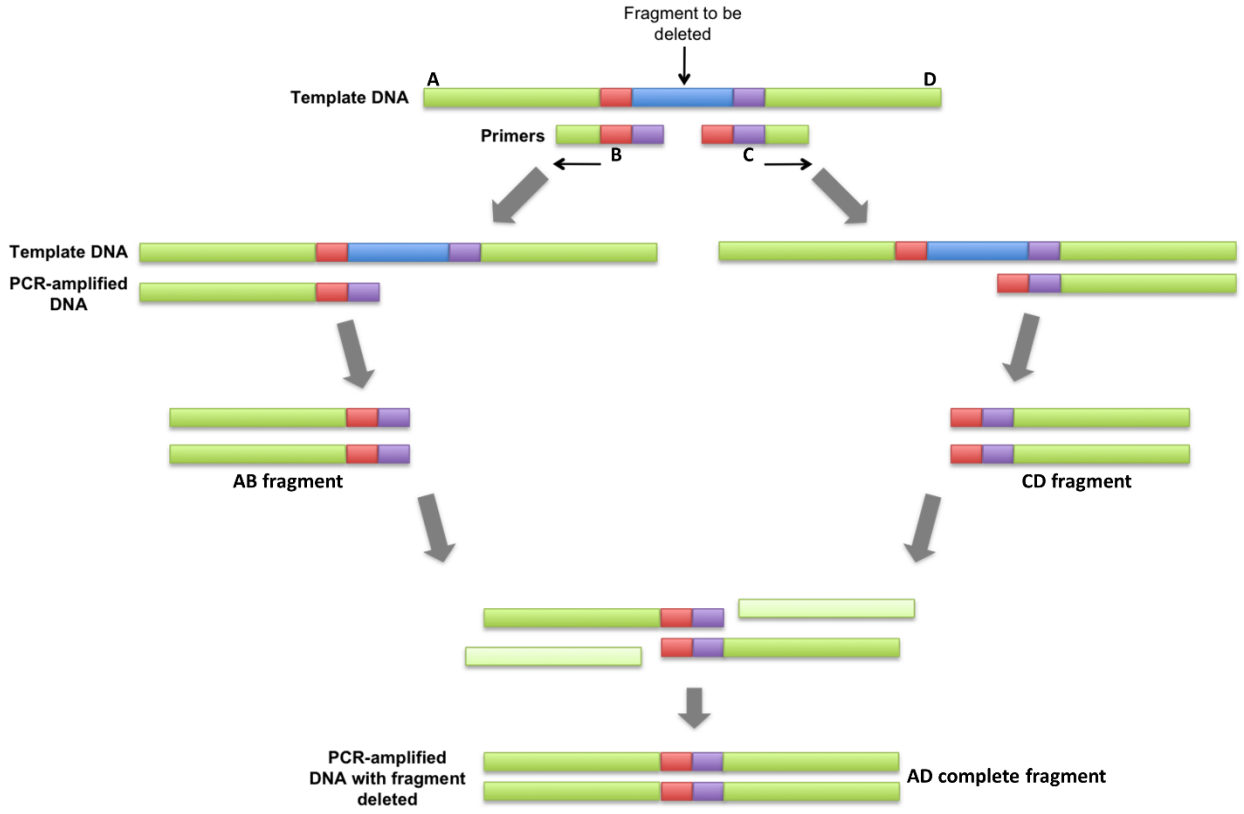

Figure 8. Schematic representation of the overlap extension technique used for deletion.[89] PCR is used to generate two fragments that correspond to the flanking regions of the cassette to be deleted. Both of these generated PCR fragments contain a terminal sequence derived from the template on the other side of the sequence to be deleted. These terminal sequences allow for hybridization of the two flanking fragments, which can be subsequently extended to generate a shortened final fragment in the secondary PCR step. In other words, deletion is essentially a ligation or recombination of the two flanking DNA fragments.

Table 3. Internal and external primers used for *Sm*DHODHΔloop cloning. Underlined sequences are corresponded to specific sites for restriction enzymes.

Primers	Sequence (5'- 3')	Melting Temperature (°C)
***Sm*DHODH *Bam*HI Fow** (external primer, A)	AGTGGATCCTTGTACTCTGGAAATGAGCACTTTTATAAAG	62.4
***Sm*DHODH *Xho*I Rev** (external primer, D)	CTGCTCGAGTTAAGATGTCATTTTTAATTTATTAATTTCT	58.3
***Sm*DHODHΔloop Fow** (internal primer, B)	GCTGTAGCTAAACAAAATGTTGTATATGGC	57.5
***Sm*DHODHΔloop Rev** (internal primer, C)	ATTTTGTTTAGCTACAGCCTCTTCATAAGT	56.2

The complete fragment and the pET-SUMO vector were digested with restriction enzymes BamHI and XhoI and purified from 0.8% agarose gel. Ligation of insert into vector was done using the enzyme T4 DNA ligase (NEB). *E. coli* DH5α cells were transformed with the ligation product; subsequently Colony PCR was performed for determining the presence or absence of insert DNA into plasmid construct. Positive clones were purified from the transformed cells with the QIAprep Miniprep Kit (QIAGEN).

Finally, to confirm the positive clones in the stored colonies, a small aliquot of purified DNA was subjected to digestion with the enzymes BamHI and XhoI. After digestion, the samples were analyzed into agarose gel 0.8%.

Plasmid DNA for the new construct was sequenced by using, two external oligonucleotides, Bgl II (5' – AGATCTCGATCCCGCGAAATTAAT – 3') and ExtPet 28a (5' – AAAGCCGGCGAACGTGGC – 3').

2.3.2 Heterologous expression of the enzymes SmDHODH, SmDHODHΔloop and HsDHODH

*Sm*DHODH, *Sm*DHODHΔloop and human enzyme (*Hs*DHODH) were expressed under similar protocols. A single colony of *E.coli* BL21-CodonPlus (DE3)-RIL transformed with pET-28-SUMO-*Sm*DHODH, pET-28-SUMO-*Sm*DHODHΔloop or pET-28-SUMO-*Hs*DHODH plasmid were grown overnight in 10 mL of medium (20 g/L bacto-tryptone, 15 g/L yeast extract, 2 g/L Na_2HPO_4, 1 g/L KH_2PO_4 and 8 g/L NaCl) containing 30 µg/mL kanamycin and 34 µg/mL chloramphenicol at 37 °C and 180 rpm and used to inoculate 1 L of fresh medium. When the $O.D_{600nm}$ reached 0.5, isopropylthio-β-galactoside (IPTG, Fermentas) was added to 100 µM final concentration and the temperature was reduced to 18 °C. After 24 hours the cells were isolated by centrifugation at 10,000 g for 8 minutes and kept at -20°C until used.

2.3.3 Purification of the enzymes SmDHODH, SmDHODHΔloop and HsDHODH

A single purification protocol was developed for all constructs used in this study: *Sm*DHODH, *Sm*DHODHΔloop and *Hs*DHODH. Cell pellets corresponding to 250 mL of culture were resuspended in 20 mL of lysis buffer (50 mM Tris-HCl pH 7.5, 600 mM NaCl, 0.33% Thesit (Sigma), 1 mM phenylmethanesulfonylfluoride (PMSF), 10% glycerol and EDTA free SigmaFAST™ (Sigma) protease inhibitor cocktail). The cells were lysed using 15 cycles of 30 s sonication with 30 s intervals on ice with an output power of 10 W. The lysate was then maintained on ice for 30 minutes on a rocking shaker and centrifuged at 16,100 g for 30 minutes at 4 °C.

The soluble fraction was loaded into a 1 mL HisTrap™ HP column connected to an ÄKTA-Purifier system (GE Life Sciences) previously equilibrated with buffer A (50 mM Tris-HCl pH 7.5, 600 mM NaCl, 10% glycerol, 0.05% Thesit). An isocratic chromatographic run was carried out at 1.0 mL/min. The wash steps consisted of passing through at least 5 column volumes of buffer A containing 10 mM imidazole followed by 5 column volumes of buffer A containing 25 mM imidazole. 6xHis-SUMO-DHODH was eluted with buffer A containing 500 mM imidazole. The eluted samples were concentrated to 500 µL using a 10 kDa cutoff Amicon Centrifugal filter unit and loaded in a 5 mL HiTrap Desalting column connected to an ÄKTA-Purifier system (GE Life Sciences). An isocratic chromatographic run was carried out with buffer A at 1 mL/min.

Homemade 6xHis-ubiquitin-like protein 1 (ULP1) protease[90] was incubated with the desalted protein, during 16 hours at 4 °C. The sample was once again loaded into a 1 mL HisTrap™ HP column connected to an ÄKTA-Purifier system (GE Life Sciences) pre-equilibrated in buffer A. Tag free DHODH was collected in the flow through. The 6xHis-SUMO tag and 6xHis-ULP1 were eluted from the column with buffer A containing 500 mM imidazole.

Protein purity was assessed by SDS-PAGE and quantification was carried out by absorbance using the extinction coefficient of the protein prosthetic group FMN, ε_{456nm} =

13080 $M^{-1}.cm^{-1}$ for *Sm*DHODHs; and ε_{454nm} = 14260 $M^{-1}.cm^{-1}$ for *Hs*DHODH, calculated as described elsewhere.[86]

2.3.4 Circular Dichroism

Circular dichroism was used to evaluate secondary structure content and protein stability for both *Sm*DHODH and *Sm*DHODHΔloop. CD spectra were recorded on a JASCO J-810 CD Spectrometer (Prof. Richard Ward's lab) at pH 8.5 in 20 mM sodium phosphate. For far-UV CD spectra, a 2 mm pathlength cell was used with a one second integration time and a 1 nm bandwidth. The spectra recorded from 190 nm to 250 nm with an increment of 1.0 nm are averages of three accumulation scans. The sample was maintained at room temperature. The protein concentration measured was 0.2 mg/mL. All spectra were corrected for blank absorption. The results were given in ellipticity, θ. For the represented graphs, the CD spectra were converted to molar ellipticity, [θ], using **Equation 1**.[91] The α-helix percentages were calculated using **Equation 2**, as described elsewhere.[92]

$$[\theta] = \frac{\theta_\lambda \times MRW}{10 \times l \times c}$$

Equation 1. Transformation of ellipticity into molar ellipticity. θ_λ is the experimental ellipticity in millidegrees fir each wavelength, MRW is the mean residue weight (113), c is the protein concentration ($mg.ml^{-1}$), and l is the path length (cm).

$$f\alpha = 100\left(\frac{[\theta]_{208} - 4{,}000}{29{,}000}\right)$$

Equation 2. α-helix percentage approximation factor. fα is the approximate percentage of α-helix, [θ] is the molar ellipticity value at 208 nm.

2.3.5 Activity and storage stability assays (Direct assay)

The activity assays were performed in a 96-well microplate reader, containing the activity buffer 50 mM Tris pH 8.15, 150 mM KCl, 0.05% Thesit, 500 µM DHO, 100 µM CoQ_0. To start the reaction, 5 µL *Sm*DHODH was added, to a final concentration of 90 nM. As a negative control, 5 µL enzyme buffer was added in 200 µL activity buffer. Orotate (ORO) formation was monitored each 3 s over a period of 60 s, in triplicate, for each concentration and each tested compound.

For the storage stability assay, the above procedure was performed for a period of 7 consecutive days, in six replicates, using a fresh prepared buffer. Enzyme solution was kept at 4°C and concentration was estimated previously to all measurements. The average activity measured at day 0 was considered as control, 100% activity. The storage stability curve was plotted in the software OriginPro 8.

2.3.6 Enzymatic inhibition assays (Indirect assay)

The experiments were performed in a 96-well microplate reader, containing 60 µM DCIP, 50 mM Tris pH 8.15, 150 mM KCl, 0.1 % Triton X-100, 500 µM DHO, 100 µM CoQ_0 and varied inhibitor concentrations. To start the reaction, 5 µL *Sm*DHODH or *Hs*DHODH protein solution were added, to a final concentration of 40 nM and 20 nM, respectively. As a negative control, 5 µL of each enzyme were added in 200 µL buffer, without the presence of the inhibitors. As a positive control, 5 µL of each enzyme were added in 200 µL buffer, with the presence of a inhibitor (identified during this work) for each enzyme (atovaquone and brequinar, for *Sm*DHODH and *Hs*DHODH, respectively). The reaction was monitored each 3 s over a period of 60 s, in technical triplicate, for each concentration and each tested compound. All the compounds tested in this thesis belong to both libraries described in topics 2.3.6.1 and 2.3.6.2. The IC_{50} was determined through the graph of percent of inhibition versus log of the inhibitor concentration. The dose-response curve was fit according to **Equation 3** using OriginPro 8 software.

$$y = \frac{A1 - A2}{1 + e^{(x - x_0)/dx}} + A2$$

Equation 3. Sigmoidal fitting equation used. A1 corresponds to the minimal inhibition value, A2 corresponds to the maximum inhibition value, and x0 correspond to the inflexion point that correspond to the log of the inhibitor concentration responsible for 50 % loss of enzymatic activity.

2.3.6.1 Atovaquone and derivatives library

A group of 34 compounds was evaluated as *Sm*DHODH and *Hs*DHODH inhibitors. The compounds were divided in five series (named A – E) according to their chemical similarity (**Figure 9**): A – controls are well known DHODH inhibitors; B – 2-hydroxi-3-amine-naphthoquinones; C – 1,4-naphthoquinones derivatives; D – Lapachol and its derivatives and E – Benzoquinones. Compounds from group A and E, as well as Lawsone (Compound 10) were commercially available and purchased. The other compounds were synthesized by Prof. Flávio Silva Emery group from this department.

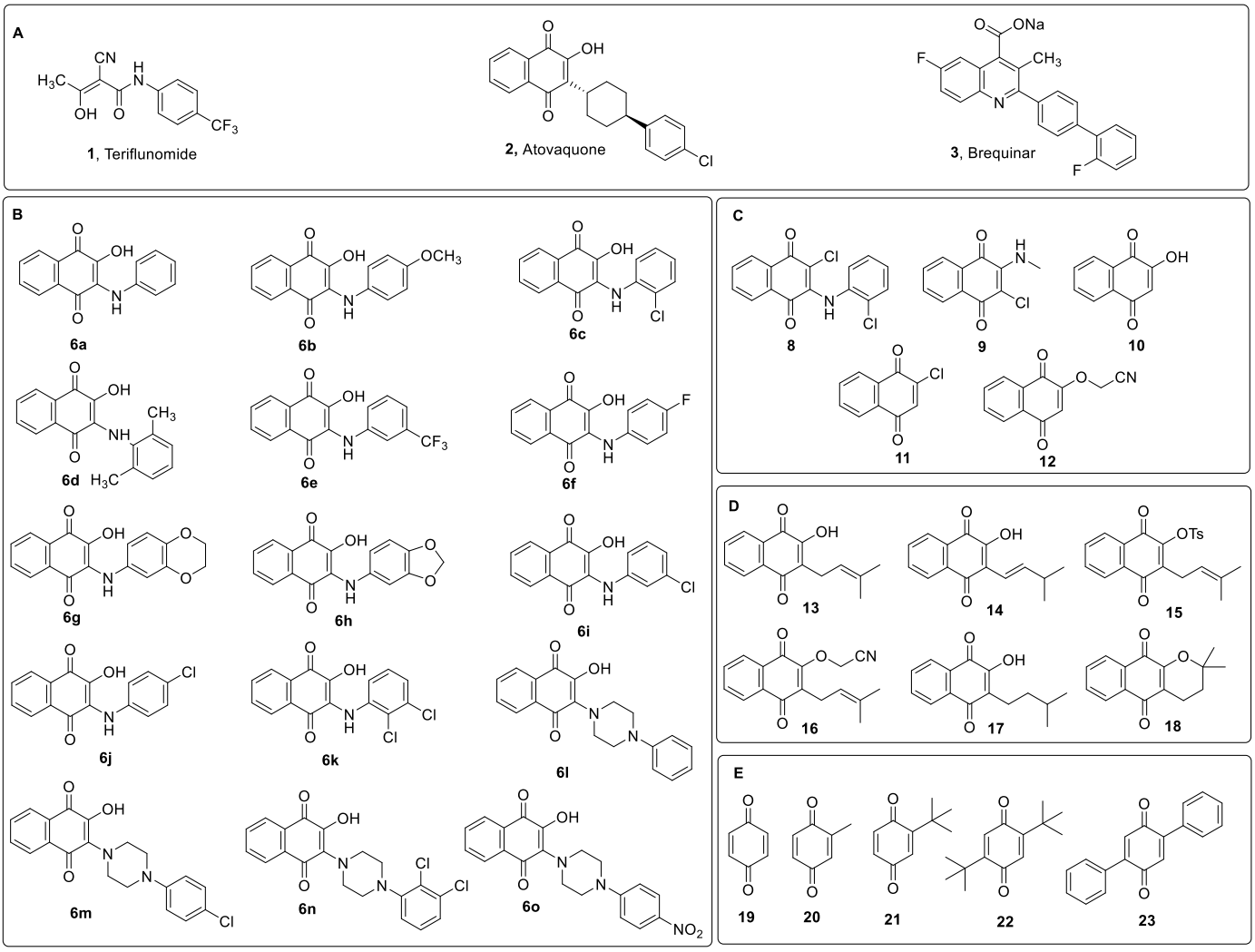

Figure 9. Compounds tested as *Sm*/*Hs*DHODH inhibitors, grouped according to their chemical scaffold. A – Known DHODH inhibitors; B – 2-hydroxi-3-amine-naphthoquinones; C – 1,4-naphthoquinones derivatives; D – Lapachol and its derivatives; E – Benzoquinones. *Compounds codes used in the submitted manuscript.

2.3.6.2 Antimalarial drugs library from Broad Institute

A wide and diverse collection of compounds, provided by Prof. Stuart Schreiber from the Broad Institute of MIT and Harvard, were evaluated as inhibitors against *Sm*DHODH and *Hs*DHODH. This group of 151 compounds is a subset of a library of molecules that were developed in collaboration with Medicines for Malaria Venture (MMV) to inhibit *Plasmodium falciparum* DHODH. Those compounds have been described to

possess antimalarial activity and some of these are already in pre-clinical stages of drug development.

The compounds were sent in 96-well plates in 100% DMSO at the concentration of 10 mM. A single-point final concentration of 10 µM was tested for all samples. The compounds that were able to inhibit the enzyme over 80% had their IC_{50} values determined.

2.3.7 Inhibition mechanism studies

The inhibition mechanism assays were performed in a 96-well microplate reader, containing the buffer 50 mM Tris pH 8.15, 150 mM KCl, 0.05% Thesit, 500 µM DHO, CoQ_0 varying from 0 to 1000 µM and varied inhibitor concentrations (according to their potency). Compounds tested were 2, 6c, 10, 17 and 19. To start the reaction, 5 µL *Sm*DHODH or *Hs*DHODH were added to a final concentration of 90 nM and 80 nM, respectively. As a control, 5 µL each enzyme was added in 200 µL buffer, without the presence of the inhibitors. The reaction of orotate (ORO) formation was monitored each 3 s over a period of 60 s, in triplicate, for each concentration and each tested compound. The inhibition mechanism was determined through the Michaelis-menten graph of k_{obs} versus CoQ_0 concentration using hyperbolic data fitting obtained in the software SigmaPlot 11.0 and also through the Lineweaver-Burk graph of $1/k_{obs}$ versus $1/CoQ_0$ concentration using linear data fitting in the software OriginPro 8.

2.3.8 ThermoFMN: A thermostability assay based on differential scanning fluorimetry

Differential scanning fluorimetry experiments were performed in a thermocycler – Mx3005P™ Real-Time PCR system (Agilent Technologies). The experiment was performed in a 96-well PCR plate, where each well contained 10 µL enzyme at 10 µM (5

µM final concentration), and 10 µL of different compounds at three concentrations (500, 250 and 50 µM final concentration), in triplicates. The fluorescence intensity was monitored using the filter FAM SyBr green I, 492 nm and 516 nm, excitation and emission, respectively. The temperature varied from 25 to 95 °C (1 °C/min). The obtained curves were used to determine the inflexion point using the software GraphPad Prism 5.03, which correlates melting temperature (Tm). Tm is also known as the temperature of hydrophobic exposure.

2.3.9 Crystallization of SmDHODH∆loop

Crystallization assays *Sm*DHODH and *Sm*DHODHΔloop were performed with pure and concentrated protein, using the sitting drop method. The sparse-matrix method [93] implemented in commercially available screening kits was used to initial crystallization experiments: PegIon 1 and 2, Natrix 1 and 2, SaltRx 1 and 2, Crystal Screen 1 and 2, PegRx 1 and 2, Index 1 and 2, and MembFac (Hampton Research); Nextal MBClass (Qiagen); and JBScreen Classic 1 to 10, JBScreen Membrane 1 to 4 (Jena Bioscience).

Previously, protein solution was incubated in presence of dihydroorotate (DHO, 2 mM), inhibitors (1 mM) and detergents (1 mM), once these help the stabilization of the enzyme and therefore aid the crystallization. Equal volumes of protein and reservoir solution were mixed, equilibrated against 500 µl reservoir solution and kept at 277 K. Several efforts were made in order to crystallize the protein by screening a wide range of different crystallization variables (protein concentration ranging from 2.0 to 20.0 mg/mL, drop volume, pH, temperature, precipitant concentration, and additives). The first crystals were obtained in presence of two conditions from PegRx within 5 days for the protein *Sm*DHODHΔloop. Other crystallization conditions are being tested in order to optimize the crystallization and also to co-crystallize with different ligands.

2.3.10 In vitro schistosomicidal activity

The *in vitro* assays were performed in collaboration with Prof. Dr. Fernanda de Freitas Anibal from the Federal University of São Carlos (UFSCar), using a protocol previously developed in her laboratory.[94]

S. mansoni parasites recovered after perfusion via hepatic portal system were washed in RPMI-1640 medium, maintained at pH 7.5 with 20 mM HEPES supplemented with penicillin (100 µL/mL), streptomycin (100 mg/mL) and 10% fetal serum bovine.

After washing, each pair of adult parasites (a male and a female) were transferred to a 24-well plate containing 2 mL of the same medium used for washing. The plates were incubated at 37 °C in a humid atmosphere containing 5% CO_2. After 24h, plates with *S. mansoni* cultures were incubated with the compounds tested against the enzyme *Sm*DHODH. Worm motor activity, egg output (oviposition), tegumental alterations, and survival of the parasites were monitored on daily basis for 4 days using a microscope. As a negative control, a culture plate was incubated only with RPMI-1640 medium with 0.5% DMSO. As a positive control, it was incubated in a culture plate 50 µM PZQ (Praziquantel) added to RPMI-1640 medium at 0.5% DMSO. The experiments were performed in six replicates.

2.4 Results and Discussion

2.4.1 Cloning of SmDHODH⊿loop

The gene fragment encoding *Sm*DHODHΔloop was successfully cloned into the plasmid pET-SUMO, using the previously cloned *Sm*DHODH construct as a template. The method colony PCR was used to screen for positive clones (**Figure 10).** Double digestion with enzymes *Bam*HI and *Xho*I were used to confirm the presence of the desirable insert. DNA sequencing confirmed the correct sequence and reading frame.

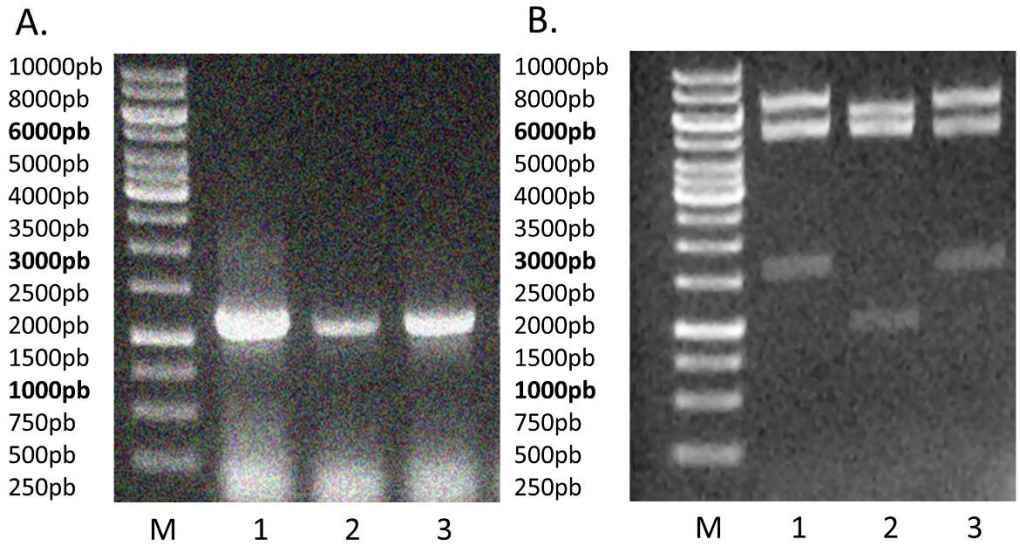

Figure 10. Electrophoresis in agarose gel. (A) colony PCR showing the potential positive colonies; and (B) double digestion to confirm the positive colony in row 2 (*Sm*DHODHΔloop, 1041bp and pET-SUMO, 5639bp).

2.4.2 Expression, purification and quantification for SmDHODH, SmDHODH⊿loop and HsDHODH

The expression and purification protocols previously established in the laboratory was adapted in order to improve yield and to speed up the purification protocol. The yield obtained, measured at 600 nm, is reproducible and around 60 mg per liter of culture for

*Sm*DHODH, 30 mg per liter of culture for *Sm*DHODHΔloop and 20 mg per liter of culture for *Hs*DHODH. SDS-PAGE gels show that the constructs were overexpressed in the soluble fraction and purification was successfully achieved by nickel affinity chromatography (**Figure 11**).

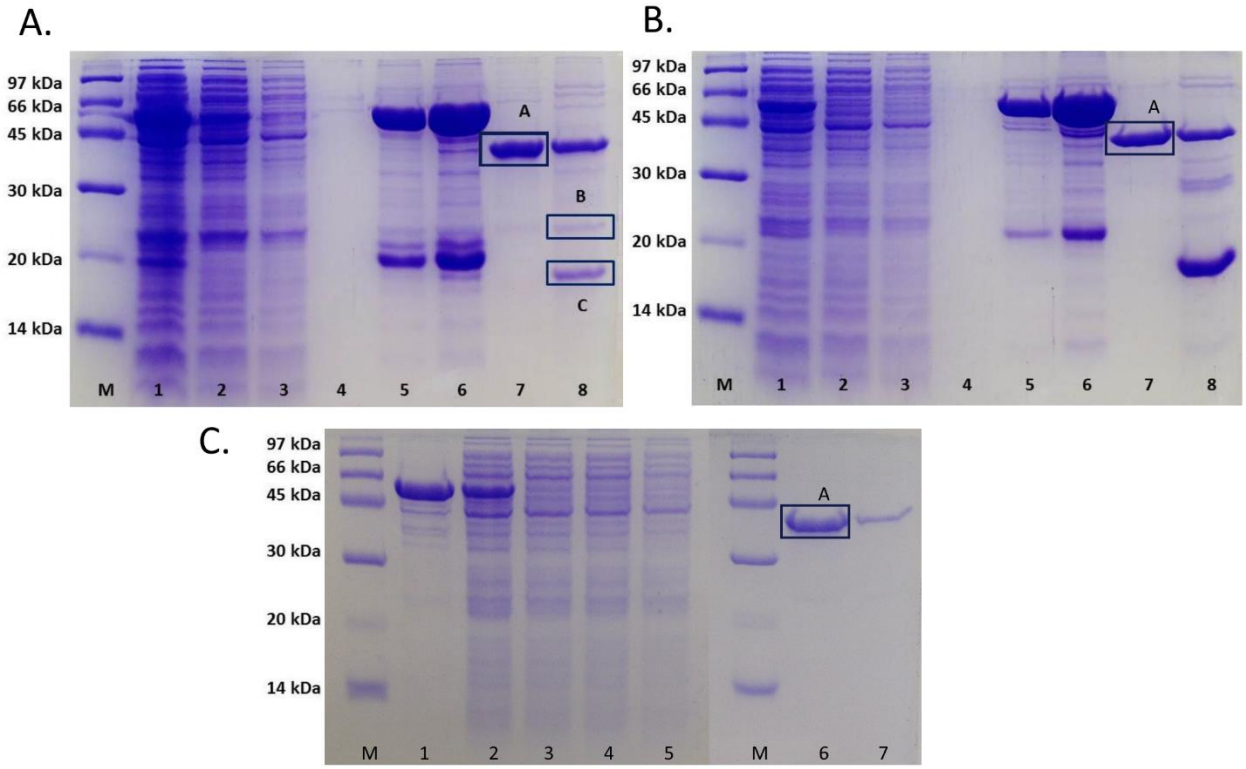

Figure 11. SDS-PAGE analysis of nickel affinity chromatography showing the purification steps. M: molecular weight marker. A: Purified proteins. B: ULP1 elution. C: 6xHis-SUMO-tag. *Sm*DHODH (A.) and *Hs*DHODH (B.): 1 – Soluble fraction; 2 – Efluent; 3 – Washing step containing 10 mM imidazole; 4 – Washing step containing 25 mM imidazole; 5 and 6 – Protein elution containing 500 mM imidazole, before SUMO cleavage with ULP1; 7 – Protein elution, after cleavage and second affinity chromatography; 8 – Elution of ULP1 and 6xHis-SUMO-tag, with 500 mM imidazole. *Sm*DHODHΔloop (C): 1 - Protein elution containing 500 mM imidazole, before SUMO cleavage with ULP1; 2 – Soluble fraction; 3 – Efluent; 4 and 5 – Washing step with 10 mM and 25 mM imidazole, respectively; 6 and 7 - Protein elution, after cleavage and second affinity chromatography.

Enzymatic activity is observed for both *Sm*DHODH and *Hs*DHODH, as previously described. Surprisingly, enzymatic activity was measured for the new construct *Sm*DHODHΔloop construct, and no activity was observed. Structural stability assays were later performed in order to further investigate this matter.

2.4.3 Storage stability assays

Using a single point assay, where activity was estimated as number of product molecules formed per time per number of protein molecules for a single substrate concentration, stability was evaluated as a function of time (hours) (**Figure 12**). Our results suggest that the enzyme remained stable from the first day (0h) through 72h. After that, activity dropped to around 80% and remained until 168h.

Evaluation of the storage stability is particularly important, especially when one needs to screen a variety of samples and one day is not enough to test them all. This experiment also highlights the need for adequate controls in order to guarantee a precise and faithful measurement of the activity and/or inhibition tests.

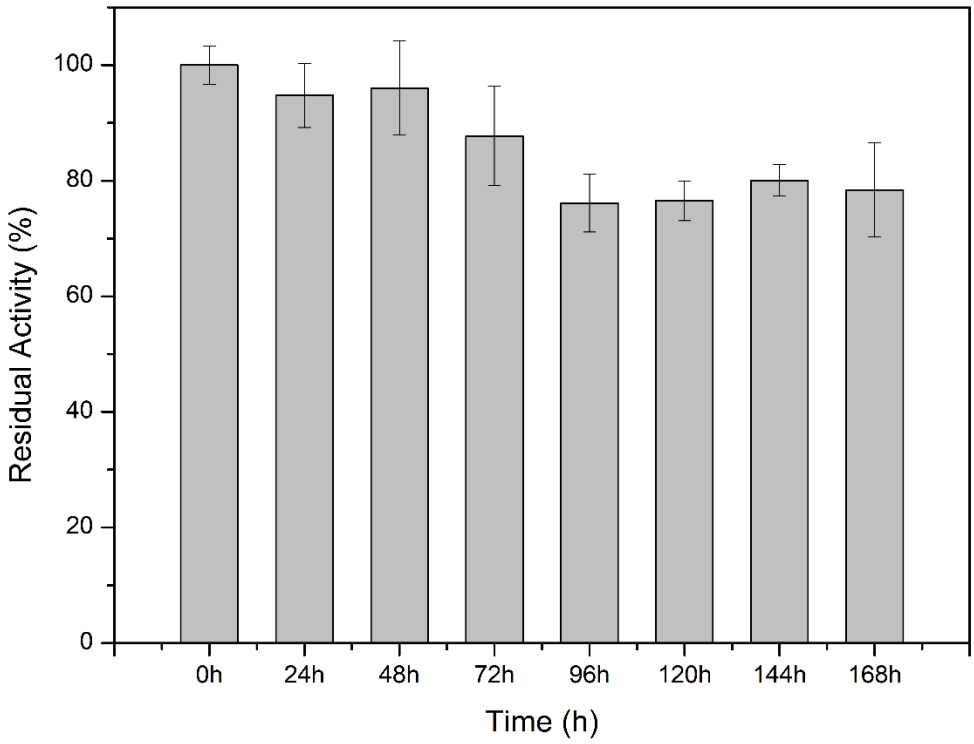

Figure 12. Residual activity versus time (hours). Activity was measure every 24h, during 7 days. The average activity measured at time 0 was considered as control, 100% activity. Bars represent means ± standard deviations for six replicates.

2.4.4 Circular Dichroism (CD)

Circular dichroism experiments were performed in order to evaluate and compare the structural integrity of both *Sm*DHODH and *Sm*DHODHΔloop. From the experiments (**Figure 13**), it was possible to observe spectra consistent to alpha/beta barrel proteins, in comparison to other reported similar structures.[95, 96] The circular dichroism spectra were characterized by two negative bands at 208 and 220 nm and a positive band at 191 nm. The minimum at 220 nm was mainly attributed to helical structures, while the negative band around 210 nm was probably the result of a mixture of the minimum at 208 nm arising from a helix structure with the band at 215 nm originating from β-sheets, which suggested a protein structure of type α/β. Moreover, the comparable intensity of the band at 208 nm and the maximum at 197 nm and minimum around 220 nm indicate substantial quantities of β-sheets. The prediction of secondary structure content was performed using the equation 2 by deconvolution of the CD spectra using K2D3.[97] The secondary structure content was estimated at 35% α-helix and 33% β-sheet, in agreement with data previously described for class 2 DHODHs.[49] *Sm*DHODHΔloop CD spectrum was very similar to the one for *Sm*DHODH, with a subtle difference at 225 nm, which might be explained as a result of the loop removal. Although the differences in the spectra are small they are detectable, and interpretable on a molecular level. The inside panel in the figure is a magnified view, which clearly shows the differences. These differences have already been observed before and can be translated into secondary structural types of the missing residues.[98]

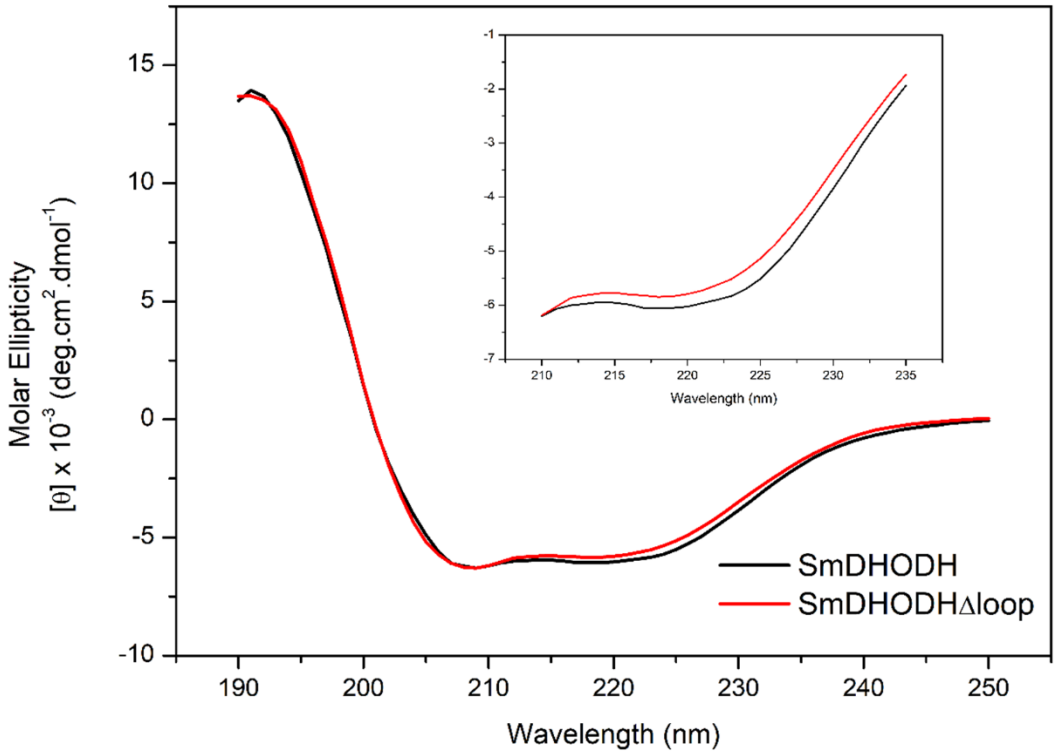

Figure 13. Circular dichroism assay performed for both *Sm*DHODH and *Sm*DHODH(Δloop). Both constructs showed similar CD spectra, suggesting that the Δloop construct retains the same tridimensional structure. Inside panel shows a magnified view ranging from 210 to 235 nm.

Structural integrity together with the lack of activity of *Sm*DHODHΔloop suggests us that this loop comprising residues Gly^{285} to Lys^{294}, and absent in other class 2 DHODHs (**Figure 7**), may be somehow involved in protein activity. The technique ThermoFMN, described later, was also used in order to help answering this matter.

It may worth mentioning that FMN scan spectra are similar and corroborate the idea that both *Sm*DHODH and *Sm*DHODHΔloop are properly and similarly folded.

2.4.5 Atovaquone and derivatives library inhibition assays

Activity measurements were carried by the indirect assay, through monitoring DCIP reduction at 610 nm. The choice of this method was due to the fact that most compounds

absorbed close to orotate maximum absorption wavelength (300 nm). Initial screening with several compounds, including atovaquone (compound 2), at single dose concentration (50 to 500 µM, according to compounds solubility limit), allowed us to select a subset of derivatives that inhibit *Sm*DHODH (**Table 4**).

Table 4. Compounds tested in the initial screening against *Sm*DHODH. Their respective codes, as in the submitted manuscript (**Figure 9**), concentration tested and percent of activity.

Code	Concentration (µM)	% Activity	Code	Concentration (µM)	% Activity
1	500	6.1 ± 0.2	**6o**	250	1.80 ± 0.01
2	500	1.0 ± 0.5	**8**	50	63.1 ± 0.5
3	500	4.4 ± 0.4	**9**	250	31 ± 1
6a	500	1.64 ± 0.05	**10**	500	9.7 ± 0.3
6b	250	3.8 ± 0.2	**11**	250	46 ± 1
6c	250	2.0 ± 0.6	**12**	500	54 ± 1
6d	500	6 ± 2	**13**	250	0.0 ± 0.2
6e	50	1.5 ± 0.4	**14**	62.5	2.9 ± 0.2
6f	50	1.8 ± 0.2	**15**	500	7.9 ± 0.2
6g	50	2.6 ± 0.1	**16**	500	4.0 ± 0.2
6h	50	3.5 ± 0.2	**17**	125	2 ± 1
6i	50	1.8 ± 0.6	**18**	500	68.1 ± 0.8
6j	50	1.4 ± 0.7	**19**	500	-1.3 ± 0.8
6k	50	1.2 ± 0.5	**20**	500	3.6 ± 0.3
6l	50	3.3 ± 0.3	**21**	500	20.6 ± 0.5
6m	50	2.7 ± 0.2	**22**	500	94 ± 1
6n	50	1.9 ± 0.2	**23**	500	86 ± 3

Compounds that reduced *Sm*DHODH activity by more than 60% in single concentration assays had their IC_{50} values (**Table 5**) determined against SmDHODH and its human homologue enzyme HsDHODH. All IC_{50} graphs are present as appendices (**Figures S2 to S50**).

Table 5. IC_{50} values and selectivity index obtained for both *Sm*DHODH and *Hs*DHODH.

Compound	*Sm*DHODH IC_{50} (nM)	*Hs*DHODH IC_{50} (nM)	Selectivity Index
1	50000 ± 2000	312 ± 27	-
2	432 ± 21	2700 ± 200	6.25 (Sm)
3	20000 ± 1000	37 ± 2	-
6a	2100 ± 200	2600 ± 500	-
6b	4700 ± 400	n.d.	-
6c	78 ± 9	808 ± 62	10.36 (Sm)
6d	9900 ± 600	10000 ± 1000	-
6e	111 ± 6	108 ± 8	-
6f	1000 ± 40	330 ± 12	-
6g	2100 ± 100	1050 ± 40	-
6h	5500 ± 100	3600 ± 100	-
6i	129 ± 10	911 ± 34	7.06 (Sm)
6j	185 ± 10	541 ± 24	2.92 (Sm)
6k	19 ± 2	123 ± 11	6.47 (Sm)
6l	711 ± 23	6800 ± 100	9.56 (Sm)
6m	227 ± 24	4600 ± 100	20.26 (Sm)

6n	436 ± 19	1800 ± 100	4.13 (Sm)
6o	375 ± 27	n.d.	-
9	79000 ± 14000	n.p.	-
10	29000 ± 3000	n.d.	-
13	19 ± 2	100 ± 7	5.26 (Sm)
14	1200 ± 100	10000 ± 900	8.33 (Sm)
15	31400 ± 900	7900 ± 900	-
16	2500 ± 100	n.d.	-
17	23 ± 4	709 ± 38	30.83 (Sm)
19	8800 ± 400	34000 ± 2000	3.86 (Sm)
20	57000 ± 2000	n.p.	–
21	768000 ± 679000	n.p.	–

n.d. – not detected at highest tested concentration; n.p. – not performed; selectivity index calculated when above 2

Among the tested compounds, 2, 6c, 6e, 6i, 6j, 6k, 6l, 6m, 6n, 6o, 13, and 17 showed nanomolar IC_{50} values against *Sm*DHODH. Both atovaquone 2 (IC_{50} = 432 ± 21 nM) and 6m (IC_{50} = 227 ± 24 nM) have aliphatic rings (cyclohexane and piperazine ring, respectively) directly attached to the quinoidal moiety and a terminal p-Cl substituted aromatic ring. As both compounds have similar steric features, it seems that electronic properties are responsible for the potency gain (approx. 2X) of 6m. However, lack of substituents in the aromatic ring (6l IC_{50}= 711 ± 23 nM) seems to be detrimental to potency. This result suggests that steric complementarity towards *Sm*DHODH is best with chlorine at para position (compare 6m *vs* 6n or 6m *vs* 6o). In order to further investigate the steric requirements for *Sm*DHODH inhibition, 2-hydroxi-3-amine-naphtoquinone derivatives 6a-k were evaluated. Although nitrogen spacing group leads to a 10-fold reduction in potency (6a IC_{50} = 2100 ± 200 nM), chlorine substitution at *ortho* (6c IC_{50} =

78 ± 9 nM) or *meta* (6i IC_{50} = 129 ± 10 nM) afford simplified, yet more potent compounds than 6m. In fact, the additive effect of these substituents leads to the most potent compound of this series (6k IC_{50} = 19 ± 2 nM). Interestingly, electron donor groups at para position is detrimental to potency, (6b IC_{50} = 4700 ± 400 nM) whereas electron withdrawing groups retain potency (6j IC_{50} = 1850 ± 10 nM). This result also supports that electronic features play a key role towards *Sm*DHODH inhibition. It is possible that the increased potency is due to activation of quinoidal ring by nitrogen electron donating effect, however the potency drops due to the substitution of quinoidal OH by Cl (8 *Sm*DHODH activity = 63.1 ± 0.5 % at 50 µM vs 6c IC_{50} = 78 ± 9 nM) suggests that other features also play an important role in *Sm*DHODH inhibition. Moreover, the presence of non-substituted OH in position 3 affords only weak *Sm*DHODH inhibitors. For instance, lawsone 10, a natural hydroxynaphthoquinone, shows IC_{50} = 29 ± 3 µM. This result suggests that the inhibitory activity reported herein is not compatible with irreversible mechanism of action due to the Michael addition to the quinoidal ring.

It also reasonable to assume that potency change might be related to the improved hydrophobic interaction of the aromatic ring, instead of piperazine ring, within *Sm*DHODH binding site. In order to evaluate this hypothesis, series D compounds were assayed against *Sm*DHODH. In case quinoidal OH is protected, or not available for hydrogen bonding, only micromolar inhibition of *Sm*DHODH is achieved (15 IC_{50} = 31400 ± 900 nM and 16 IC_{50} = 2500 ± 100 nM). On the other hand, both 13 (IC_{50} = 19 ± 2 nM) and 17 (IC_{50} = 23 ± 4 nM) are as potent *Sm*DHODH inhibitors as 6k (IC_{50} = 19 ± 2 nM).

Lapachol derivatives, with constrained side-chain, show reduced potency against *Sm*DHODH (14 IC_{50} = 1200 ± 100 nM and 18 *Sm*DHODH activity = 68.1 ± 0.8 % at 500 µM). Although it is tempting to assume that rigid analogs fail to adopt the bioactive conformation, it is also possible that electronic features are responsible for this potency decrease: the double bond in the side chain of Isolapachol 14 is conjugated to the quinoidal ring, whereas the double bond of Lapachol 13 is not. Therefore, both 13 and 17 have more electron deficient side chains than 14. Furthermore, the hydrophobicity of these side-chains is similar to the one found in ubiquinone, CoQ_{10} (Class 2 DHODHs physiological substrate).

Whenever the macromolecular target is also present at the host, drug development efforts must balance potency and selectivity, if a high quality lead compound is wanted. Accordingly, all compounds with IC_{50} values lower than 50 µM, in previous assays, had their inhibition profile against *Hs*DHODH investigated. The IC_{50} values (**Table 5**) against the human enzyme show that 2-hydroxy-3-amine-naphtoquinone derivatives 6f and 6g present low selectivity for the human enzyme, whereas 6a, 6b, 6d, 6e, 6h and 6o inhibit both parasite and human DHODH likewise. The most potent compound against *Sm*DHODH (6k SI = 6.47) is less selective than either 6c (SI = 10.36) or 6m (SI = 20.26). In fact, 6c is approximately 66% more selective and 5 fold more potent than atovaquone 2. Then, this compound can be considered the most promising compound from this series.

Among lapachol derivatives (group D), only tosylated lapachol 15 shows a minor selectivity index towards *Hs*DHODH, whereas reduced lapachol 17 presented the largest SI (30.83). The comparison of 13 and 17 IC_{50} values for *Hs*DHODH (100 ± 7 nM vs 709 ± 38 nM, respectively) shows that one double bond is responsible for approximately 6-fold selectivity increase. As none of these compounds have a side chain conjugated to the quinoidal ring, it is reasonable to conclude that side chain flexibility is crucial to the selective inhibition of *Sm*DHODH. This hypothesis is in good agreement with 6m higher selectivity than 6c: Intra-molecular hydrogen-bonding in 6c might restrain its conformational space, whereas 6m would explore the torsional space around the single bond that links the piperazine ring (chair conformation) to the quinoidal ring. Then, *para* substituted phenyl ring would be positioned in dissimilar pockets in human or parasite DHODH, thus providing a higher selectivity profile. Considering all stated above, Compound 17 was considered the best compound for *Sm*DHODH selective inhibition.

3D pharmacophore models were also build (performed by Prof. Marcelo Castilho, data not shown) in order to identify pharmacophore requirements that are essential to *Sm*DHODH inhibition and selectivity. The pharmacophore model also helps to explain the fact that benzoquinones are weak *Sm*DHODH inhibitors and that the naphthoquinone ring is required for potency.

2.4.6 Atovaquone derivatives inhibition mechanism studies

Despite the chemical similarities among *Sm*DHODH inhibitors described so far, there is no proof, up to this point, that all of them have similar binding profile towards their macromolecular target. In order to further investigate this matter, one compound from each group (A – 2, B – 6c, C – 10, D – 17 and E – 19, **Figure 9**) had its mode of inhibition determined. Double reciprocal plot at increasing inhibitor concentrations were drawn (Appendices, **Figures S51 to S56**). Compound 19 shows that substrate affinity towards *Sm*DHODH decreases, whereas the slope of the curve changes This result suggests a competitive inhibition mechanism, which is expected once its structure is very similar to the substrate ubiquinone (a benzoquinone). On the other hand, compounds 6c, 17 and 10 show that substrate affinity towards *Sm*DHODH remains unchanged, whereas the slope of the curve increases. These results suggest a non-competitive inhibition mechanism of inhibition. Compound 2 result shows a mixed-type inhibition which is a mixture of both competitive and non-competitive events, where both slope of the curve and substrate affinity changes with increasing inhibitor concentrations. This mixed-type inhibition mechanism could be explained as a result of the flexibility of the two N-terminal helices, as previously reported, which could result in different binding modes for the inhibitor.

Aiming to validate the proposed experiment, compound 17 (best compound for SmDHODH selective inhibition) was chosen and tested against the human enzyme; it presented the same mechanism of inhibition as for the parasite enzyme, suggesting that despite differences between the DHODH from both human and parasite species, the binding mode must be similar. **Table 6** summarizes all the tested inhibitors and their respective inhibition mechanisms.

Table 6. Inhibition mechanism data.

Species + Inhibitor	Type of Inhibition
Schistosoma + **2**	mixed-type
Schistosoma + **6c**	non-competitive
Schistosoma + **10**	non-competitive
Schistosoma + **17**	non-competitive
Schistosoma + **19**	competitive
Human + **17**	non-competitive

Those results raise questions regarding the non-competitive inhibition mechanism observed for the majority of the compounds tested. The first hypothesis is related to binding site differences: when looking at the tridimensional structures available for other class 2 DHODHs (**Figure 14**), it is possible to observe that the tunnel created behind the two N-terminal helices, in which CoQ_0 binds, is deep. Smaller compounds, such as compound 19 (benzoquinone) could be able to go through all the way to the end of the tunnel, and sit near the FMN prosthetic group, while the other tested compounds (naphthoquinones, **Figure 9**) would interact in the entrance of the tunnel, allowing substrate binding.

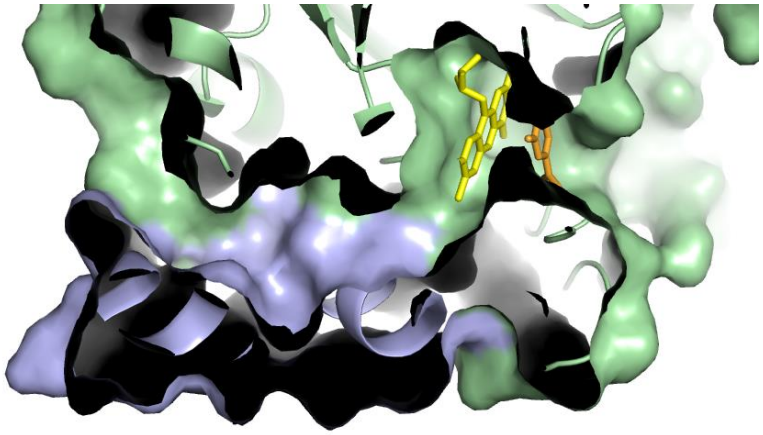

Figure 14. Cartoon and surface representation of partial *Rn*DHODH (PDBID: 1UUM) showing the deep tunnel behind the N-terminal helices (light blue) known to be the second substrate and inhibitors binding-site. Alpha-beta barrel, FMN and orotate is represented in pale green, yellow and orange, respectively.

The second hypothesis was the possibility of the existence of a different binding site for this class of compounds, such as an allosteric inhibitor binding site in the protein. The tridimensional structure in complex with these compounds, kinetic studies testing different quinones, as well as evaluating different constructs (deletion and mutations of residues) are strategies that can be used to evaluate the results found.

2.4.7 ThermoFMN: A thermostability assay based on differential scanning fluorimetry (DSF)

Thermostability assays were performed by using differential scanning fluorimetry technique (DSF). In this assay, the protein unfolding process is monitored as a function of increasing in temperature. In general, the SYPRO® Orange dye is used as a probe, due to its ability to activate fluorescence when binding to hydrophobic patches exposed as a result of conformational changes.[99-101] However, once detergent (Thesit®) is present in the purification procedure, the traditional methodology is infeasible. An alternative methodology, called ThermoFMN,[102] was then applied. In this technique, DSF is performed in the absence of dye, exploring the prosthetic group FMN from flavoproteins as the fluorescence marker. The unfolding process can then be followed by monitoring differences in fluorescence intensity. The fluorescence intensity is plotted as a function of temperature, which usually describe a sigmoidal curve. The curve inflexion point allows the determination of the protein melting temperature, T_m. This technique is a method with broad applications, both for scanning conditions that stabilize proteins as well as, especially in this case, searching for ligands.

Considering the application, simplicity and low-consuming sample features of the ThermoFMN technique, we decided to investigate the feasibility of using this technique for screening larger chemical libraries. The twenty-eight compounds that had their IC_{50} previously determined were selected and assayed, using three concentrations (500, 250 and 50 µM). **Table 7** shows all Tm shifts for the three concentrations tested for each compound against the enzyme *Sm*DHODH. It was possible to identify ligands capable of

stabilizing (compounds 1, 3, 6c, 6k, 13, 17) and destabilizing (compounds 15, 19, 20, 21) the enzyme at the concentration of 500 µM. The other compounds showed ΔT_m not greater than ± 2.00.

A similar experiment was performed against *Sm*DHODHΔloop and **Table 8** shows Tm shifts for the three concentrations tested for each compound. Interestingly, similar positive thermal shifts were observed for compounds 6c, 6k, 13 and 17, which are the compounds that presents the best IC_{50} values against *Sm*DHODH. On the other hand, new significant positive ΔT_ms were observed for compounds 6d and 14, while compounds 19, 20 and 21 showed no longer negative ΔT_ms.

At first, analysis of our thermal stability studies suggested a correlation between IC_{50} and thermal shift: The compounds that stabilized the enzyme displayed lower IC_{50} values (most in nM range, with the exception of compounds 1 and 3) than the ones with destabilizing values, negative thermal shift, which display IC_{50} in µM range. However, a more and careful analysis of both kinetics and DSF results suggest a correlation between thermal stability and mechanism of inhibition. Since ThermoFMN uses FMN as a probe, the negative thermal shift, observed for the small compounds that display competitive mechanism of inhibition (compound 19 and possibly 20 and 21), could be explained as a result of a direct talk between substrate/compound and FMN. We hypothesize whether this negative thermal shift could be directly related to the ping-pong mechanism of catalysis adopted by class 2 DHODHs (**Figure 3**). According to this model, dihydroorotate is oxidized concomitant to FMN reduction, and the product of catalysis, orotate, has to be released before the second substrate, ubiquinone, recycles FMN for new cycles of catalysis. According to previous studies performed by our group for class 1A DHODHs,[24] we know that both reduction and reoxidizing steps have to be orchestrated and depend on the control of opening and closing of the active site loop. Thus, considering that negative thermal shift is directly associated to the release of FMN, it is tempting to speculate whether the direct binding of those small compounds to the very end of binding site channel, in direct contact with FMN, could mimic the interaction of quinone with FMN, favoring the opening of the active site loop and inducing the release of orotate. In the case of our ligands, binding near the FMN could induce the opening of the active site loop and,

under increase of temperature, could favor the release of the prosthetic group. Similar thermofluor experiments, conduct for the construct *Sm*DHODHΔloop, showed no significant change in thermal stability when testing the same group of compounds, suggesting that the removal of this loop may interfere either with the direct binding of the substrate or the cross-talk between reduction and reoxidizing steps, or both.

Compounds that have been identified as non-competitive inhibitors (compounds 6c, 10, and 17) are the ones that display higher thermal shift (**Table 7**). Non-competitive inhibitors are expected to bind in a different site rather than Q_0 binding site. Due to their chemical properties, the compounds are expected to bind to the hydrophobic patch created by the N-terminal helical domain, where all class 2 inhibitors are found. However, probably due to their inability to reach the end of the channel and bind near the FMN, they may stabilize the protein by holding still the helical domain and/or even interfere with the cross talk between dihydroorotate and quinone binding sites, locking the active site loop in a closed conformation.

Atovaquone, compound 2, displayed a mixed-type mechanism of inhibition and do not induce significant thermal shift for either constructs (**Table 7** and **Table 8**). The contribution of competitive (negative thermal shift) and non-competitive (positive thermal shift) mechanisms of inhibition for thermal stability can cancel each other out and no significant thermal shift becomes evident.

Table 7. ΔTm shifts for the tested compounds at three different concentrations (500, 250 and 50 µM) against *Sm*DHODH. Green cells are ≥ 2 °C from reference and red cells are ≤ -2 °C from reference (54.73 °C).

Compound	1	2	3	6a	6b	6c	6d
500 µM	2.74	-0.51	2.66	-1.46	-0.05	3.22	1.26
250 µM	2.46	-0.23	2.63	-0.68	-0.23	3.05	1.92
50 µM	1.52	-0.04	1.70	0.05	-0.13	1.87	1.45
Compound	**6e**	**6f**	**6g**	**6h**	**6i**	**6j**	**6k**
500 µM	1.81	1.80	0.19	-1.64	1.72	1.60	4.74
250 µM	1.91	1.95	0.52	-0.81	1.68	1.53	4.02
50 µM	1.91	1.52	0.62	0.16	1.27	0.79	2.31
Compound	**6l**	**6m**	**6n**	**6o**	**9**	**10**	**13**
500 µM	0.54	0.83	0.52	1.40	-0.32	0.52	3.99
250 µM	0.21	0.84	0.21	1.16	-0.14	0.44	3.59
50 µM	0.03	0.76	0.01	0.58	0.01	0.26	2.34
Compound	**14**	**15**	**16**	**17**	**19**	**20**	**21**
500 µM	-0.20	-4.48	-0.93	12.05	-4.60	-2.00	-7.35
250 µM	0.29	-3.32	-0.55	8.16	-3.28	-2.07	-5.55
50 µM	0.39	-0.60	0.12	3.78	-5.89	-5.35	-5.05

Table 8. ΔTm shifts for the tested compounds at three different concentrations (500, 250 and 50 µM) against *Sm*DHODHΔloop. Green cells are ≥ 2 °C from reference and red cells are ≤ -2 °C from reference (50.40 °C).

Compound	1	2	3	6a	6b	6c	6d
500 µM	-0.14	0.70	0.54	-0.11	-0.33	2.91	5.88
250 µM	-0.23	0.54	0.33	-0.26	-0.45	2.44	2.32
50 µM	-0.14	0.33	0.03	-0.23	-0.11	0.99	0.23
Compound	**6e**	**6f**	**6g**	**6h**	**6i**	**6j**	**6k**
500 µM	1.64	1.88	1.00	0.25	1.29	1.25	3.83
250 µM	1.27	1.75	0.85	0.12	1.18	1.08	3.46
50 µM	0.47	0.82	0.32	-0.04	0.43	0.68	1.76
Compound	**6l**	**6m**	**6n**	**6o**	**9**	**10**	**13**
500 µM	0.37	0.13	-0.25	0.07	0.04	-0.05	5.09
250 µM	0.12	0.19	-0.20	-0.04	0.03	-0.19	4.18
50 µM	-0.15	-0.07	-0.19	-0.16	-0.07	-0.16	2.90
Compound	**14**	**15**	**16**	**17**	**19**	**20**	**21**
500 µM	4.07	0.76	-0.08	7.82	-0.19	-0.14	-0.40
250 µM	2.79	-0.26	-0.23	2.71	-0.04	-0.23	-0.45
50 µM	1.41	-0.14	-0.09	1.50	0.90	-0.24	-0.18

In order to fully characterized the enzymes in study, the same experiment was also performed against *Hs*DHODH and **Table 9** shows all Tm shifts for the three concentrations tested for each compound.

Table 9. ΔTm shifts for the tested compounds at three different concentrations (500, 250 and 50 µM) against *Hs*DHODH. Green cells are ≥ 2 °C from reference and red cells are ≤ -2 °C from reference (53.66 °C).

Compound	1	2	3	6a	6b	6c	6d
500 µM	10.94	4.50	20.82	3.87	1.45	10.52	5.95
250 µM	9.47	4.26	19.75	2.89	0.88	9.76	3.50
50 µM	3.82	3.73	17.08	0.91	0.21	6.56	1.08
Compound	**6e**	**6f**	**6g**	**6h**	**6i**	**6j**	**6k**
500 µM	10.51	9.14	7.19	5.95	9.37	8.98	12.27
250 µM	10.48	8.51	7.31	5.09	8.96	8.58	12.06
50 µM	7.97	5.64	4.31	2.49	6.19	6.31	9.06
Compound	**6l**	**6m**	**6n**	**6o**	**9**	**10**	**13**
500 µM	3.05	2.51	1.60	1.34	0.59	0.76	14.16
250 µM	2.62	2.55	1.25	0.91	0.30	0.35	13.19
50 µM	1.05	1.40	0.41	-0.01	0.01	0.03	10.41
Compound	**14**	**15**	**16**	**17**	**19**	**20**	**21**
500 µM	11.95	4.53	-0.21	10.56	-0.22	-0.25	-0.13
250 µM	10.62	3.30	-0.13	9.17	-0.14	-0.21	-0.02
50 µM	7.22	0.82	-0.10	5.98	-0.08	-0.10	0.03

The results obtained for *Hs*DHODH showed that most compounds display positive ΔT_ms, and no significant negative ΔT_m was observed. Since, absolute thermal shift values can be used to compare potency and binding mechanism of compounds among different proteins, our analysis was restricted to the effects of all tested compounds against the human enzyme. It is possible to observe that compounds which presented positive thermal shift for *Hs*DHODH, such as 6c, 6k, 13 and 17, display IC_{50} in the low nanomolar range. Important to highlight that compounds 1 and 3 (known *Hs*DHODH potent inhibitors) also presented a high positive ΔT_m (10.94 and 20.82 °C, respectively), which had already been observed before by our group.[102]

It was also observed that compounds that do not inhibit the enzyme (compounds 6b, 6o, 9, 10, 16, 20 and 21 at **Table 5**), did not display a thermal shift higher than 2 °C

either, suggesting that thermofluor can indeed be used as a tool to search for ligands/inhibitors of *Hs*DHODH.

2.4.8 Antimalarial drugs library from Broad Institute

The Broad Institute of MIT and Harvard has been working in a partnership with MMV (Medicine for Malaria Venture) in order to develop new compounds to treat malaria. Through a collaboration between our research group and Prof. Stuart Schreiber from Harvard Medical School, a library containing 151 compounds developed at Broad Institute was sent to us to evaluate its impact on *Sm*DHODH enzyme. Activity measurements were carried by the indirect assay, through monitoring DCIP reduction at 610 nm. Initial screening at single dose concentration (**Table S2**) was performed at 10 µM. This low concentration was used in order to select compounds that could inhibit *Sm*DHODH with lower IC_{50} values.

Compounds that reduced *Sm*DHODH activity by more than 80% in single concentration assays (20 compounds) had their IC_{50} values (**Table 10**) calculated by non-linear regression fit. All IC_{50} graphs are present in appendices (**Figures S57 to S76**). By our request, the compounds from this library are sent to us for a blind test. That means that no chemical structure for the compounds are available. Having that said, it is impossible at this point to make structural-activity relationships as discussed for the atovaquone and derivatives library.

Table 10. IC_{50} values obtained for SmDHODH against the antimalarial drugs library provided by the Broad Institute.

Compound	*Sm*DHODH IC_{50} (µM)	*Hs*DHODH IC_{50}
BRD-K33197954-001-01-4	0.78 ± 0.03	n.p.
BRD-K02955208-001-01-6	0.7 ± 0.1	n.p.
BRD-K27505055-001-01-4	0.86 ± 0.03	n.p.
BRD-K32075950-001-01-7	0.70 ± 0.05	n.p.
BRD-K31857539-001-04-3	0.71 ± 0.03	n.p.
BRD-K09681131-001-01-3	**0.46 ± 0.03**	**n.d.**
BRD-K31655302-001-01-2	0.78 ± 0.01	n.p.
BRD-K18887044-001-01-1	1.18 ± 0.08	n.p.
BRD-K37218351-001-01-3	0.86 ± 0.04	n.p.
BRD-K84953102-001-01-9	**0.26 ± 0.01**	**n.d.**
BRD-K22505729-001-01-5	0.70 ± 0.07	n.p.
BRD-K94234276-001-01-2	0.61 ± 0.02	n.p.
BRD-K31021301-001-01-8	1.3 ± 0.1	n.p.
BRD-K88402291-001-01-4	0.76 ± 0.08	n.p.
BRD-K60263288-001-01-7	0.59 ± 0.07	n.p.
BRD-K15879709-001-01-7	**0.077 ± 0.005**	**n.d**.
BRD-K45235328-001-01-7	1.3 ± 0.1	n.p.
BRD-K99869451-001-01-7	1.09 ± 0.02	n.p.
BRD-K08187511-001-01-2	0.95 ± 0.04	n.p.
BRD-K86496683-001-01-4	1.10 ± 0.06	n.p.

n.d. – not detected at highest tested concentration; n.p. – not performed

Three compounds presented IC_{50} lower than 500 nM: BRD-K09681131-001-01-3, BRD-K84953102-001-01-9 and BRD-K15879709-001-01-7, with 460 ± 30, 260 ± 10 and 77 ± 5 nM, respectively. These results are extremely good and surprising, considering that this is a wide library, with different kinds of molecules and no design of new molecules have been made whatsoever.

After identifying these compounds with good inhibitory potency, we also decided to perform a cross-validation experiment against the human enzyme. Unexpectedly, no inhibition has been observed for the compounds at the concentration of 10 µM. This selectivity has not been observed before for any compound against DHODHs in literature and can be used in future tests or yet to the design of new and even better inhibitors.

Co-crystal structures bound to these inhibitors can provide valuable information to elucidate ligand-receptor mechanism of interaction. Work towards this goal is currently in progress.

2.4.9 Crystallization

Crystals were obtained for *Sm*DHODHΔloop using the following conditions: Sodium citrate pH 5.5, 18% PEG 3350; and 31 – Sodium Acetate pH 4.0, 10% PEG 4000 (PegRx 1, solution 29). The final protein solution concentration was 20 mg/mL; together with 2 mM DHO, as substrate, 1 mM Compound 13 as inhibitor and LDAO, as detergent. In **Figure 15**, we can observe pictures from the obtained crystals. Yellow crystals, due to the presence of the prosthetic FMN group, have been recently obtained. Data collection at Soleil Synchrotron Source is planned for December.

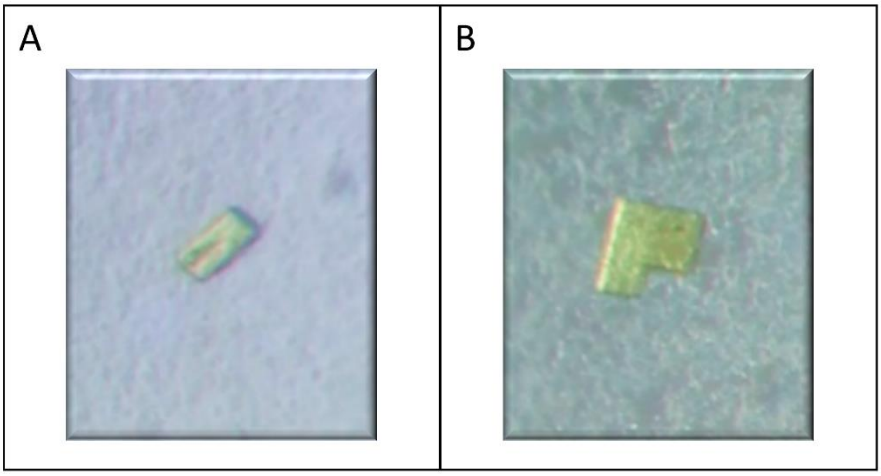

Figure 15. *Sm*DHODHΔloop crystals obtained in A) PegRx1 (29): Sodium citrate pH 5.5, 18% PEG 3350; and B) PegRx1 (31): Sodium Acetate pH 4.0, 10% PEG 4000.

Data has not been collected/processed yet for the obtained crystals, since they have crystallized recently. Data collection in both synchrotrons (LNLS in Campinas and SOLEIL in France) are planned. The data collected from these crystals can provide important information, especially how compound 13 is bound to *Sm*DHODH.

2.4.10 In vitro schistosomicidal activity

Firstly, in an attempt to identify compounds that presents schistosomicidal activity, we selected 11 compounds that presented the best inhibitory potential and/or higher selectivity against the enzyme *Sm*DHODH: 6c, 6i, 6j, 6k, 6l, 6m, 6n, 6o, 13, 14 and 17. In this first preliminary experiment, we tested a single dose concentration for the selected compounds at 5 µM final concentration in the culture. The results can be found at **Table S1**. As a global result, we observed that all compounds tested were able to affect the parasites tegument. Most of the compounds affected more the male worms than the female. However, apparently, the concentration used was insufficient to kill worms, even in the positive control group (PZQ) and no clear distinguishing between the compounds

could be observed, with exception to compound 17, which was capable of affecting the teguments from all female and male worms, similarly what was observed for PZQ.

Considering that, we decided to continue the study by selecting the top 4 compounds (either by selectivity and potency) identified in the enzymatic inhibition assays (i.e. compounds 6c, 6i, 6m and 17). Atovaquone (compound 2) was not present in the preliminary assays, but considering it is already a market drug and all the compounds were its precursors or derivatives, we also decided to include it in this experiment. Three different concentrations were used: 500, 50 and 5 µM. Up to this moment, only the compounds 2, 6i and 17 have been tested, however compounds 6c and 6m are currently under test.

The effect on the mortality rate of both male and female adult worms were analyzed with respect to the concentration and incubation time as observed at **Table 11** below. The worms remained viable in the negative control group until the end of the incubation period (96 h), whereas PZQ 50 µM, the positive control, caused the death of all the parasites within 24 h. Compound 2 was capable of killing 66% of both male and female parasites at the concentration of 50 µM in 96 h, while compounds 6i and 17 were capable of killing parasites only at the concentration of 500 µM. Between compounds 6i and 17, 6i seems to present a better mortality rate, once it was capable of killing parasites in 24 h, while compound 17 mortality rate appeared after 48 h. Difference was also observed in the mortality rate between male and female parasites, especially for compound 17. Subsequently, the effect on the motor activity of the worms was examined, and a dose-dependent reduction of activity was observed for all compounds.

In addition to the mortality rate and effect on the motor activity of adult *S. mansoni*, the results highlighted the effect on the parasite's tegument. The alterations in the tegument occurred in a dose-dependent manner, and were more evident in male than in female adults. This evidence has already been described for other compounds in literature.[103, 104] No tegumental variations in adult worms were perceived in the negative control group, while the 50 µM PZQ group presented tegumental alterations in all worms.

Table 11. *In vitro* effects of Compounds 2, 6i and 17 against 49-day-old adult *Schistosoma mansoni*.

Group	Incubation period (h)	Sex	Dead worms (%)[a]	Motor activity (%)[a]		Worms with tegumental alterations (%)[a]	
				Normal	Altered	Partial	Extensive
Control[b]	24	Male	0	100	0	0	0
		Female	0	100	0	0	0
	48	Male	0	100	0	0	0
		Female	0	100	0	0	0
	72	Male	0	100	0	0	0
		Female	0	100	0	0	0
	96	Male	0	100	0	0	0
		Female	0	100	0	0	0
PZQ[c]	24	Male	100	0	0	0	100
		Female	100	0	0	0	100
	48	Male	100	0	0	0	100
		Female	100	0	0	0	100
	72	Male	100	0	0	0	100
		Female	100	0	0	0	100
	96	Male	100	0	0	0	100
		Female	100	0	0	0	100
Compound 2							
50 µM	24	Male	17	17	66	17	50
		Female	0	17	83	17	0
	48	Male	17	17	66	50	50
		Female	17	0	83	33	66
	72	Male	17	0	83	0	100
		Female	66	0	33	0	100
	96	Male	66	0	33	0	100
		Female	66	0	33	0	100
Compound 6i							
5 µM	24	Male	0	100	0	0	0
		Female	0	83	17	0	0
	48	Male	0	100	0	17	0
		Female	0	100	0	0	0
	72	Male	0	100	0	17	0
		Female	0	100	0	0	0
	96	Male	0	100	0	17	0
		Female	0	100	0	0	0
50 µM	24	Male	0	66	33	17	50
		Female	0	83	17	0	17
	48	Male	0	66	33	33	50
		Female	0	83	17	0	17
	72	Male	0	66	33	17	66
		Female	0	66	33	0	50
	96	Male	0	33	66	17	66
		Female	0	66	33	0	50
500 µM	24	Male	83	0	17	0	100
		Female	50	0	50	17	83
	48	Male	100	0	0	0	100
		Female	100	0	0	0	100
	72	Male	100	0	0	0	100

		Female	100	0	0	0	100
	96	Male	100	0	0	0	100
		Female	100	0	0	0	100
Compound 17							
5 µM	24	Male	0	100	0	0	17
		Female	0	100	0	0	0
	48	Male	0	83	17	17	0
		Female	0	83	17	17	0
	72	Male	0	83	17	17	0
		Female	0	83	17	17	0
	96	Male	0	83	17	17	33
		Female	0	83	17	0	17
50 µM	24	Male	0	66	33	33	17
		Female	0	83	17	0	0
	48	Male	0	83	17	0	33
		Female	0	83	17	0	0
	72	Male	0	66	33	17	33
		Female	0	66	33	33	0
	96	Male	0	50	50	33	33
		Female	0	50	50	50	0
500 µM	24	Male	0	0	100	17	50
		Female	0	0	100	0	33
	48	Male	50	0	50	0	100
		Female	0	0	100	0	100
	72	Male	50	0	50	0	100
		Female	17	0	83	0	100
	96	Male	100	0	0	0	100
		Female	100	0	0	0	100

The effects of the compounds on motor activity and tegumental alterations of adult *S. mansoni* were assessed qualitatively and were monitored under a microscope.

[a] Percentages relative to the 6 worms investigated.

[b] 0.5% DMSO.

[c] Tested at concentration of 50 µM.

The *in vitro* oviposition was also continually monitored during the experiment to assess the sexual fitness of treated worms (**Figure 16**). All the compounds tested at higher doses presented a significant inhibition of egg laying when compared to the control group (DMSO). Overall, compound 2 presents the lowest oviposition, once it shows similar number of eggs at 50 µM as the other compounds at 500 µM. This can be explained due to its higher mortality rate when compared to the other compounds at this same concentration.

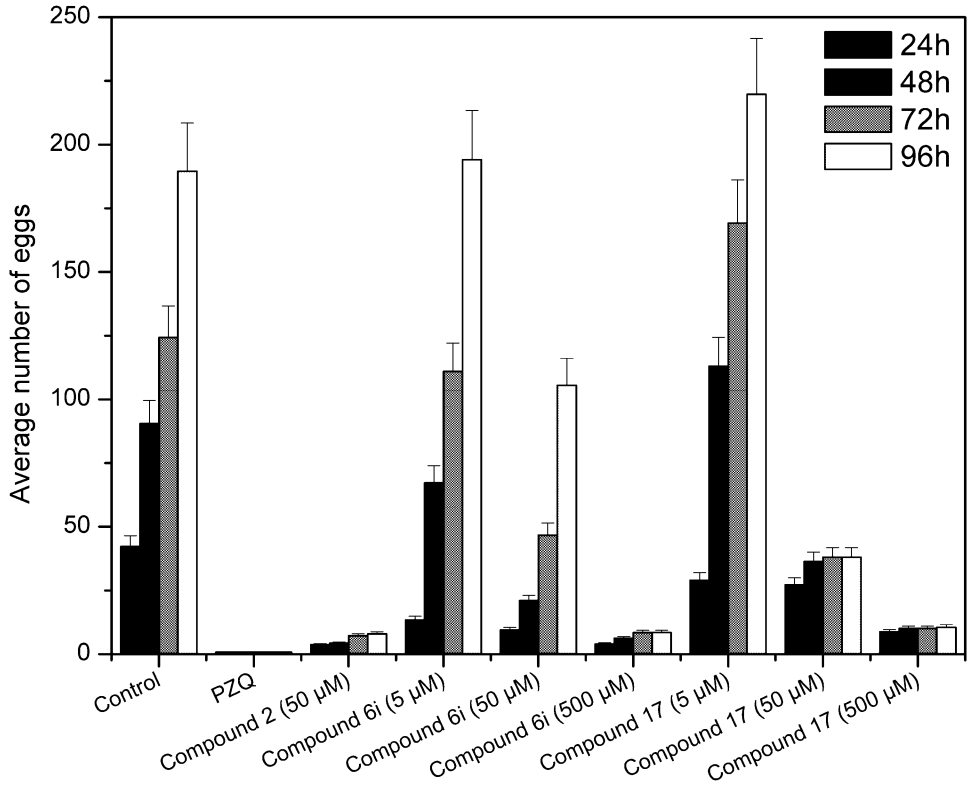

Figure 16. *In vitro* effect of Compounds 2, 6i and 17 on *Schistosoma mansoni* oviposition. Adult worm couples were incubated with Compounds 2, 6i and 17, and at the indicated time periods, the cumulative number of eggs per worm couple was assessed and scored using an inverted microscope. Values are means ± SD (bars) for six worm couples.

2.5 Conclusions

The present work describes the search for new selective inhibitors against *Sm*DHODH through the use of the strategy called drug repurposing as a strategy to develop new therapeutics to treat schistosomiasis. A total of 185 molecules and analogues that have been develop to treat malaria through the selective inhibition of the enzyme dihydroorotate dehydrogenase were tested and evaluated against *Sm*DHODH. Using both biochemical and biophysical assays with *Sm*DHODH, we were able to identify potent ligands/inhibitors. Several compounds displayed IC_{50} values in the low nanomolar range and some also showed highly selective against the parasite enzyme. Overall, compound 17 (2-hydroxy-3-isopentylnaphthalene-1,4-dione) was considered the best compound for *Sm*DHODH selective inhibition. Inhibition mechanism assays were used to address the understand the binding mode for the best compounds. In order to fully characterize the binding mechanism of those compounds, and to determine the structural basis for enzyme selectivity, structural studies for *Sm*DHODH are currently in progress.

CHAPTER 3. *PLASMODIUM FALCIPARUM* DHODH

3.1 Introduction

According to the WHO, 216 million cases of malaria occurred worldwide in 2016; these led to 445,000 deaths, mainly among children under 5 years of age in African countries. Malaria is found in both tropical and subtropical regions of the planet and in 91 countries (**Figure 17**). The increasing number of malaria cases that have occurred in first-world countries due to globalization have drawn attention to this disease, which, together with AIDS and tuberculosis, represents one of the most serious global public health problems.[105]

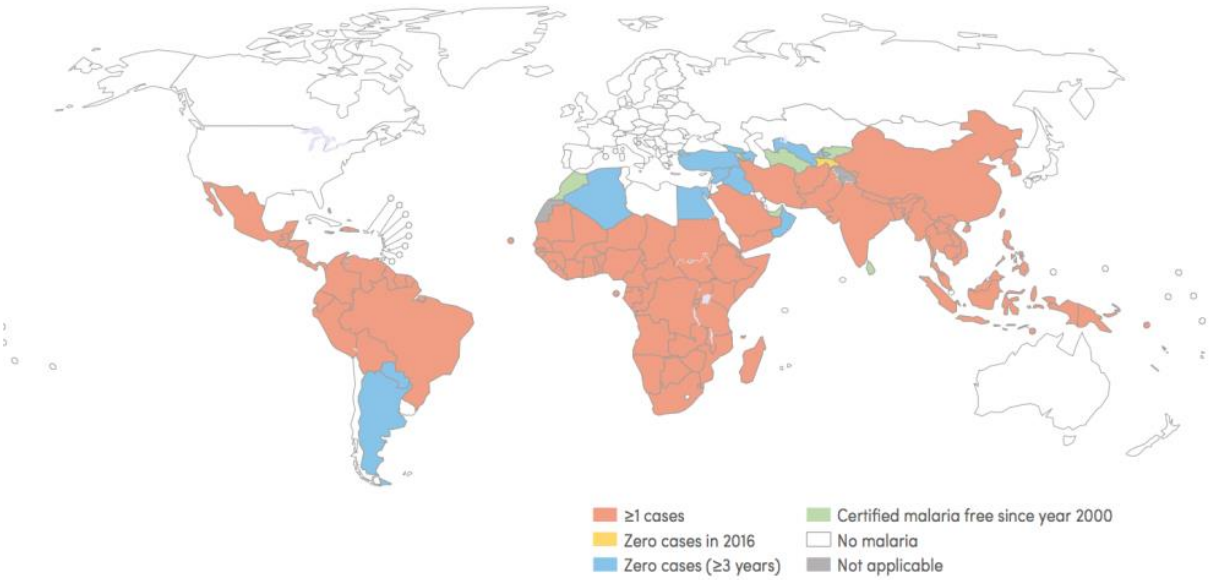

Figure 17. Countries and territories with indigenous cases in 2000 and their status by 2016 (extracted from WHO, 2017 [105]).

Malaria is caused by a protozoan of the genus *Plasmodium*, of which five species are infectious to humans: *Plasmodium falciparum*, which produces the most severe form of malaria; *Plasmodium vivax*, *Plasmodium malariae*, *Plasmodium knowlesi* and *Plasmodium ovale*, which were recently divided into *P. ovale wallikeri* and *P. ovale curtisi*.

These species are primarily transmitted by the bite of infected female mosquitoes of the genus *Anopheles*.[106-108]

Vector control, chemoprophylaxis and chemotherapy with antimalarial drugs are the primary methods used to eliminate or reduce the number of cases of malaria.[109] Most antimalarials operate via mechanisms that target one or two phases of the parasite's life cycle (**Figure 18**).[108] Several drugs are available, each of which acts at a different phase of the parasite's life cycle to prevent development of the parasite in the host.[110] However, the ability of *Plasmodium* species to evade the action of current drugs by developing resistance has become a great challenge to malaria treatment in recent decades, requiring the discovery of more available and effective drugs.[111-113]

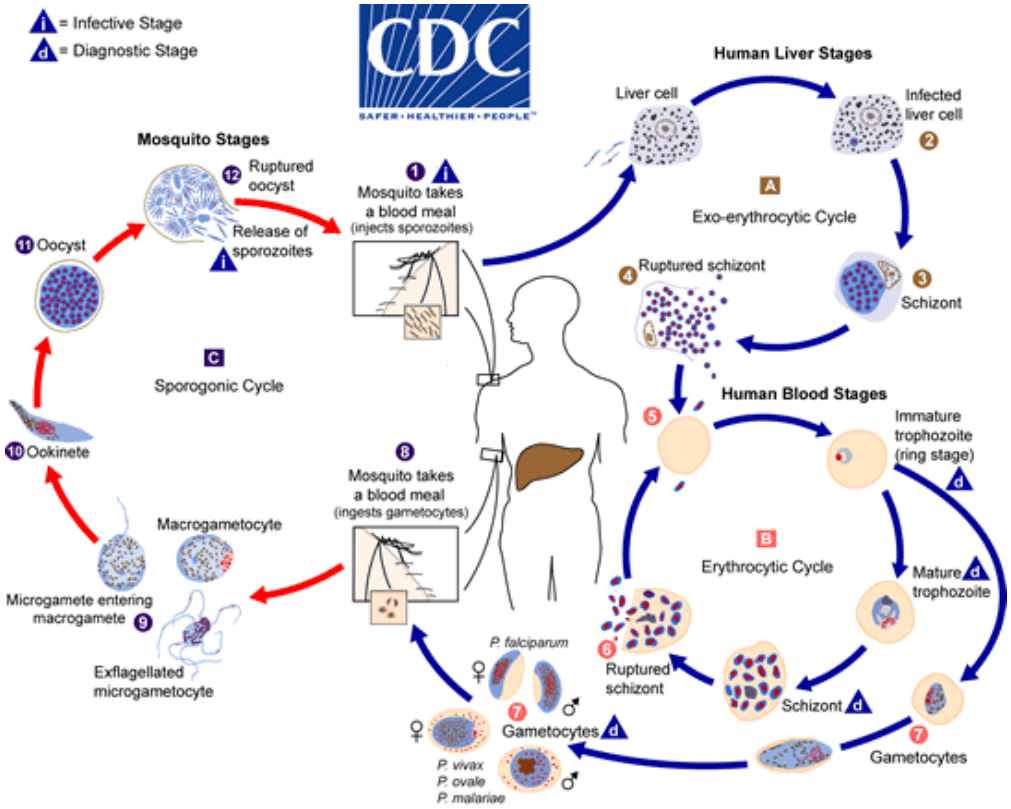

Figure 18. Malaria parasite life cycle involving two hosts. During a blood meal, a malaria-infected female *Anopheles* mosquito inoculates sporozoites into the human host (1). Sporozoites infect liver cells (2) and mature into schizonts, which rupture and release merozoites (4). After this initial replication in the liver (exo-erythrocytic schizogony, A), the parasites undergo asexual multiplication in the erythrocytes (erythrocytic schizogony, B). Merozoites infect red blood cells (5). The ring stage trophozoites mature into schizonts, which rupture releasing merozoites (5). Some parasites differentiate into sexual erythrocytic stages

(gametocytes) (7). Blood stage parasites are responsible for the clinical manifestations of the disease. The gametocytes, male (microgametocytes) and female (macrogametocytes), are ingested by an Anopheles mosquito during a blood meal (8). The parasites' multiplication in the mosquito is known as the sporogonic cycle (C). While in the mosquito's stomach, the microgametes penetrate the macrogametes generating zygotes (9). The zygotes in turn become motile and elongated (ookinetes) (10) which invade the midgut wall of the mosquito where they develop into oocysts (11). The oocysts grow, rupture, and release sporozoites (12), which make their way to the mosquito's salivary glands. Inoculation of the sporozoites (1) into a new human host perpetuates the malaria life cycle (extracted from CDC, 2018 [108])

The antimalarial drugs that are currently in use fall into the following classes[113-115]:

- Quinoline derivatives. Quinine, an alkaloid isolated from Cinchona bark, was the first compound used to treat malaria. Its use led to the development of synthetic derivatives such as chloroquine (CQ), amodiaquine, primaquine, mefloquine, pyronaridine and piperaquine. Cases of resistance to these drugs have also been reported.[113, 115] The quinolines are active against the erythrocytic forms of *P. falciparum* and *P. vivax*. CQ was originally the most effective drug and has been the first choice for antimalarial treatment for a long time, but abusive use has led to the emergence of CQ-resistant parasites, rendering this drug ineffective in many regions of the world.[115] If used against *P. vivax* and *P. ovale* hypnozoites, primaquine, which inhibits the formation of gametocytes, acts against the slowly developing hepatic forms of *P. vivax* infection that are responsible for relapses.[113]
- Antifolates. These compounds constitute a class of antimalarials that act as schizonticides in the blood and are divided into classes I and II:

Class I. Sulfadoxine, which belongs to the type I class of antifolate drugs, has a structure similar to that of p-aminobenzoic acid. Sulfadoxine interrupts the formation of dihydrofolic acid by inhibiting dihydropteroate synthase, which is necessary for the synthesis of nucleic acids.[116]

Class II. Cycloguanil and pyrimethamine belong to the type II class of antifolate drugs; they inhibit dihydrofolate (DHF) reductase in the parasite, thereby preventing the reduction of DHF to tetrahydrofolate, which is important in the synthesis of nucleic acids and amino acids. DHF reductase inhibitors are potent schizonticidal agents that act on

asexual forms of the parasite. The use of this class of drugs has been reduced due to the capacity of the parasites to develop resistance.[116]

- Artemisinin and its derivatives. Dihydroartemisinin, artemether, arteether and artesunate are known for their ability to rapidly reduce the number of parasites present. These drugs are poorly effective as monotherapies for treatment of malaria due to their low bioavailability and short half-life, and due to cases of resistance, their use is primarily indicated as part of artemisinin-based combination therapy.[105, 117] The endoperoxide bridge of these compounds can undergo reductive cleavage in the presence of ferrous ions from the heme group of hemoglobin, thus generating free radicals that alkylate or modify the proteins of the parasite and lead to its death.[110]
- An antimalarial drug that is used in combination with proguanil for the treatment of malaria is atovaquone. This hydroxyl-1,4-naphthoquinone derivative inhibits oocyst development in the mosquito and pre-erythrocytic development in the liver, interferes with cytochrome electron transport, and also presents low inhibition against the enzyme dihydroorotate dehydrogenase.

Among *P. falciparum* enzymes, *P. falciparum* dihydroorotate dehydrogenase has been identified as an important target in drug discovery. Interference with the activity of this enzyme inhibits *de novo* pyrimidine biosynthesis and consequently prevents malarial infection. *P. falciparum* DHODH (*Pf*DHODH) is a Class 2 DHODH enzyme that contains 569 amino acids (**Figure 6**).

Due to its importance as a drug target, *Pf*DHODH has already been successfully crystallized and had its structure determined 15 times, bound to different ligands. The first *Pf*DHODH structure was determined (2.4 Å) by Hurt et al. in 2006.[118] The *Pf*DHODH crystals complexed with A771726 (teriflunomide) and orotate were obtained by removal of the signal peptide and the transmembrane region and grown using the sitting-drop vapor-diffusion technique at 277 K with sulfate salt as the precipitant, ammonium acetate as a buffer and the detergent pentaethylene glycol monooctyl ether (C8E5) in the crystallization solution. In fact, the use of a detergent in both the purification and crystallization steps is considered obligatory for stabilization of the Class 2 DHODH N-terminal membrane-associated domain.

All of the other DHODHs whose structures were determined later were crystallized using the hanging-drop vapor-diffusion technique at 293 K, also in the presence of sulfate salt and ammonium acetate. The only exception was described by Ross et al. in 2014; those authors used lithium chloride and/or 2-(N-morpholino)ethanesulfonic acid (MES) associated with polyethylene glycol (PEG) 3350.[119] Other components used include PEG 4000, glycerol, dithiothreitol (DTT) and the detergent N,N-dimethyldodecylamine N-oxide, which was used in the purification protocol and/or during crystallization.[19, 21, 37, 53, 119-123]

The first crystal structure of *Pf*DHODH described by Hurt et al. was found to contain a missing or disordered region (residues 375–414) that is not present in Class 2 enzymes such as those of humans or *Schistosoma* species.[118] In fact, removal of a 30-residue-long loop (residues 384–413, shown in **Figure 6**) was found to be necessary to obtain reproducible diffraction-quality crystals.[120] Steady-state kinetic analysis of the construct lacking amino acid residues 384–413 (*Pf*DHODHΔloop) demonstrated that the catalytic efficiency and inhibitor-binding properties of the loop free enzyme were similar to those of the wild-type enzyme.[120] It is worth mentioning that all *Pf*DHODH crystal structures available in the PDB have been solved in the presence of both orotate and potent Class 2 DHODH inhibitors.

The studies described next shows the expression, purification and cloning of the enzymes *Pf*DHODH and *Pf*DHODHΔloop, as well as the search for ligands, as a first step to evaluate the potential of the selective inhibition of the enzyme *Pf*DHODH. Inhibitors identified had their mode of action determined. Crystallization and crystallographic studies were also performed, for the first time in our lab, which can allow the study of binding and design of new candidate molecules. The study described in this Chapter can be helpful, in the future, as a therapeutic strategy in the fight against malaria.

3.2 Objectives

The general goal of this work was to evaluate the potential of compounds as selective inhibitors of the enzyme dihydroorotate dehydrogenase from *Plasmodium falciparum* as a strategy for the development of new therapies for the treatment of malaria.

The specific steps can be summarized in:

- Cloning of a new construct, named *Pf*DHODHΔloop, where the protruding loop is removed;
- Heterologous expression in *E. coli* and purification for the enzymes *Pf*DHODH and *Pf*DHODHΔloop;
- Inhibitory assays for *Pf*DHODH and determination of the inhibition mechanism;
- Crystallization assays and structural elucidation of *Pf*DHODHΔloop by X-ray diffraction techniques;

3.3 Materials and Methods

3.3.1 Cloning of PfDHODH and PfDHODHΔloop

The gene encoding active *Pf*DHODH enzyme (Glu^{159} to Ser^{569}) had been previously cloned in our laboratory using the pET-SUMO expression vector.

In order to favor crystallization in a reproducible manner, a novel construct, named *Pf*DHODHΔloop, was prepared where the flexible region (Ser^{384} to Asp^{413}) was removed from the target protein. *Pf*DHODH enzyme was used as template for carrying out gene amplification.

Using the overlap extension technique (**Figure 8**), the fragment of interest was deleted through a sequence of three polymerase chain reactions (PCR). In the first two PCR reactions, two external oligonucleotides (A and D) were used together with two internal oligonucleotides (B and C) to create two fragments (**Table 12**). Amplifications of both fragments (AB and CD) were performed according to the specifications indicated in the manual of the polymerase enzyme used Phusion DNA Polymerase (Thermo Scientific). The third step was divided into two PCRs, the first for the extension of incomplete fragments (AB and CD) and the second for amplification, through the external oligonucleotides, of the complete fragment (AD). The fragments obtained in the PCR reactions were purified from the 0.8% agarose gel using the QIAquick Gel Extraction Kit (QIAGEN) and then cloned into the pET-SUMO vector.

Table 12. Internal and external primers used for *Pf*DHODHΔloop cloning. Underlined sequences are corresponded to specific sites for restriction enzymes.

Primers	Sequence (5'- 3')	Melting Temperature (°C)
***Pf*DHODH *Bam*HI Fow** (external primer A)	GACGACGGATCCGAATCCTATAACCCGGAATTT	64.4
***Pf*DHODH *Xho*I Rev** (external primer D)	GACGACCTCGAGTTACGATTTGGAGTGTTTGCG	65.6
***Pf*DHODHΔloop Fow** (internal primer B)	GAACGATGAATTTCTGTGGTTCAATACCACCAAG	62.0
***Pf*DHODHΔloop Rev** (internal primer C)	ACCACAGAAATTCATCGTTCATGATGTTGTTTTTCTCC	62.3

The complete fragment and the pET-SUMO vector were digested with restriction enzymes BamHI and XhoI and purified from 0.8% agarose gel. Ligation of insert into vector was done using the enzyme T4 DNA ligase (NEB). *E. coli* DH5α cells were transformed with the ligation product; subsequently Colony PCR was performed for determining the presence or absence of insert DNA into plasmid construct. Positive clones were purified from the transformed cells with the QIAprep Miniprep Kit (QIAGEN).

Finally, to confirm the positive clones in the stored colonies, a small aliquot of purified DNA was subjected to digestion with the enzymes BamHI and XhoI. After digestion, the samples were analyzed into agarose gel 0.8%.

Plasmid DNA for the new construct was sequenced by using, two external oligonucleotides, Bgl II (5' – AGATCTCGATCCCGCGAAATTAAT – 3') and ExtPet 28a (5' – AAAGCCGGCGAACGTGGC – 3').

3.3.2 Heterologous expression of PfDHODH and PfDHODHΔloop

*Pf*DHODH or *Pf*DHODHΔloop were expressed under similar protocols. A single colony of *E.coli* BL21 (DE3) transformed with pET-28-SUMO-*Pf*DHODH or pET-28-SUMO-*Pf*DHODHΔloop was grown overnight in 10 mL of medium (20 g/L bacto-tryptone, 15 g/L yeast extract, 2 g/L Na_2HPO_4, 1 g/L KH_2PO_4 and 8 g/L NaCl) containing 30 µg/mL

kanamycin at 37 °C and 180 rpm and used to inoculate 1 L of fresh medium. When the $O.D_{600nm}$ reached 0.6, isopropylthio-β-galactoside (IPTG, Fermentas) was added to 250 µM final concentration and the temperature was reduced to 18 °C. After 24 hours the cells were isolated by centrifugation at 9,500 g for 8 minutes and kept at -20°C until used.

3.3.3 Purification of the enzymes PfDHODH and PfDHODHΔloop

Cell pellets corresponding to 250 mL of culture were resuspended in 20 mL of lysis buffer (50 mM NaH_2PO_4 pH 8.0, 300 mM NaCl, 0.33% Thesit (Sigma), 1 mM phenylmethanesulfonylfluoride (PMSF), 10% glycerol). The cells were lysed using 15 cycles of 30 s sonication with 30 s intervals on ice with an output power of 10 W. The lysate was then maintained on ice for 30 minutes on a rocking shaker and centrifuged at 16,100 g for 30 minutes at 4 °C.

The soluble fraction was loaded into a 1 mL HisTrap™ HP column connected to an ÄKTA-Purifier system (GE Life Sciences) previously equilibrated with buffer A (50 mM NaH_2PO_4 pH 8.0, 300 mM NaCl, 0.05% Thesit (Sigma), 10% glycerol). An isocratic chromatographic run was carried out at 1.0 mL/min. The wash steps consisted of passing through at least 5 column volumes of buffer A containing 10 mM imidazole followed by 5 column volumes of buffer A containing 25 mM imidazole. 6xHis-SUMO-DHODH was eluted with buffer A containing 500 mM imidazole. The eluted samples were concentrated to 500 µL using a 10 kDa cutoff Amicon Centrifugal filter unit and loaded in a 5 mL HiTrap Desalting column connected to an ÄKTA-Purifier system (GE Life Sciences). An isocratic chromatographic run was carried out with buffer A at 1 mL/min.

Homemade 6xHis-ubiquitin-like protein 1 (ULP1) protease[90] was incubated with the desalted protein, during 16 hours at 4 °C. The sample was once again loaded into a 1 mL HisTrap™ HP column connected to an ÄKTA-Purifier system (GE Life Sciences) pre-equilibrated in buffer A. Tag free DHODH was collected in the flow through. The 6xHis-SUMO tag and 6xHis-ULP1 were eluted from the column with buffer A containing 500 mM imidazole.

Protein purity was assessed by SDS-PAGE and quantification was carried out by absorbance using the extinction coefficient of the protein cofactor FMN, ε_{456nm} = 12137 $M^{-1}.cm^{-1}$ for *Pf*DHODH; calculated as described elsewhere.[86]

3.3.4 Inhibition mechanism studies (Broad Institute compounds)

The experiments were performed in a 96-well microplate reader, containing the assay buffer: 60 µM DCIP, 50 mM Tris pH 8.15, 150 mM KCl, 0.1 % Triton X-100, 500 µM DHO, CoQ_D varying from 6.25 to 100 µM and inhibitor concentrations varying from 11.7 to 6000 nM (serial dilution). To start the reaction 200 µL were added in 5 µL *Pf*DHODH, to a final enzyme concentration of 40 nM. As a negative control, 200 µL assay buffer were added in 5 µL enzyme buffer, without the presence of enzyme. Also, 200 µL buffer were added in 5 µL *Pf*DHODH, without the presence of the inhibitors to determine the activity for each substrate concentration. The reactions were monitored each 3 s over a period of 60 s, in triplicate, for each concentration and each tested compound. The inhibition mechanism was determined through the graph of IC_{50} versus CoQ_D concentration using linear data fitting obtained in the software Origin 2016.

3.3.5 Crystallization of PfDHODHΔloop

Crystallization assays *Sm*DHODH and *Sm*DHODHΔloop were performed with pure and concentrated protein, using the sitting drop method. The sparse-matrix method implemented in commercially available screening kits was used to initial crystallization experiments: PegIon 1 and 2, Natrix 1 and 2, SaltRx 1 and 2, Crystal Screen 1 and 2, PegRx 1 and 2, Index 1 and 2, and MembFac (Hampton Research); Nextal MBClass (Qiagen); and JBScreen Classic 1 to 10, JBScreen Membrane 1 to 4 (Jena Bioscience) and also prepared conditions, according to what has already been identified as crystallization conditions for *Pf*DHODH.

Previously, protein solution was incubated in presence of dihydroorotate (DHO, 2 mM), inhibitors (1 mM) and detergents (1 mM), once these help the stabilization of the enzyme and therefore aid the crystallization. Equal volumes of protein and reservoir solution were mixed, equilibrated against 500 µL reservoir solution and kept at 293 K. Several efforts were made in order to crystallize the protein by screening a wide range of different crystallization variables (protein concentration ranging from 2.0 to 20.0 mg/mL, drop volume, pH, temperature, precipitant concentration, and additives). The first crystals were obtained in presence of two conditions within 14 days for the protein *Pf*DHODHΔloop. Other crystallization conditions are being tested, in order to optimize the crystallization and also to co-crystallize with different ligands.

3.3.6 Data collection, processing and phasing

Prior to data collection, *Pf*DHODHΔloop crystals were harvested with cryo loops, protected using a cryo-protective solution, and were cooled in liquid nitrogen. The data set was collected at 100 K on a synchrotron facility (PROXIMA1 - SOLEIL, France) using a PILATUS 6M detector (Dectris, Baden, Switzerland). Crystallographic data reduction and scaling was carried out with the software autoPROC.[124] Initial phases were obtained by the molecular replacement method using MOLREP[125] and the atomic coordinates of the *Pf*DHODHΔloop protein (PDBID: 4RX0)[37] as search model. The structure has been initially refined with REFMAC,[126] intercepted with manual map inspection and model building using Coot.[127]

3.4 Results and Discussion

3.4.1 Cloning of PfDHODH∆loop

The gene fragment encoding *Pf*DHODHΔloop was successfully cloned into the plasmid pET-SUMO, using the previously cloned *Sm*DHODH construct as a template. The high-throuput method colony PCR was used to screen for positive clones (**Figure 19**). Double digestion with enzymes BamHI and XhoI were used to confirm the presence of the desirable insert. DNA sequencing confirmed the correct sequence and reading frame.

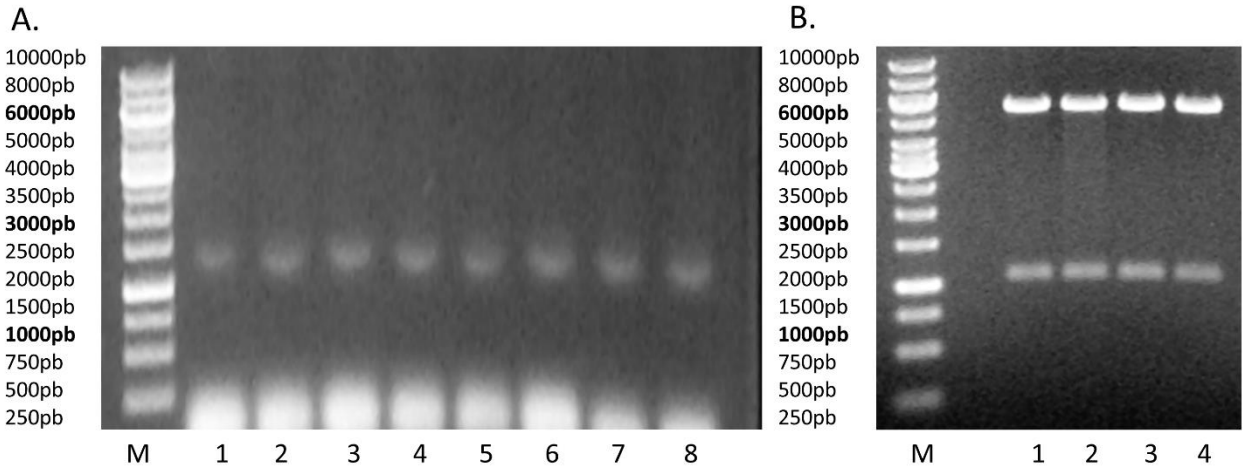

Figure 19. Electrophoresis in agarose gels related to the *Pf*DHODHΔloop-pET-SUMO construction, (A) colony PCR showing the positive colonies; and (B) double digestion to confirm the positive colonies (*Pf*DHODHΔloop, 1146bp and pET-SUMO, 5639bp).

3.4.2 Expression, purification and quantification for PfDHODH and PfDHODH∆loop

The expression and purification protocols previously established in the laboratory was adapted in order to improve the yield and purification time. The yield obtained, measured at 600 nm, is around 60 mg per liter of culture for *Pf*DHODH, and 40 mg per liter of culture for *Pf*DHODHΔloop. SDS-PAGE gels show that the constructs were

overexpressed in the soluble fraction and that were purified by the Nickel affinity chromatographic column (**Figure 20**).

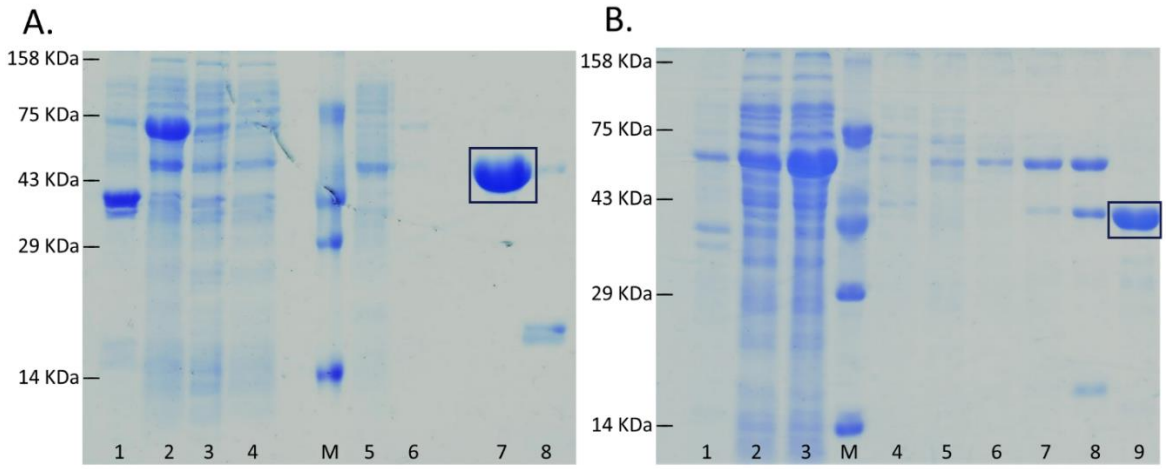

Figure 20. SDS-PAGE analyses of nickel affinity chromatography showing the purification steps. M: molecular weight marker. Black Square: Purified proteins. *Pf*DHODH (A.): 1 – Pellet; 2 – Soluble fraction; 3 – Efluent; 4 – Washing step containing 10 mM imidazole; 5 – Washing step containing 25 mM imidazole; 6 – Protein elution containing 500 mM imidazole, before SUMO cleavage with ULP1; 7 – Protein elution, after cleavage and second affinity chromatography; 8 – Elution of ULP1 and 6xHis-SUMO-tag, with 500 mM imidazole. *Pf*DHODHΔloop (B.): 1 – Pellet; 2 – Efluent; 3 – Soluble fraction 4 – Washing step containing 10 mM imidazole; 5 – Washing step containing 25 mM imidazole; 6 and 7 – Protein elution containing 500 mM imidazole, before SUMO cleavage with ULP1; 8 – Elution of ULP1 and 6xHis-SUMO-tag, with 500 mM imidazole; 9 – Protein elution, after cleavage and second affinity chromatography.

3.4.3 Inhibition mechanism studies (Broad Institute compounds)

Similar to what has been described for *Sm*DHODH, several compounds have also been provided by the Broad Institute for evaluation of inhibition against the enzyme *Pf*DHODH. The collaboration between the institutions has several years and many inhibitors have already been identified against *Pf*DHODH. Among these, 3 compounds (codes: TV0557742, TV057745 and TV057747) were previously tested as inhibitors (by the lab specialist Valquíria Jabor) and their IC_{50} values were determined. With the interest in identifying the site of inhibition for these compounds, we have also performed inhibition mechanism assays. The graphs IC_{50} value versus varying concentration of decylubiquinone for *Pf*DHODH are found in the following **Figure 21**.

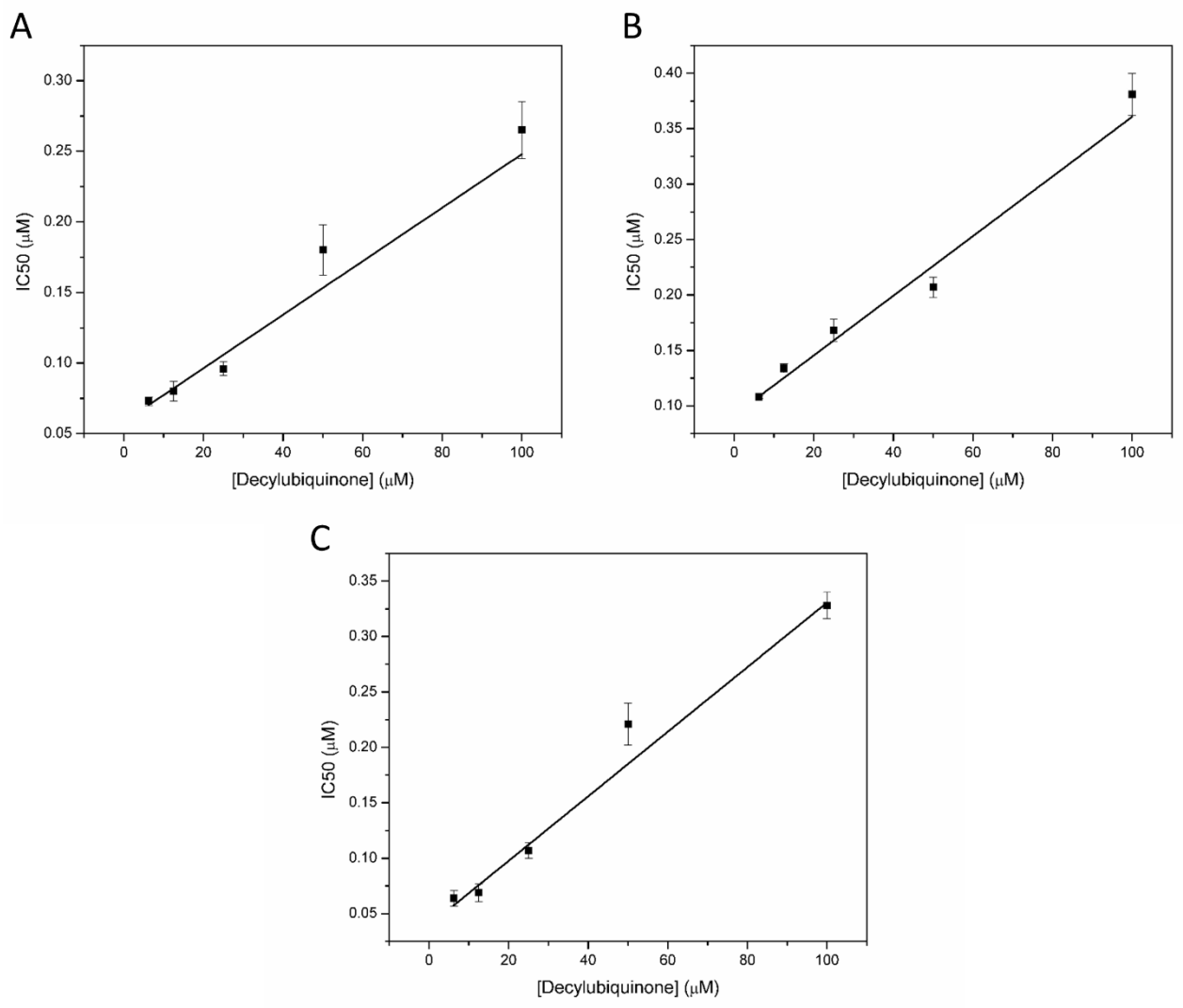

Figure 21. Inhibition mechanism assays. Compounds IC_{50} values vs varying concentration of decylubiquinone for *Pf*DHODH. Single experiment in triplicate. A) Compound TV057742, B) Compound TV057745, C) Compound TV057747, shows positive slope of the curves, meaning competitive inhibition mechanism against decylubiquinone for *Pf*DHODH.

According to the figure above, all the compounds tested presented a competitive inhibition mechanism. This is observed by the positive slope of the curves, in which higher concentrations of substrate (decylubiquinone) presents a higher IC_{50} value, which means competition for the same site of interaction. This information can help the design of new molecules as inhibitors of *Pf*DHODH.

3.4.4 Crystallization of PfDHODHΔloop

Crystals were obtained for *Pf*DHODHΔloop using the following conditions: 0.1 M Sodium acetate pH 4.6, 24% PEG 4000, 0.14 - 0.2 M Ammonium sulfate, 25% Glycerol and 10 mM DTT; and also condition E6 from kit JBScreen Membrane (2M Ammonium Sulfate). The final protein solution concentration was 15 mg/mL; together with 2 mM DHO, as substrate, 1 mM DSM265 as inhibitor and LDAO, as detergent. In **Figure 22**, we can observe pictures from the obtained crystals. Yellow crystals, due to the presence of the prosthetic FMN group, have been recently obtained.

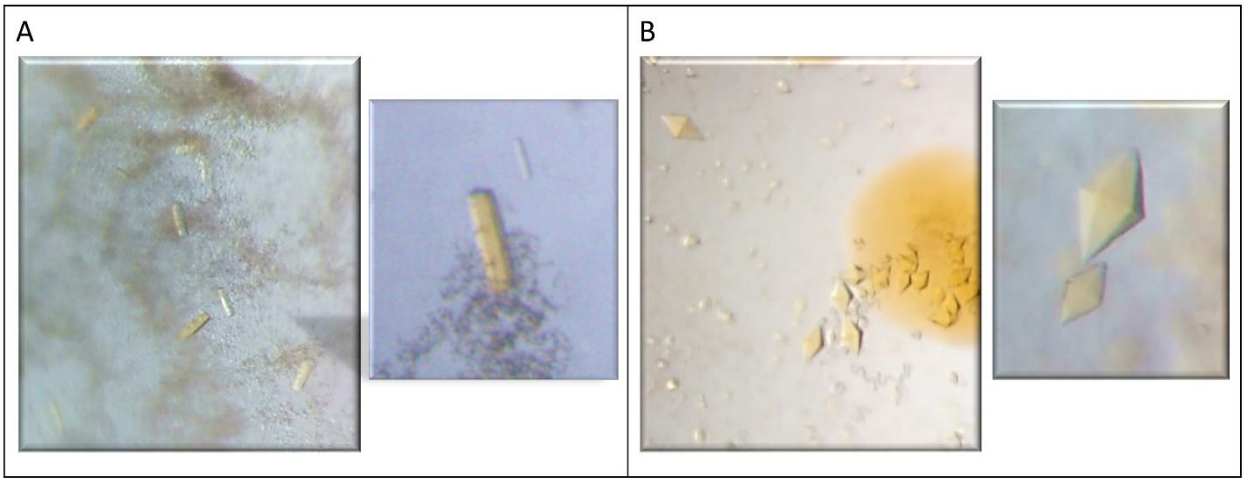

Figure 22. *Pf*DHODHΔloop crystals obtained in A) 0.1 M Sodium acetate pH 4.6, 24% PEG 4000, 0.14 - 0.2 M Ammonium sulfate, 25% Glycerol and 10 mM DTT; and B) 2 M Ammonium sulfate: condition E6 from kit JBScreen Membrane (Jena Bioscience). Left panel are general views of the drop, while right panels are focused on crystals.

3.4.5 Data collection, processing and phasing for PfDHODHΔloop

Data collection was performed for the first crystal form **Figure 22A**. Although crystals in **Figure 22B** presented a defined external morphology in a clear drop, they only diffract up to 5.0 Å of resolution. *Pf*DHODHΔloop crystals belong to trigonal space group

P321, with cell unit parameters a=172.66, b=172.66, c=73.21 and diffract up 3.17 Å resolution (**Table S3**). A single refining process was performed. It was possible to observe the electronic density for the cofactor FMN and also for the co-crystallized ligand DSM265 (**Figure 23A**). Overall, the structure obtained for *Pf*DHODHΔloop, presents similar folding as to the ones previously solved before for *Pf*DHODHΔloop (**Figure 23B**). Crystallization of *Pf*DHODHΔloop corresponds to an important step towards characterizing the mechanism of binding of *Pf*DHODH inhibitors.

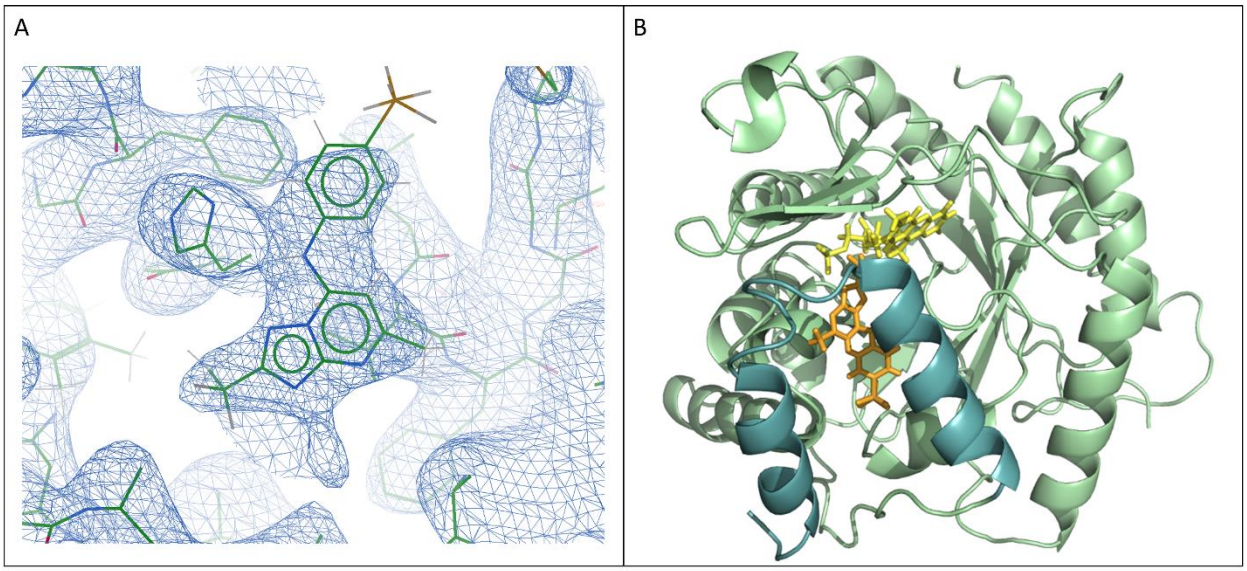

Figure 23. A) Electronic density map 2Fobs-Fcalc, with σ (contour level) equals to 1.2, represented in blue for *Pf*DHODHΔloop. At the center is highlighted the electronic density fitted with the ligand DSM265. B) Cartoon representation of *Pf*DHODHΔloop. Alpha-beta barrel, N-terminal helices, FMN and DSM265 is represented in pale green, light teal, yellow and orange, respectively.

3.5 Conclusions

The increasing number of malaria cases that have occurred in first-world countries due to globalization have drawn attention to this disease. Due to resistance, new drugs are required to overcome this important issue. The present work describes the search for new selective inhibitors against *Pf*DHODH. Using biochemical assays, we were able to identify potent inhibitors. With the interest in identifying the site of inhibition for these compounds, inhibition mechanism assays were performed. Cloning of a new construct, named *Pf*DHODHΔloop, where a protruding loop present in the protein was removed, in order to fully characterize the binding mechanism of the identified inhibitors. Crystals were obtained in different conditions, in which the best data set obtained, was processed at 3.17 Å of resolution. Overall, the structure obtained for *Pf*DHODHΔloop, presents similar folding as to the ones previously solved. Reproducibility was obtained for the crystallization of this enzyme, which guarantees the possibility of acquiring new crystals bound to different compounds.

CHAPTER 4. FINAL REMARKS

4.1 Final Remarks

The work here described and entitled “Repurposing of antimalarial drugs in the treatment of schistosomiasis based on the selective inhibition of the enzyme dihydroorotate dehydrogenase” was carried out between March 2016 and October 2018.

Initially, our work focused on the enzyme dihydroorotate dehydrogenase from *Schistosoma mansoni* (Chapter 2). We were interested in pursuing the search for new potent and selective inhibitors, taking advantage of the previous work performed by the former master student Juliana S. David, which described in her dissertation, the preliminary expression and purification protocols and biochemical characterization for this enzyme. The compounds originally tested had been previously identified as inhibitors of the homologous enzyme from *Plasmodium falciparum*, including molecules under clinical trials such as DSM265 and atovaquone. Potent inhibitors were identified, and the design of analogues (in collaboration with Prof. Flávio Emery) allowed the identification of highly potent (in nanomolar range) and selective inhibitors (cross validation against the human enzyme, *Hs*DHODH).

In order to provide the structural basis for potency and selectivity, different techniques were used, including traditional biochemical assays; inhibition mechanism assays; and the home designed technique ThermoFMN. Considering our lab expertise, structural characterization was also extensively attempted through the use of the X-ray crystallography. Despite testing thousands of conditions, the major challenge of this work was to obtain *Sm*DHODH crystals.

Based on our results, it was possible to characterize three distinct mechanisms of inhibition among the identified ligands: competitive against CoQ_0, non-competitive and mixed-type. Moreover, they effect on thermostability, measured by monitoring the prosthetic group FMN, raised very important questions regarding the mechanism of catalysis adopted by class 2 DHODHs, in particular *Sm*DHODH.

First, by using a small cofactor, we predicted that similar compounds could exploit different interactions in the inhibitor binding site. The competitive ones can reach the end

of the quinone binding site and get in close proximity to the FMN. The non-competitive inhibitors, even though sitting in the same binding pocket, are predicted to bind far away from FMN, holding the helical domain and stabilizing the protein. Mixed-type mechanism, not only corroborate the idea that some of our compounds can exploit different interactions in the pocket, but support previous findings regarding the relevance of the mobility of the helical domain for catalysis as well as binding mechanism of inhibition, including potency and selectivity.

A critical analysis of *Sm*DHODH structure through building a homology model helped us to identify the presence of a flexible loop (Gly^{285} to Lys^{294}), absent in other class 2 DHODHs. Unexpectedly, this region proved to be essential to catalysis and work towards understanding the relevance of this region for protein activity is currently in progress. We recently obtained crystals of our construct *Sm*DHODHΔloop that together with our biophysical assays can provide a starting point to understand the mechanism of catalysis adopted *Sm*DHODH and class 2 DHODH in general. We strongly believe that the understanding on how our target works have a beneficial impact on the rational design of selective inhibitors. Thus, we emphasize here that despite our interest in identifying potent and selective ligands for *Sm*DHODH, our work also focused on contributing for the full characterization of protein function.

In vitro studies using adult *S. mansoni* worms have also been performed. By testing the best inhibitors, it was possible to evaluate their impact on schistosomicidal morphology and activity. Results show a potent activity against the parasites, especially for the compound atovaquone, which it is already a drug in use against malaria. Those exciting, despite preliminary results, provide strong encouragement to keep on pursuing the idea of using inhibition of DHODH, including drug repurposing, as a strategy to search for alternative strategies to treat schistosomiasis.

Considering structural and functional similarity between *Sm*DHODH and *Pf*DHODH, and considering the fact that DHODH is a validated target for malaria, we invested our knowledge on DHODHs and efforts in developing a pipeline to allow the screening and characterization of inhibitors for *Pf*DHODH.

During the development of this work, several molecules have been screened against *Pf*DHODH in our laboratory. This work is performed on regular basis by our Screening Center, under the coordination of Dr. Valquiria Jabor. Several potent inhibitors have been identified from different collaborators in Brazil and abroad. Specifically, for the compounds sent by the Broad Institute of MIT and Harvard in a partnership with MMV (Medicine for Malaria Venture), our laboratory performed not only the determination of inhibitory constants but we were able to map the mechanism of inhibition (as shown in Chapter 3). The protocol developed for this work is now implemented in our pipeline and is being used for other ongoing partnerships. In addition to biochemical studies, the *Pf*DHODHΔloop protein was successfully crystallized and provide us the ability to add structural studies in our pipeline, a required step during drug development based on the selective inhibition of a protein target.

This work is part of a major effort of our laboratory to contribute for the development of new therapeutic strategies to combat neglected diseases as well as the training of human resources in the field of structural biology applied to medicinal chemistry.

4.2 Manuscripts published related to this thesis

Calil, Felipe A.; David, Juliana S.; Chiappetta, Estela R. C.; Fumagalli, Fernando; Mello, Rodrigo B.; Leite, Franco H.; Castilho, Marcelo S.; Emery, Flávio S.; Nonato, M. Cristina. Ligand-Based Design, Synthesis, and Biochemical Evaluation of Potent and Selective Inhibitors of Dihydroorotate Dehydrogenase for the Treatment of Schistosomiasis. *European Journal of Medicinal Chemistry*. v. 106, p. 357-366, 2019.

Nonato, Maria Cristina; De Padua, Ricardo A. P.; David, Juliana S.; Reis, Renata A. G.; Tomaleri, Giovani P.; Pereira, Humberto D.; **Calil, Felipe A.** Structural basis for the design of selective inhibitors for *Schistosoma mansoni* dihydroorotate dehydrogenase. *Biochimie*, v. 158, p. 180-190, 2019.

Hoelz, Lucas V. B.*; **Calil, Felipe A.***; Nonato, Maria Cristina; Pinheiro, Luiz C. S.; Boechat, Nubia. *Plasmodium falciparum* Dihydroorotate Dehydrogenase: a Drug Target Against Malaria. *Future Medicinal Chemistry*, 10(15):1853-1874. 2018 *authors equally contributed to the work.

Reis, Renata Almeida Garcia*; **Calil, Felipe Antunes***; Feliciano, Patricia Rosa*; Pinheiro, Matheus Pinto*; Nonato, Maria Cristina*. The dihydroorotate dehydrogenases: past and present. *Archives of Biochemistry and Biophysics*, v. 632, p. 175-191, 2017. *all authors equally contributed to the work.

Maetani, Micah; Kato, Nobutaka; Jabor, Valquiria A. P.; **Calil, Felipe Antunes**; Nonato, Maria Cristina; Scherer, Christina A.; Schreiber, Stuart L. Discovery of antimalarial azetidine-2-carbonitriles that inhibit *P. falciparum* dihydroorotate dehydrogenase. *ACS Medicinal Chemistry Letters*, v. 8, p. 438-442, 2017.

4.3 Bibliography

1. Saker, L.; Lee, K.; Cannito, B.; Gilmore, A.; Campbell-Lendrum, D. *Globalization and infectious diseases : a review of the linkages*; World Health Institute: 2004; p 64.

2. Molina-Cruz, A.; Canepa, G. E.; Kamath, N.; Pavlovic, N. V.; Mu, J.; Ramphul, U. N.; Ramirez, J. L.; Barillas-Mury, C. *Plasmodium* evasion of mosquito immunity and global malaria transmission: The lock-and-key theory. *Proceedings of the National Academy of Sciences of the United States of America* **2015,** 112, 15178-15183.

3. Lancet. Ebola: lessons for future pandemics. *The Lancet* **2015,** 386, 2118.

4. Musso, D.; Nilles, E. J.; Cao-Lormeau, V. M. Rapid spread of emerging Zika virus in the Pacific area. *Clinical Microbiology and Infection* **2014,** 20, O595-O596.

5. Petersen, E. E.; Staples, J. E.; Meaney-Delman, D.; Fischer, M.; Ellington, S. R.; Callaghan, W. M.; Jamieson, D. J. Interim Guidelines for Pregnant Women During a Zika Virus Outbreak — United States, 2016. *MMWR Morb Mortal Wkly Rep* **2016,** 65, 30-33.

6. Hennessey, M.; Fischer, M.; Staples, J. E. Zika Virus Spreads to New Areas — Region of the Americas, May 2015–January 2016. *MMWR Morb Mortal Wkly Rep* **2016,** 65, 55–58.

7. Lancet. Neglected tropical diseases: becoming less neglected. *The Lancet* **2014,** 383, 1269-1269.

8. Liese, B.; Rosenberg, M.; Schratz, A. Neglected Tropical Diseases 1 Programmes, partnerships, and governance for elimination and control of neglected tropical diseases. *Lancet* **2010,** 375, 67-76.

9. Knobler, S.; Mahmoud, A.; Lemon, S.; Pray, L. *The Impact of Globalization on Infectious Disease Emergence and Control: Exploring the Consequences and Opportunities: Workshop Summary*. National Academies Press (US): Washington (DC), 2006.

10. Gushulak, B. D.; MacPherson, D. W. Globalization of Infectious Diseases: The Impact of Migration. *Clinical Infectious Diseases* **2004,** 38, 1742-1748.

11. Pinto-Almeida, A.; Mendes, T.; de Oliveira, R. N.; Corrêa, S. d. A. P.; Allegretti, S. M.; Belo, S.; Tomás, A.; Anibal, F. d. F.; Carrilho, E.; Afonso, A. Morphological Characteristics of *Schistosoma mansoni* PZQ-Resistant and -Susceptible Strains Are Different in Presence of Praziquantel. *Frontiers in Microbiology* **2016,** 7, 594.

12. Matthews, H.; Hanison, J.; Nirmalan, N. "Omics"-Informed Drug and Biomarker Discovery: Opportunities, Challenges and Future Perspectives. *Proteomes* **2016,** 4.

13. Lotharius, J.; Gamo-Benito, F. J.; Angulo-Barturen, I.; Clark, J.; Connelly, M.; Ferrer-Bazaga, S.; Parkinson, T.; Viswanath, P.; Bandodkar, B.; Rautela, N.; Bharath, S.; Duffy, S.; Avery, V. M.; Mohrle, J. J.; Guy, R. K.; Wells, T. Repositioning: the fast track to new anti-malarial medicines? *Malaria Journal* **2014,** 13.

14. Abdulla, M. H.; Ruelas, D. S.; Wolff, B.; Snedecor, J.; Lim, K. C.; Xu, F. Y.; Renslo, A. R.; Williams, J.; McKerrow, J. H.; Caffrey, C. R. Drug Discovery for Schistosomiasis: Hit and Lead Compounds Identified in a Library of Known Drugs by Medium-Throughput Phenotypic Screening. *Plos Neglected Tropical Diseases* **2009,** 3.

15. Caffrey, C. R.; Steverding, D. Recent initiatives and strategies to developing new drugs for tropical parasitic diseases. *Expert Opinion on Drug Discovery* **2008,** 3, 173-186.

16. Ashburn, T. T.; Thor, K. B. Drug repositioning: Identifying and developing new uses for existing drugs. *Nature Reviews Drug Discovery* **2004,** 3, 673-683.

17. RepurposingDrugs101. What has worked? http://repurposingdrugs101.com/what-has-worked/ (August 2018).

18. Allarakhia, M. Open-source approaches for the repurposing of existing or failed candidate drugs: learning from and applying the lessons across diseases. *Drug Design Development and Therapy* **2013,** 7, 753-766.

19. Booker, M. L.; Bastos, C. M.; Kramer, M. L.; Barker, R. H.; Skerlj, R.; Sidhu, A. B.; Deng, X. Y.; Celatka, C.; Cortese, J. F.; Bravo, J. E. G.; Llado, K. N. C.; Serrano, A. E.; Angulo-Barturen, I.; Jimenez-Diaz, M. B.; Viera, S.; Garuti, H.; Wittlin, S.; Papastogiannidis, P.; Lin, J. W.; Janse, C. J.; Khan, S. M.; Duraisingh, M.; Coleman, B.; Goldsmith, E. J.; Phillips, M. A.; Munoz, B.; Wirth, D. F.; Klinger, J. D.; Wiegand, R.; Sybertz, E. Novel Inhibitors of *Plasmodium falciparum* Dihydroorotate Dehydrogenase with Anti-malarial Activity in the Mouse Model. *Journal of Biological Chemistry* **2010,** 285, 33054-33064.

20. Patel, V.; Booker, M.; Kramer, M.; Ross, L.; Celatka, C. A.; Kennedy, L. M.; Dvorin, J. D.; Duraisingh, M. T.; Sliz, P.; Wirth, D. F.; Clardy, J. Identification and Characterization of Small Molecule Inhibitors of *Plasmodium falciparum* Dihydroorotate Dehydrogenase. *Journal of Biological Chemistry* **2008,** 283, 35078-35085.

21. Coteron, J. M.; Marco, M.; Esquivias, J.; Deng, X. Y.; White, K. L.; White, J.; Koltun, M.; El Mazouni, F.; Kokkonda, S.; Katneni, K.; Bhamidipati, R.; Shackleford, D. M.; Angulo-Barturen, I.; Ferrer, S. B.; Jimenez-

Diaz, M. B.; Gamo, F. J.; Goldsmith, E. J.; Charman, W. N.; Bathurst, I.; Floyd, D.; Matthews, D.; Burrows, J. N.; Rathod, P. K.; Charman, S. A.; Phillips, M. A. Structure-Guided Lead Optimization of Triazolopyrimidine-Ring Substituents Identifies Potent *Plasmodium falciparum* Dihydroorotate Dehydrogenase Inhibitors with Clinical Candidate Potential. *Journal of Medicinal Chemistry* **2011,** 54, 5540-5561.

22. Feliciano, P. R.; Cordeiro, A. T.; Costa, A. J.; Nonato, M. C. Cloning, expression, purification, and characterization of *Leishmania major* dihydroorotate dehydrogenase. *Protein Expression and Purification* **2006,** 48, 98-103.

23. Hines, V.; Johnston, M. Analysis of the Kinetic Mechanism of the Bovine Liver Mitochondrial Dihydroorotate Dehydrogenase. *Biochemistry* **1989,** 28, 1222-1226.

24. Reis, R. A. G.; Ferreira, P.; Medina, M.; Nonato, M. C. The mechanistic study of *Leishmania major* dihydro-orotate dehydrogenase based on steady- and pre-steady-state kinetic analysis. *Biochemical Journal* **2016,** 473, 651-660.

25. Lieberman, I.; Kornberg, A. Enzymic Synthesis and Breakdown of a Pyrimidine, Orotic Acid .1. Dihydro-Orotic Dehydrogenase. *Biochimica Et Biophysica Acta* **1953,** 12, 223-234.

26. Dimitrijevic, M.; Bartlett, R. R. Leflunomide, a novel immunomodulating drug, inhibits homotypic adhesion of peripheral blood and synovial fluid mononuclear cells in rheumatoid arthritis. *Inflammation Research* **1996,** 45, 550-556.

27. Smolen, J. S.; Kalden, J. R.; Scott, D. L.; Rozman, B.; Kvien, T. K.; Larsen, A.; Loew-Friedrich, I.; Oed, C.; Rosenburg, R.; Grp, E. L. S. Efficacy and safety of leflunomide compared with placebo and sulphasalazine in active rheumatoid arthritis: a double-blind, randomised, multicentre trial. *Lancet* **1999,** 353, 259-266.

28. Rowland, P.; Bjornberg, O.; Nielsen, F. S.; Jensen, K. F.; Larsen, S. The crystal structure of *Lactococcus lactis* dihydroorotate dehydrogenase A complexed with the enzyme reaction product throws light on its enzymatic function. *Protein Science* **1998,** 7, 1269-1279.

29. Knecht, W.; Henseling, J.; Löffler, M. Kinetics of inhibition of human and rat dihydroorotate dehydrogenase by atovaquone, lawsone derivatives, brequinar sodium and polyporic acid. *Chemico-Biological Interactions* **2000,** 124, 61-76.

30. Vyas, V. K.; Ghate, M. Recent Developments in the Medicinal Chemistry and Therapeutic Potential of Dihydroorotate Dehydrogenase (DHODH) Inhibitors. *Mini-Reviews in Medicinal Chemistry* **2011,** 11, 1039-1055.

31. Munier-Lehmann, H.; Vidalain, P.-O.; Tangy, F.; Janin, Y. L. On Dihydroorotate Dehydrogenases and Their Inhibitors and Uses. *Journal of Medicinal Chemistry* **2013,** 56, 3148-3167.

32. Pinheiro, M. P.; Emery, F. D.; Nonato, M. C. Target Sites for the Design of Anti-trypanosomatid Drugs Based on the Structure of Dihydroorotate Dehydrogenase. *Current Pharmaceutical Design* **2013,** 19, 2615-2627.

33. Nonato, M. C.; Costa-Filho, A. J. The dihydroorotate dehydrogenases. In *Handbook of Flavoproteins, Volume 1 Oxidases, Dehydrogenases and Related Systems*, Hille, R.; Miller, S.; Palfey, B., Eds. De Gruyter: Berlin, 2013; Vol. 1, pp 297-312.

34. Sulyok, M.; Ruckle, T.; Roth, A.; Murbeth, R. E.; Chalon, S.; Kerr, N.; Samec, S. S.; Gobeau, N.; Calle, C. L.; Ibanez, J.; Sulyok, Z.; Held, J.; Gebru, T.; Granados, P.; Bruckner, S.; Nguetse, C.; Mengue, J.; Lalremruata, A.; Sim, B. K. L.; Hoffman, S. L.; Mohrle, J. J.; Kremsner, P. G.; Mordmuller, B. DSM265 for *Plasmodium falciparum* chemoprophylaxis: a randomised, double blinded, phase 1 trial with controlled human malaria infection. *Lancet Infectious Diseases* **2017,** 17, 636-644.

35. Murphy, S. C.; Duke, E. R.; Shipman, K. J.; Jensen, R. L.; Fong, Y. Y.; Ferguson, S.; Janes, H. E.; Gillespie, K.; Seilie, A. M.; Hanron, A. E.; Rinn, L.; Fishbaugher, M.; VonGoedert, T.; Fritzen, E.; Kappe, S. H.; Chang, M.; Sousa, J. C.; Marcsisin, S. R.; Chalon, S.; Duparc, S.; Kerr, N.; Mohrle, J. J.; Andenmatten, N.; Rueckle, T.; Kublin, J. G. A Randomized Trial Evaluating the Prophylactic Activity of DSM265 Against Preerythrocytic *Plasmodium falciparum* Infection During Controlled Human Malarial Infection by Mosquito Bites and Direct Venous Inoculation. *Journal of Infectious Diseases* **2018,** 217, 693-702.

36. McCarthy, J. S.; Lotharius, J.; Ruckle, T.; Chalon, S.; Phillips, M. A.; Elliott, S.; Sekuloski, S.; Griffin, P.; Ng, C. L.; Fidock, D. A.; Marquart, L.; Williams, N. S.; Gobeau, N.; Bebrevska, L.; Rosario, M.; Marsh, K.; Mohrle, J. J. Safety, tolerability, pharmacokinetics, and activity of the novel long-acting antimalarial DSM265: a two-part first-in-human phase 1a/1b randomised study. *Lancet Infectious Diseases* **2017,** 17, 626-635.

37. Phillips, M. A.; Lotharius, J.; Marsh, K.; White, J.; Dayan, A.; White, K. L.; Njoroge, J. W.; El Mazouni, F.; Lao, Y. B.; Kokkonda, S.; Tomchick, D. R.; Deng, X. Y.; Laird, T.; Bhatia, S. N.; March, S.; Ng, C. L.; Fidock, D. A.; Wittlin, S.; Lafuente-Monasterio, M.; Benito, F. J. G.; Alonso, L. M. S.; Martinez, M. S.; Jimenez-Diaz, M. B.; Bazaga, S. F.; Angulo-Barturen, I.; Haselden, J. N.; Louttit, J.; Cui, Y.; Sridhar, A.; Zeeman, A. M.; Kocken, C.; Sauerwein, R.; Dechering, K.; Avery, V. M.; Duffy, S.; Delves, M.; Sinden, R.; Ruecker, A.; Wickham, K. S.; Rochford, R.; Gahagen, J.; Iyer, L.; Riccio, E.; Mirsalis, J.; Bathhurst, I.; Rueckle, T.; Ding, X.; Campo, B.; Leroy, D.; Rogers, M. J.; Rathod, P. K.; Burrows, J. N.; Charman, S. A. A long-duration dihydroorotate dehydrogenase inhibitor (DSM265) for prevention and treatment of malaria. *Science Translational Medicine* **2015,** 7.

38. Llanos-Cuentas, A.; Casapia, M.; Chuquiyauri, R.; Hinojosa, J. C.; Kerr, N.; Rosario, M.; Toovey, S.; Arch, R. H.; Phillips, M. A.; Rozenberg, F. D.; Bath, J.; Ng, C. L.; Cowell, A. N.; Winzeler, E. A.; Fidock, D. A.; Baker, M.; Mohrle, J. J.; van Huijsduijnen, R. H.; Gobeau, N.; Araeipour, N.; Andenmatten, N.; Ruckle, T.;

Duparc, S. Antimalarial activity of single-dose DSM265, a novel *Plasmodium* dihydroorotate dehydrogenase inhibitor, in patients with uncomplicated *Plasmodium falciparum* or *Plasmodium vivax* malaria infection: a proof-of-concept, open-label, phase 2a study. *Lancet Infectious Diseases* **2018,** 18, 874-883.

39. Baldwin, J.; Farajallah, A. M.; Malmquist, N. A.; Rathod, P. K.; Phillips, M. A. Malarial dihydroorotate dehydrogenase. *Journal of Biological Chemistry* **2002,** 277, 41827-41834.

40. Bjornberg, O.; Rowland, P.; Larsen, S.; Jensen, K. F. Active site of dihydroorotate dehydrogenase A from *Lactococcus lactis* investigated by chemical modification and mutagenesis. *Biochemistry* **1997,** 36, 16197-16205.

41. Sørensen, P.; Dandanell, G. A new type of dihydroorotate dehydrogenase, type 1S, from the thermoacidophilic archaeon *Sulfolobus solfataricus*. *Extremophiles* **2002,** 6, 245-251.

42. Liu, S. P.; Neidhardt, E. A.; Grossman, T. H.; Ocain, T.; Clardy, J. Structures of human dihydroorotate dehydrogenase in complex with antiproliferative agents. *Structure with Folding & Design* **2000,** 8, 25-33.

43. Norager, S.; Jensen, K. F.; Bjornberg, O.; Larsen, S. *E. coli* dihydroorotate dehydrogenase reveals structural and functional distinctions between different classes of dihydroorotate dehydrogenases. *Structure* **2002,** 10, 1211-1223.

44. Couto, S. G.; Nonato, M. C.; Costa, A. J. Site directed spin labeling studies of *Escherichia coli* dihydroorotate dehydrogenase N-terminal extension. *Biochemical and Biophysical Research Communications* **2011,** 414, 487-492.

45. Couto, S. G.; Nonato, M. C.; Costa-Filho, A. J. Defects in vesicle core induced by *Escherichia coli* dihydroorotate dehydrogenase. *Biophysical Journal* **2008,** 94, 1746-1753.

46. Nielsen, F. S.; Andersen, P. S.; Jensen, K. F. The B form of dihydroorotate dehydrogenase from *Lactococcus lactis* consists of two different subunits, encoded by the pyrDb and pyrK genes, and contains FMN, FAD, and [FeS] redox centers. *Journal of Biological Chemistry* **1996,** 271, 29359-29365.

47. Rowland, P.; Norager, S.; Jensen, K. F.; Larsen, S. Structure of dihydroorotate dehydrogenase B: Electron transfer between two flavin groups bridged by an iron-sulphur cluster. *Structure* **2000,** 8, 1227-1238.

48. Jones, M. E. Pyrimidine Nucleotide Biosynthesis in Animals - Genes, Enzymes, and Regulation of Ump Biosynthesis. *Annual Review of Biochemistry* **1980,** 49, 253-279.

49. Reis, R. A. G.; Calil, F. A.; Feliciano, P. R.; Pinheiro, M. P.; Nonato, M. C. The dihydroorotate dehydrogenases: Past and present. *Arch Biochem Biophys* **2017,** 632, 175-191.

50. Hines, V.; Keys, L. D., 3rd; Johnston, M. Purification and properties of the bovine liver mitochondrial dihydroorotate dehydrogenase. *Journal of Biological Chemistry* **1986,** 261, 11386-92.

51. Knecht, W.; Bergjohann, U.; Gonski, S.; Kirschbaum, B.; Loffler, M. Functional expression of a fragment of human dihydroorotate dehydrogenase by means of the baculovirus expression vector system, and kinetic investigation of the purified recombinant enzyme. *Eur J Biochem* **1996,** 240, 292-301.

52. Davis, J. P.; Cain, G. A.; Pitts, W. J.; Magolda, R. L.; Copeland, R. A. The immunosuppressive metabolite of leflunomide is a potent inhibitor of human dihydroorotate dehydrogenase. *Biochemistry* **1996,** 35, 1270-3.

53. Deng, X.; Kokkonda, S.; El Mazouni, F.; White, J.; Burrows, J. N.; Kaminsky, W.; Charman, S. A.; Matthews, D.; Rathod, P. K.; Phillips, M. A. Fluorine modulates species selectivity in the triazolopyrimidine class of *Plasmodium falciparum* dihydroorotate dehydrogenase inhibitors. *J Med Chem* **2014,** 57, 5381-94.

54. Phillips, M. A.; Rathod, P. K. *Plasmodium* dihydroorotate dehydrogenase: a promising target for novel anti-malarial chemotherapy. *Infect Disord Drug Targets* **2010,** 10, 226-39.

55. Azeredo, L. F.; Coutinho, J. P.; Jabor, V. A. P.; Feliciano, P. R.; Nonato, M. C.; Kaiser, C. R.; Menezes, C. M. S.; Hammes, A. S. O.; Caffarena, E. R.; Hoelz, L. V. B.; de Souza, N. B.; Pereira, G. A. N.; Ceravolo, I. P.; Krettli, A. U.; Boechat, N. Evaluation of 7-arylaminopyrazolo[1,5-a]pyrimidines as anti-*Plasmodium falciparum*, antimalarial, and Pf-dihydroorotate dehydrogenase inhibitors. *Eur J Med Chem* **2017,** 126, 72-83.

56. Maetani, M.; Kato, N.; Jabor, V. A. P.; Calil, F. A.; Nonato, M. C.; Scherer, C. A.; Schreiber, S. L. Discovery of Antimalarial Azetidine-2-carbonitriles That Inhibit *P. falciparum* Dihydroorotate Dehydrogenase. *ACS Med Chem Lett* **2017,** 8, 438-442.

57. Caballero, I.; Lafuente, M. J.; Gamo, F. J.; Cid, C. A high-throughput fluorescence-based assay for *Plasmodium* dihydroorotate dehydrogenase inhibitor screening. *Anal Biochem* **2016,** 506, 13-21.

58. Horak, P.; Kolarova, L. Bird schistosomes: do they die in mammalian skin? *Trends in Parasitology* **2001,** 17, 66-69.

59. Martins, D. D.; Xavier, M. F.; Masiero, F. D.; Cordeiro, J.; Thyssen, P. J. Schistosomiasis in Southern Brazil 17 years after the confirmation of the first autochthonous case. *Revista Da Sociedade Brasileira De Medicina Tropical* **2015,** 48, 354-357.

60. Ferrari, T. C. A.; Moreira, P. R. R. Neuroschistosomiasis: clinical symptoms and pathogenesis. *Lancet Neurology* **2011,** 10, 853-864.

61. Zhang, S.-M.; Coultas, K. A. Identification of plumbagin and sanguinarine as effective chemotherapeutic agents for treatment of schistosomiasis. *International Journal for Parasitology, Drugs and Drug Resistance* **2013,** 3, 28-34.

62. Blach, O.; Rai, B.; Oates, K.; Franklin, G.; Bramwell, S. An outbreak of schistosomiasis in travellers returning from endemic areas: the importance of rigorous tracing in peer groups exposed to risk of infection. *Journal of Public Health* **2012,** 34, 32-36.

63. Redman, C.; Spence, G.; Smith, H.; Smith, K. Travel medicine: schistosomiasis in Scotland 2005 – 2009. *HPS Surveill Rep* **2010,** 44, 24-26.

64. Boissier, J.; Moné, H.; Mitta, G.; Bargues, M. D.; Molyneux, D.; Mas-Coma, S. Schistosomiasis reaches Europe. *The Lancet Infectious Diseases* **2015,** 15, 757-758.

65. Antoine, B.; Hélène, M.; Xavier, I.; Gabriel, M.; Olivier, A.; Jérôme, B.; Judith, F.; Sophie, C.; Cécile, D.; Alexis, V.; Guillaume, M.; André, T.; Jean-François, M. Schistosomiasis Haematobium, Corsica, France. *Emerging Infectious Disease journal* **2014,** 20, 1595.

66. Pan, X.; Zhou, Y.-B.; Yang, Y.; Song, X.-X.; Jiang, Q.-W. Epidemic characteristics and security implications of Africa schistosomiasis on people who go to Africa. *Chin J Schisto Control* **2015,** 27, 436-439.

67. CDC. Schistosomiasis: about schistosomiasis: biology. https://www.cdc.gov/parasites/schistosomiasis/biology.html (September 2018).

68. Tucker, M. S.; Karunaratne, L. B.; Lewis, F. A.; Freitas, T. C.; Liang, Y.-s. Schistosomiasis. *Current protocols in immunology* **2001,** 19, 1-80.

69. de Souza, F. P. C.; Vitorino, R. R.; Costa, A. d. P.; de Faria Jr., F. C.; Santana, L. A.; Gomes, A. P. Esquistossomose mansônica: aspectos gerais, imunologia, patogênese e história natural. *Revista da Sociedade Brasileira de Clínica Médica* **2011**, 300-307.

70. Pinto-Almeida, A.; Mendes, T.; Armada, A.; Belo, S.; Carrilho, E.; Viveiros, M.; Afonso, A. The Role of Efflux Pumps in *Schistosoma mansoni* Praziquantel Resistant Phenotype. *PLoS One* **2015,** 10, e0140147.

71. Aoki, T.; Oya, H. Glutamine-dependent carbamoyl-phosphate synthetase and control of pyrimidine biosynthesis in the parasitic helminth *Schistosoma mansoni*. *Comparative Biochemistry and Physiology Part B: Comparative Biochemistry* **1979,** 63, 511-515.

72. Hill, B.; Kilsby, J.; Rogerson, G. W.; McIntosh, R. T.; Ginger, C. D. The enzymes of pyrimidine biosynthesis in a range of parasitic protozoa and helminths. *Molecular and Biochemical Parasitology* **1981,** 2, 123-134.

73. El Kouni, M. H.; Naguib, F. N. M. Pyrimidine salvage pathways in adult *Schistosoma mansoni*. *International Journal for Parasitology* **1990,** 20, 37-44.

74. Jaffe, J. J.; McCormack, J. J.; Meymarian, E. Comparative properties of schistosomal and filarial dihydrofolate reductases. *Biochemical Pharmacology* **1972,** 21, 719-731.

75. Jaffe, J. J. Dihydrofolate Reductase From Filarial Worms and Schistosomes. *Annals of the New York Academy of Sciences* **1971,** 186, 113-114.

76. Christopherson, R. I.; Lyons, S. D.; Wilson, P. K. Inhibitors of de Novo Nucleotide Biosynthesis as Drugs. *Accounts of Chemical Research* **2002,** 35, 961-971.

77. Jöckel, J.; Wendt, B.; Löffler, M. Structural and functional comparison of agents interfering with dihydroorotate, succinate and NADH oxidation of rat liver mitochondria. *Biochemical Pharmacology* **1998,** 56, 1053-1060.

78. Ittarat, I.; Asawamahasakda, W.; Bartlett, M. S.; Smith, J. W.; Meshnick, S. R. Effects of atovaquone and other inhibitors on *Pneumocystis carinii* dihydroorotate dehydrogenase. *Antimicrobial Agents and Chemotherapy* **1995,** 39, 325-8.

79. Corpet, F. Multiple sequence alignment with hierarchical clustering. *Nucleic Acids Research* **1988,** 16, 10881-10890.

80. Robert, X.; Gouet, P. Deciphering key features in protein structures with the new ENDscript server. *Nucleic Acids Research* **2014,** 42, W320-W324.

81. Hansen, M.; Le Nours, J.; Johansson, E.; Antal, T.; Ullrich, A.; Löffler, M.; Larsen, S. Inhibitor binding in a class 2 dihydroorotate dehydrogenase causes variations in the membrane-associated N-terminal domain. *Protein Science : A Publication of the Protein Society* **2004,** 13, 1031-1042.

82. Pinto, A. V.; Pinto, M. d. C. R.; Gilbert, B.; Pellegrino, J.; Mello, R. T. Schistosomiasis mansoni: blockage of cercarial skin penetration by chemical agents: I. naphthoquinones and derivatives. *Transactions of The Royal Society of Tropical Medicine and Hygiene* **1977,** 71, 133-135.

83. Cichewicz, R. H.; Lim, K.-C.; McKerrow, J. H.; Nair, M. G. Kwanzoquinones A–G and other constituents of Hemerocallis fulva 'Kwanzo' roots and their activity against the human pathogenic trematode *Schistosoma mansoni*. *Tetrahedron* **2002,** 58, 8597-8606.

84. Neves, B.; Andrade, C.; Cravo, P. Natural Products as Leads in Schistosome Drug Discovery. *Molecules* **2015,** 20, 1872.

85. Lima, N. M. F.; dos Santos, A. F.; Porfírio, Z.; Goulart, M. l. O. F.; Sant'Ana, A. E. G. Toxicity of lapachol and isolapachol and their potassium salts against *Biomphalaria glabrata*, *Schistosoma mansoni* cercariae, *Artemia salina* and *Tilapia nilotica*. *Acta Tropica* **2002,** 83, 43-47.

86. Costacurta, J. S. D. Caracterização bioquímica, biofísica e estudos inibitórios da enzima diidroorotate desidrogenase de *Schistosoma mansoni*. Universidade de São Paulo, Brasil, 2014.

87. Nonato, M. C.; Pádua, R. A. P.; David, J. S.; Reis, R. A. G.; Tomaleri, G. P.; Pereira, H. D. M.; Calil, F. A. Structural basis for the design of selective inhibitors for *Schistosoma mansoni* dihydroorotate dehydrogenase. *Biochimie* **2018,** (to be published).

88. Marti-Renom, M. A.; Stuart, A. C.; Fiser, A.; Sanchez, R.; Melo, F.; Sali, A. Comparative protein structure modeling of genes and genomes. *Annual Review of Biophysics and Biomolecular Structure* **2000,** 29, 291-325.

89. Commons. Overlap Extension PCR. https://commons.wikimedia.org/wiki/File:Overlap_Extension_PCR.png (September 2018).

90. Navarro, M. V.; De, N.; Bae, N.; Wang, Q.; Sondermann, H. Structural analysis of the GGDEF-EAL domain-containing c-di-GMP receptor FimX. *Structure* **2009,** 17, 1104-16.

91. Woody, R. W. Circular Dichroism of Intrinsically Disordered Proteins. In *Instrumental Analysis of Intrinsically Disordered Proteins: Assessing Structure and Conformation*, Uversky, V. N.; Longhi, S., Eds. Wiley New Jersey, USA, 2010; pp 303-321.

92. Greenfield, N.; Fasman, G. D. Computed circular dichroism spectra for the evaluation of protein conformation. *Biochemistry* **1969,** 8, 4108-16.

93. Jancarik, J.; Kim, S. H. Sparse-matrix sampling - A screening method for crystallization of proteins. *Journal of Applied Crystallography* **1991,** 24, 409-411.

94. Dejani, N. N.; Souza, L. C.; Oliveira, S. R.; Neris, D. M.; Rodolpho, J. M.; Correia, R. O.; Rodrigues, V.; Sacramento, L. V.; Faccioli, L. H.; Afonso, A.; Anibal, F. F. Immunological and parasitological parameters in *Schistosoma mansoni*-infected mice treated with crude extract from the leaves of Mentha x piperita L. *Immunobiology* **2014,** 219, 627-32.

95. Offredi, F.; Dubail, F.; Kischel, P.; Sarinski, K.; Stern, A. S.; Van de Weerdt, C.; Hoch, J. C.; Prosperi, C.; Francois, J. M.; Mayo, S. L.; Martial, J. A. De novo backbone and sequence design of an idealized alpha/beta-barrel protein: evidence of stable tertiary structure. *J Mol Biol* **2003,** 325, 163-74.

96. Nagarajan, D.; Deka, G.; Rao, M. Design of symmetric TIM barrel proteins from first principles. *BMC Biochem* **2015,** 16, 18.

97. Louis-Jeune, C.; Andrade-Navarro, M. A.; Perez-Iratxeta, C. Prediction of protein secondary structure from circular dichroism using theoretically derived spectra. *Proteins* **2012,** 80, 374-81.

98. Miles, A. J.; Wallace, B. A. Circular dichroism spectroscopy of membrane proteins. *Chem Soc Rev* **2016,** 45, 4859-72.

99. Niesen, F. H.; Berglund, H.; Vedadi, M. The use of differential scanning fluorimetry to detect ligand interactions that promote protein stability. *Nat Protoc* **2007,** 2, 2212-21.

100. Pantoliano, M. W.; Petrella, E. C.; Kwasnoski, J. D.; Lobanov, V. S.; Myslik, J.; Graf, E.; Carver, T.; Asel, E.; Springer, B. A.; Lane, P.; Salemme, F. R. High-density miniaturized thermal shift assays as a general strategy for drug discovery. *J Biomol Screen* **2001,** 6, 429-40.

101. Lo, M. C.; Aulabaugh, A.; Jin, G.; Cowling, R.; Bard, J.; Malamas, M.; Ellestad, G. Evaluation of fluorescence-based thermal shift assays for hit identification in drug discovery. *Anal Biochem* **2004,** 332, 153-9.

102. Pádua, R. A. P.; Tomaleri, G. P.; Reis, R. A. G.; David, J. S.; Silva, V. C.; Pinheiro, M. P.; Nonato, M. C. ThermoFMN - a thermofluor assay developed for ligand-screening as an alternative strategy for drug discovery. *Journal of the Brazilian Chemical Society* **2014,** 25, 1864-1871.

103. Sanderson, L.; Bartlett, A.; Whitfield, P. J. In vitro and in vivo studies on the bioactivity of a ginger (*Zingiber officinale*) extract towards adult schistosomes and their egg production. *J Helminthol* **2002,** 76, 241-7.

104. Moraes, J.; Nascimento, C.; Lopes, P. O.; Nakano, E.; Yamaguchi, L. F.; Kato, M. J.; Kawano, T. *Schistosoma mansoni*: *In vitro* schistosomicidal activity of piplartine. *Exp Parasitol* **2011,** 127, 357-64.

105. WHO. *World Malaria Report 2017*; World Health Organization: Geneva, 2017.

106. Garcia, L. S. Malaria. *Clinics in Laboratory Medicine* **2010,** 30, 93-+.

107. Greenwood, B. M.; Bojang, K.; Whitty, C. J. M.; Targett, G. A. T. Malaria. *The Lancet* **2005,** 365, 1487-1498.

108. CDC. Malaria: about malaria: biology. https://www.cdc.gov/malaria/about/biology/index.html (September 2018).

109. Rappuoli, R.; Aderem, A. A 2020 vision for vaccines against HIV, tuberculosis and malaria. *Nature* **2011,** 473, 463-469.

110. O'Neill, P. M.; Barton, V. E.; Ward, S. A. The Molecular Mechanism of Action of Artemisinin-The Debate Continues. *Molecules* **2010,** 15, 1705-1721.

111. Seder, R. A.; Chang, L. J.; Enama, M. E.; Zephir, K. L.; Sarwar, U. N.; Gordon, I. J.; Holman, L. A.; James, E. R.; Billingsley, P. F.; Gunasekera, A.; Richman, A.; Chakravarty, S.; Manoj, A.; Velmurugan, S.; Li, M. L.; Ruben, A. J.; Li, T.; Eappen, A. G.; Stafford, R. E.; Plummer, S. H.; Hendel, C. S.; Novik, L.; Costner, P. J. M.; Mendoza, F. H.; Saunders, J. G.; Nason, M. C.; Richardson, J. H.; Murphy, J.; Davidson, S. A.; Richie, T. L.; Sedegah, M.; Sutamihardja, A.; Fahle, G. A.; Lyke, K. E.; Laurens, M. B.; Roederer, M.; Tewari, K.; Epstein, J. E.; Sim, B. K. L.; Ledgerwood, J. E.; Graham, B. S.; Hoffman, S. L.; Team, V. S. Protection Against Malaria by Intravenous Immunization with a Nonreplicating Sporozoite Vaccine. *Science* **2013,** 341, 1359-1365.

112. Raj, D. K.; Nixon, C. P.; Nixon, C. E.; Dvorin, J. D.; DiPetrillo, C. G.; Pond-Tor, S.; Wu, H. W.; Jolly, G.; Pischel, L.; Lu, A. L.; Michelow, I. C.; Cheng, L.; Conteh, S.; McDonald, E. A.; Absalon, S.; Holte, S. E.; Friedman, J. F.; Fried, M.; Duffy, P. E.; Kurtis, J. D. Antibodies to PfSEA-1 block parasite egress from RBCs and protect against malaria infection. *Science* **2014,** 344, 871-877.

113. Teixeira, C.; Vale, N.; Perez, B.; Gomes, A.; Gomes, J. R. B.; Gomes, P. "Recycling" Classical Drugs for Malaria. *Chemical Reviews* **2014,** 114, 11164-11220.

114. Wells, T. N.; Hooft van Huijsduijnen, R.; Van Voorhis, W. C. Malaria medicines: a glass half full? *Nature Reviews Drug Discovery* **2015,** 14, 424-42.

115. Kaur, K.; Jain, M.; Reddy, R. P.; Jain, R. Quinolines and structurally related heterocycles as antimalarials. *Eur J Med Chem* **2010,** 45, 3245-64.

116. Staines, H. M.; Krishna, S. *Treatment and Prevention of Malaria*. Springer: Basel, Switzerland, 2012.

117. Barnett, D. S.; Guy, R. K. Antimalarials in development in 2014. *Chemical Reviews* **2014,** 114, 11221-41.

118. Hurt, D. E.; Widom, J.; Clardy, J. Structure of *Plasmodium falciparum* dihydroorotate dehydrogenase with a bound inhibitor. *Acta Crystallogr D Biol Crystallogr* **2006,** 62, 312-23.

119. Ross, L. S.; Gamo, F. J.; Lafuente-Monasterio, M. J.; Singh, O. M.; Rowland, P.; Wiegand, R. C.; Wirth, D. F. In vitro resistance selections for *Plasmodium falciparum* dihydroorotate dehydrogenase inhibitors give mutants with multiple point mutations in the drug-binding site and altered growth. *Journal of Biological Chemistry* **2014,** 289, 17980-95.

120. Deng, X.; Gujjar, R.; El Mazouni, F.; Kaminsky, W.; Malmquist, N. A.; Goldsmith, E. J.; Rathod, P. K.; Phillips, M. A. Structural plasticity of malaria dihydroorotate dehydrogenase allows selective binding of diverse chemical scaffolds. *Journal of Biological Chemistry* **2009,** 284, 26999-7009.

121. Deng, X.; Matthews, D.; Rathod, P. K.; Phillips, M. A. The X-ray structure of *Plasmodium falciparum* dihydroorotate dehydrogenase bound to a potent and selective N-phenylbenzamide inhibitor reveals novel binding-site interactions. *Acta Crystallogr F Struct Biol Commun* **2015,** 71, 553-9.

122. Kokkonda, S.; Deng, X.; White, K. L.; Coteron, J. M.; Marco, M.; de Las Heras, L.; White, J.; El Mazouni, F.; Tomchick, D. R.; Manjalanagara, K.; Rudra, K. R.; Chen, G.; Morizzi, J.; Ryan, E.; Kaminsky, W.; Leroy, D.; Martinez-Martinez, M. S.; Jimenez-Diaz, M. B.; Bazaga, S. F.; Angulo-Barturen, I.; Waterson, D.; Burrows, J. N.; Matthews, D.; Charman, S. A.; Phillips, M. A.; Rathod, P. K. Tetrahydro-2-naphthyl and 2-Indanyl Triazolopyrimidines Targeting *Plasmodium falciparum* Dihydroorotate Dehydrogenase Display Potent and Selective Antimalarial Activity. *J Med Chem* **2016,** 59, 5416-31.

123. Phillips, M. A.; White, K. L.; Kokkonda, S.; Deng, X.; White, J.; El Mazouni, F.; Marsh, K.; Tomchick, D. R.; Manjalanagara, K.; Rudra, K. R.; Wirjanata, G.; Noviyanti, R.; Price, R. N.; Marfurt, J.; Shackleford, D. M.; Chiu, F. C.; Campbell, M.; Jimenez-Diaz, M. B.; Bazaga, S. F.; Angulo-Barturen, I.; Martinez, M. S.; Lafuente-Monasterio, M.; Kaminsky, W.; Silue, K.; Zeeman, A. M.; Kocken, C.; Leroy, D.; Blasco, B.; Rossignol, E.; Rueckle, T.; Matthews, D.; Burrows, J. N.; Waterson, D.; Palmer, M. J.; Rathod, P. K.; Charman, S. A. A Triazolopyrimidine-Based Dihydroorotate Dehydrogenase Inhibitor with Improved Drug-like Properties for Treatment and Prevention of Malaria. *ACS Infect Dis* **2016,** 2, 945-957.

124. Vonrhein, C.; Flensburg, C.; Keller, P.; Sharff, A.; Smart, O.; Paciorek, W.; Womack, T.; Bricogne, G. Data processing and analysis with the autoPROC toolbox. *Acta Crystallographica Section D-Biological Crystallography* **2011,** 67, 293-302.

125. Winn, M. D.; Ballard, C. C.; Cowtan, K. D.; Dodson, E. J.; Emsley, P.; Evans, P. R.; Keegan, R. M.; Krissinel, E. B.; Leslie, A. G. W.; McCoy, A.; McNicholas, S. J.; Murshudov, G. N.; Pannu, N. S.; Potterton, E. A.; Powell, H. R.; Read, R. J.; Vagin, A.; Wilson, K. S. Overview of the CCP4 suite and current developments. *Acta Crystallographica Section D-Biological Crystallography* **2011,** 67, 235-242.

126. Vagin, A. A.; Steiner, R. A.; Lebedev, A. A.; Potterton, L.; McNicholas, S.; Long, F.; Murshudov, G. N. REFMAC5 dictionary: organization of prior chemical knowledge and guidelines for its use. *Acta Crystallographica Section D-Biological Crystallography* **2004,** 60, 2184-2195.

127. Emsley, P.; Cowtan, K. Coot: model-building tools for molecular graphics. *Acta Crystallographica Section D-Biological Crystallography* **2004,** 60, 2126-2132.

APPENDICES

Figures S1. A) DCIP assay. In the enzymatic reaction coupled to DCIP, the first substrate DHO is oxidized to ORO, while the cofactor FMN is reduced to $FMNH_2$. The reoxidation of QH_2 into Q is stoichiometrically equivalent to reduction of DCIP (blue) to $DCIPH_2$ (colorless). This reaction is usually monitored spectrophotometrically at 600 nm. B) Reaction for the resazurin fluorescence intensity (FLINT) high-throughput assay. In the enzymatic reaction, first substrate DHO is oxidized to ORO, while the cofactor FMN is reduced to $FMNH_2$; then resazurin (blue), acting as second substrate, changes to resorufin, a pink highly fluorescent state measured at 590 nm.

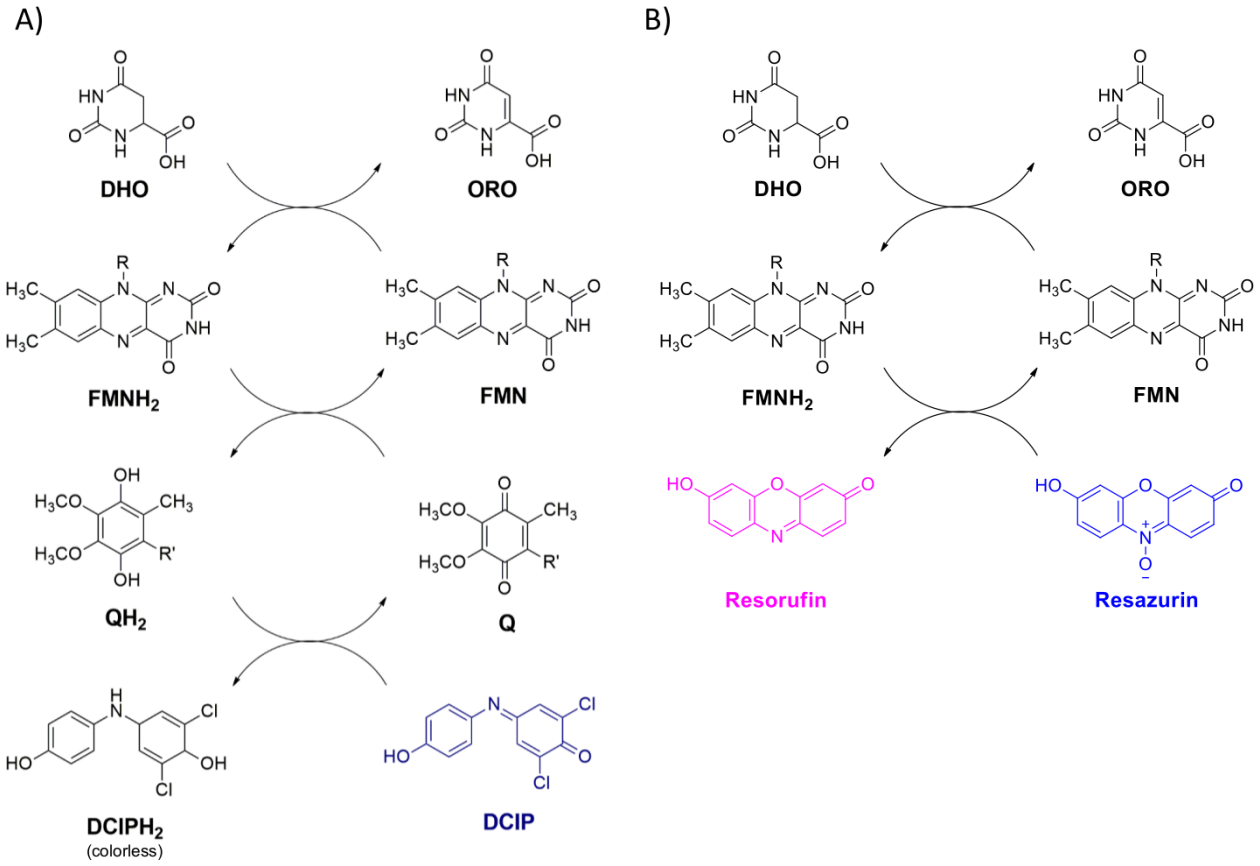

Figures S2 to S29. Graphs showing the log of the inhibitor concentration versus the percent of inhibition, for obtaining the compounds IC_{50} against ***Sm*DHODH**.

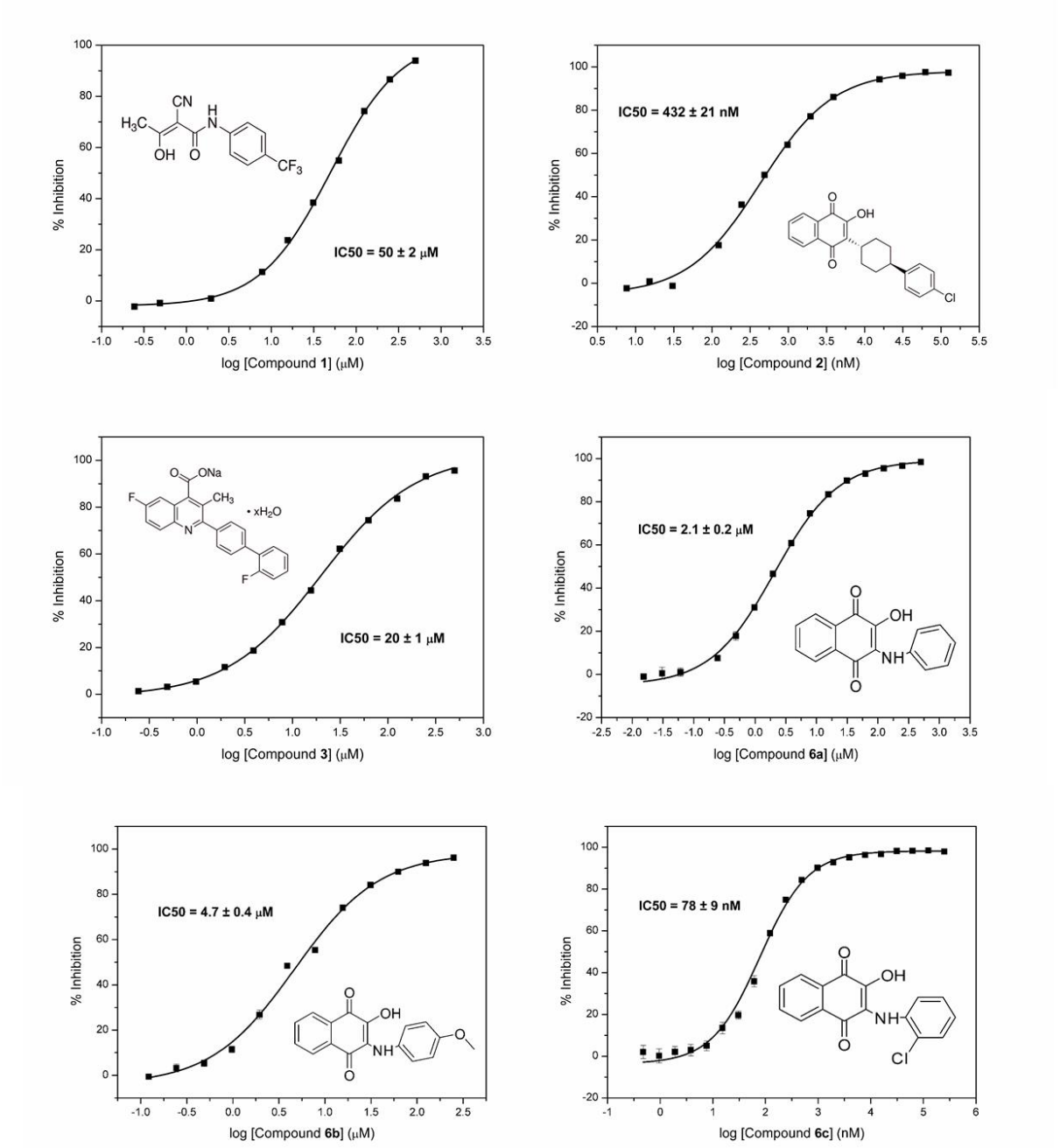

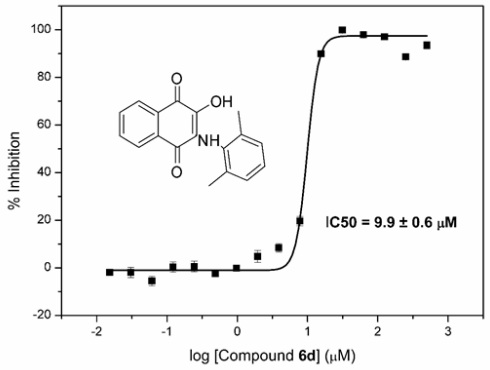
% Inhibition
log [Compound 6d] (μM)
IC50 = 9.9 ± 0.6 μM
O
OH
NH
O

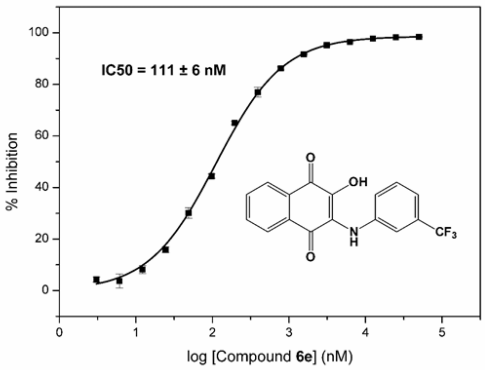
% Inhibition
log [Compound 6e] (nM)
IC50 = 111 ± 6 nM
O
OH
N
H
CF3

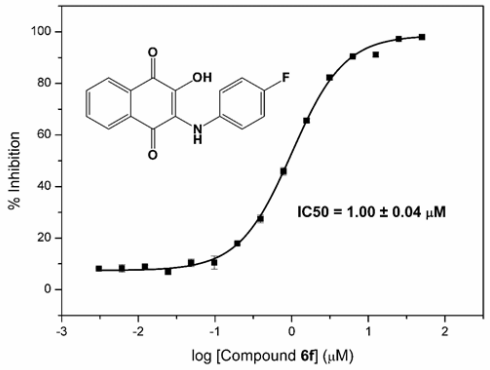
% Inhibition
log [Compound 6f] (μM)
IC50 = 1.00 ± 0.04 μM
O
OH
F
N
H

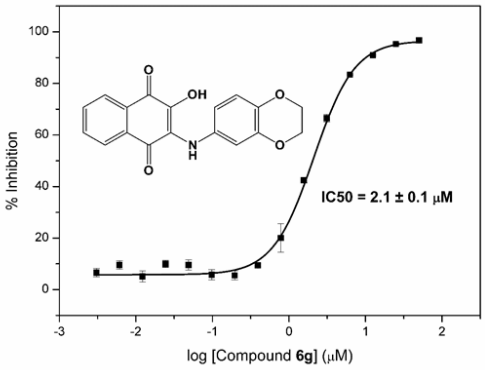
% Inhibition
log [Compound 6g] (μM)
IC50 = 2.1 ± 0.1 μM
O
OH
O
N
H

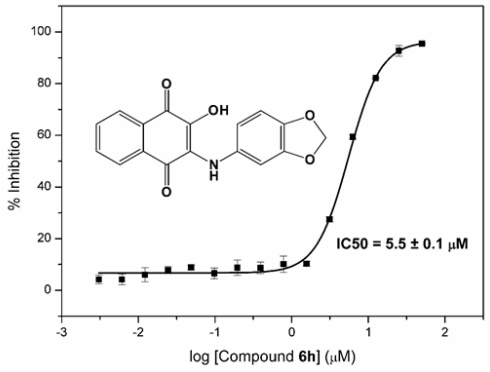
% Inhibition
log [Compound 6h] (μM)
IC50 = 5.5 ± 0.1 μM
O
OH
O
N
H

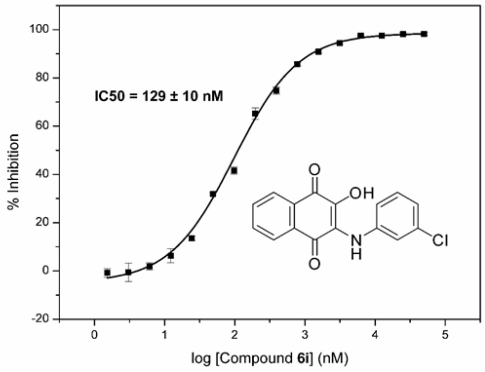
% Inhibition
log [Compound 6i] (nM)
IC50 = 129 ± 10 nM
O
OH
N
H
Cl

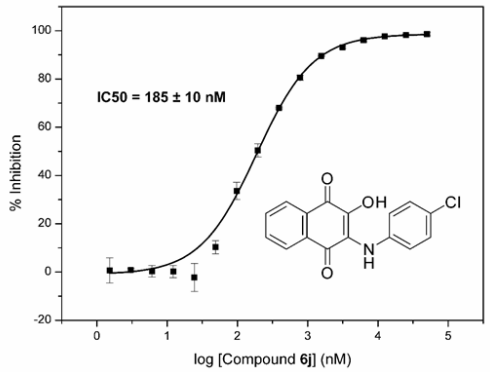
% Inhibition
log [Compound 6j] (nM)
IC50 = 185 ± 10 nM
O
OH
Cl
N
H

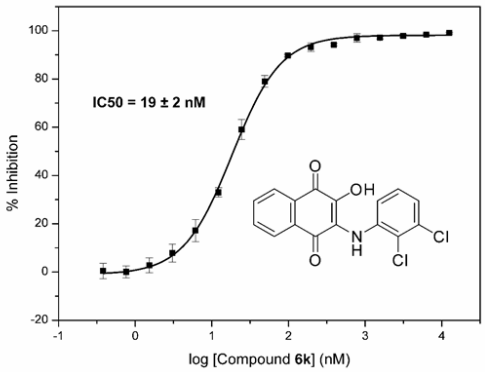
% Inhibition
log [Compound 6k] (nM)
IC50 = 19 ± 2 nM
O
OH
N
H
Cl
Cl

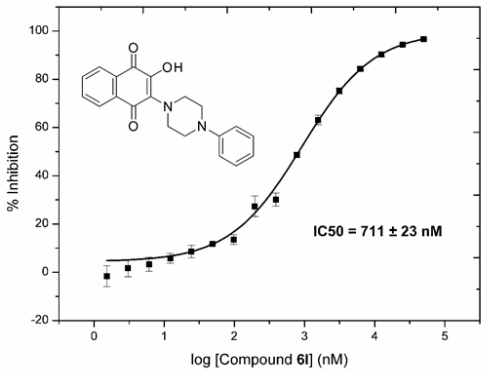
% Inhibition
log [Compound 6l] (nM)
IC50 = 711 ± 23 nM

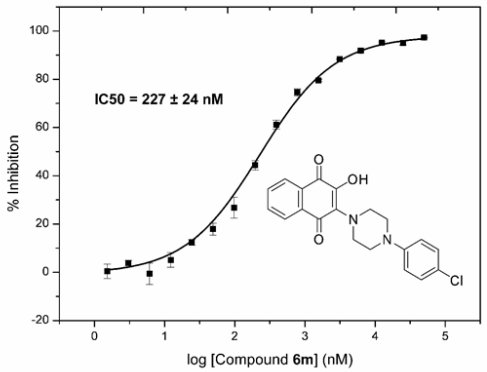
% Inhibition
log [Compound 6m] (nM)
IC50 = 227 ± 24 nM

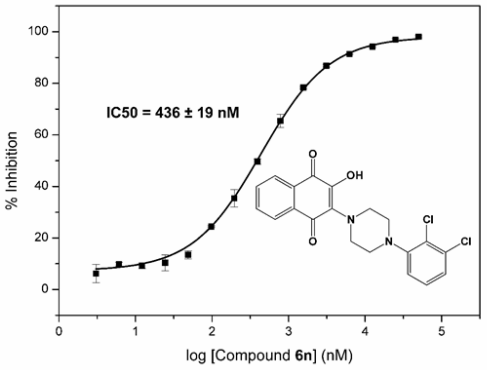
% Inhibition
log [Compound 6n] (nM)
IC50 = 436 ± 19 nM

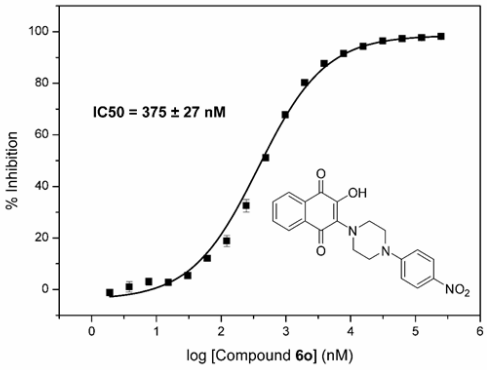
% Inhibition
log [Compound 6o] (nM)
IC50 = 375 ± 27 nM

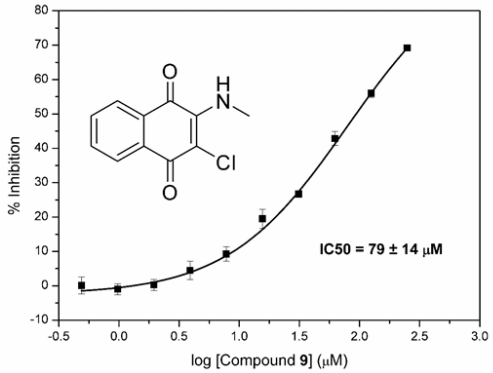
% Inhibition
log [Compound 9] (μM)
IC50 = 79 ± 14 μM

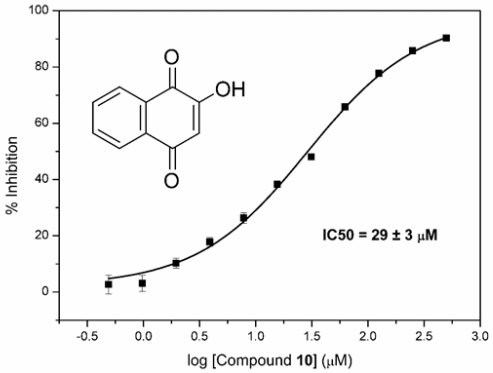
% Inhibition
log [Compound 10] (μM)
IC50 = 29 ± 3 μM

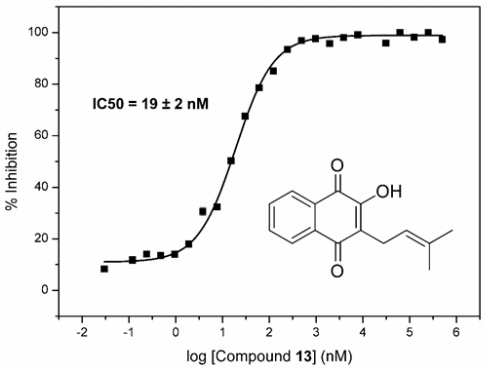
% Inhibition
log [Compound 13] (nM)
IC50 = 19 ± 2 nM

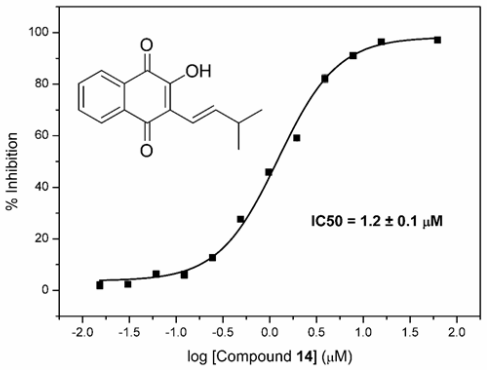
% Inhibition
log [Compound 14] (μM)
IC50 = 1.2 ± 0.1 μM

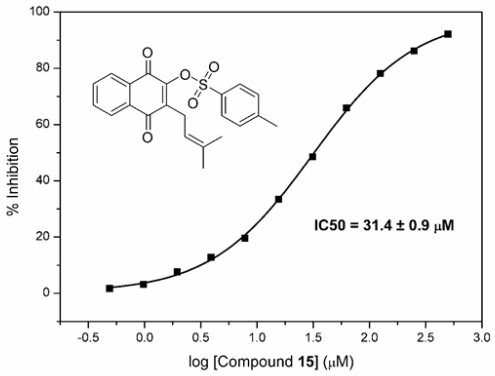
% Inhibition
log [Compound 15] (μM)
IC50 = 31.4 ± 0.9 μM

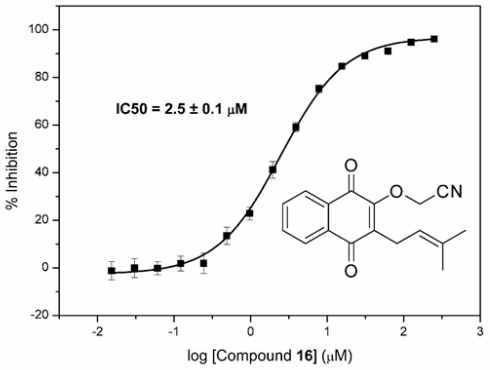
% Inhibition
log [Compound 16] (μM)
IC50 = 2.5 ± 0.1 μM
CN

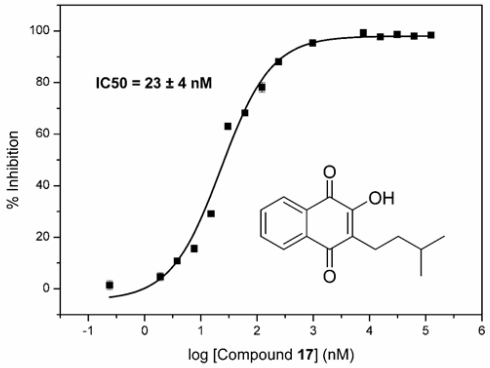
% Inhibition
log [Compound 17] (nM)
IC50 = 23 ± 4 nM
OH

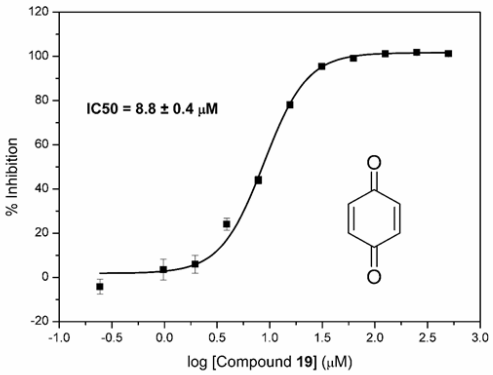
% Inhibition
log [Compound 19] (μM)
IC50 = 8.8 ± 0.4 μM

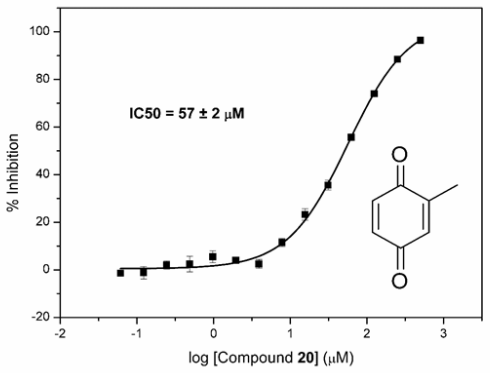
% Inhibition
log [Compound 20] (μM)
IC50 = 57 ± 2 μM

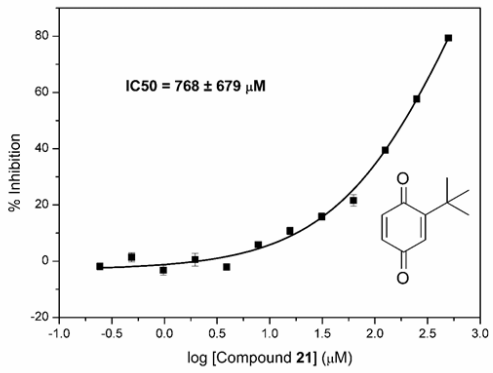
% Inhibition
log [Compound 21] (μM)
IC50 = 768 ± 679 μM

Figures S30 to S50. Graphs showing the log of the inhibitor concentration versus the percent of inhibition, for obtaining the compounds IC_{50} against ***Hs*DHODH**.

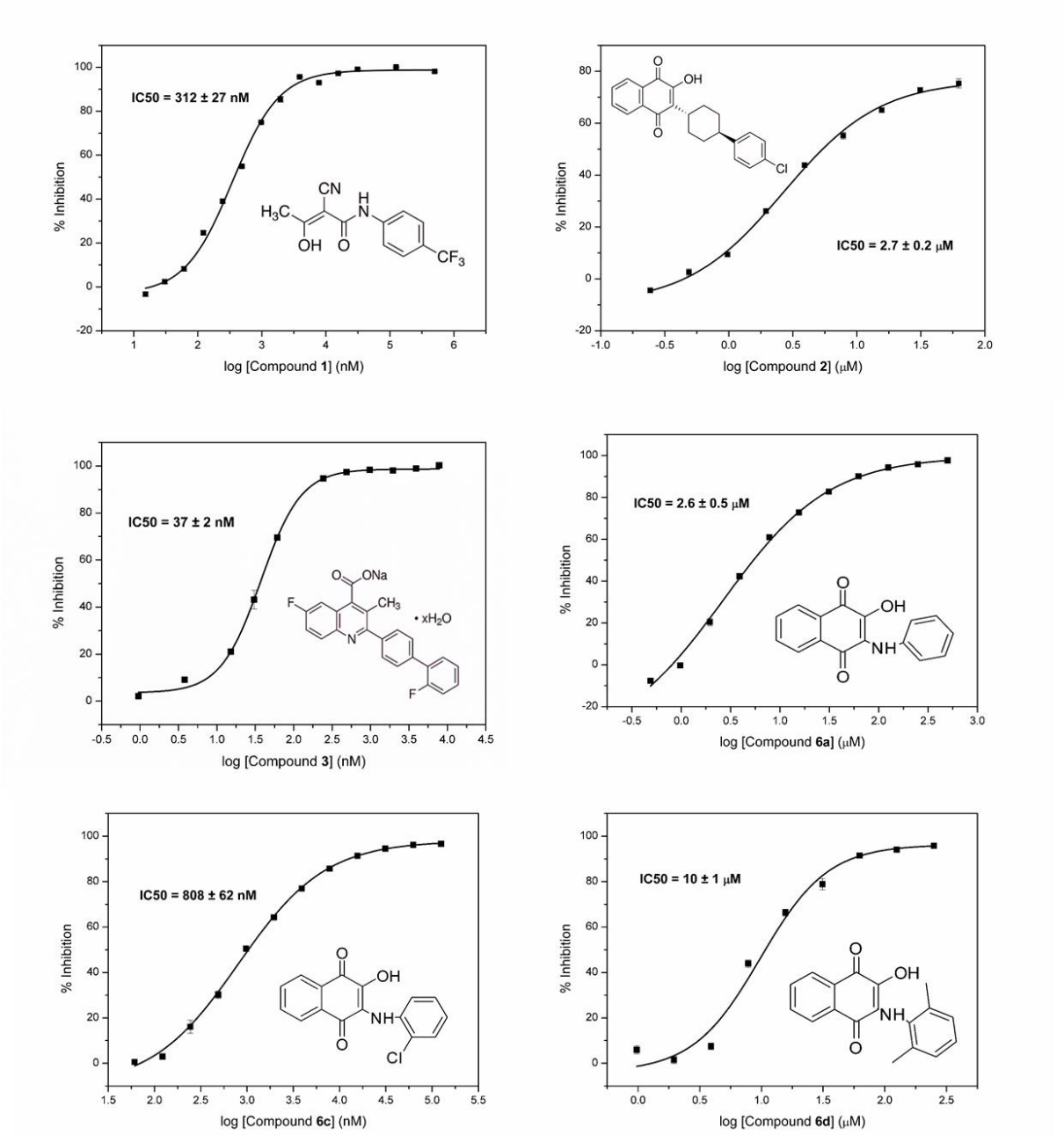

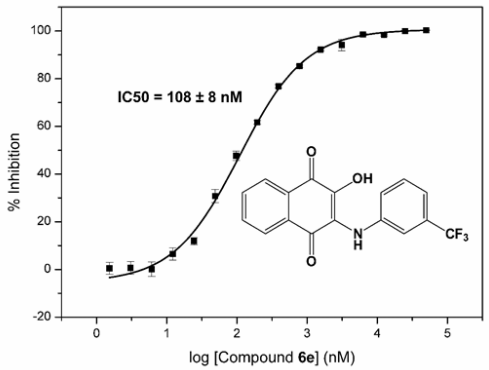
IC50 = 108 ± 8 nM
% Inhibition
log [Compound 6e] (nM)

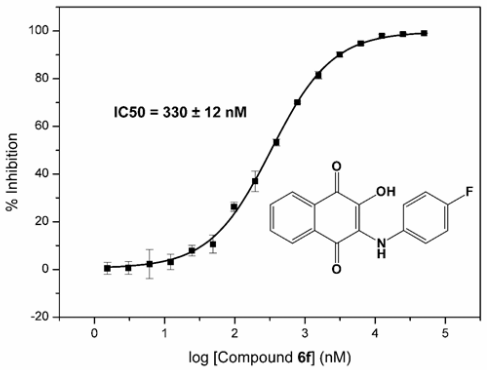
IC50 = 330 ± 12 nM
% Inhibition
log [Compound 6f] (nM)

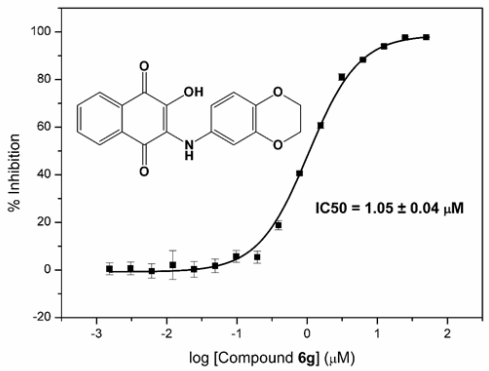
IC50 = 1.05 ± 0.04 μM
% Inhibition
log [Compound 6g] (μM)

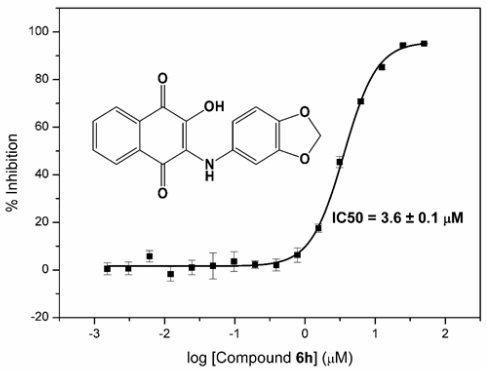
IC50 = 3.6 ± 0.1 μM
% Inhibition
log [Compound 6h] (μM)

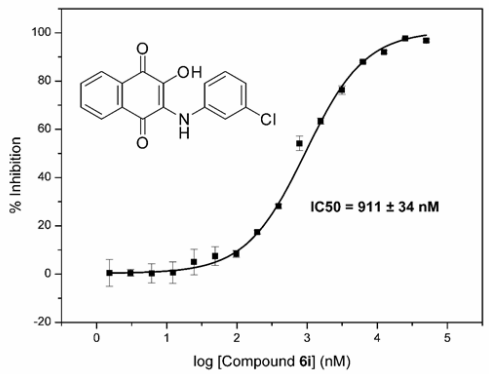
IC50 = 911 ± 34 nM
% Inhibition
log [Compound 6i] (nM)

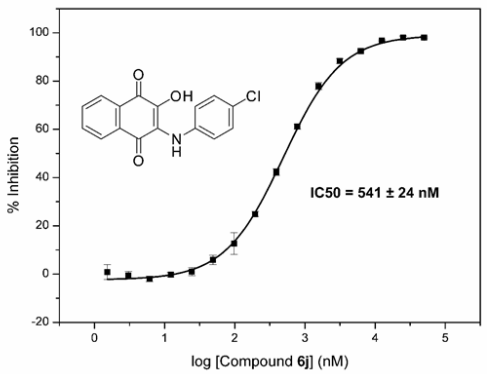
IC50 = 541 ± 24 nM
% Inhibition
log [Compound 6j] (nM)

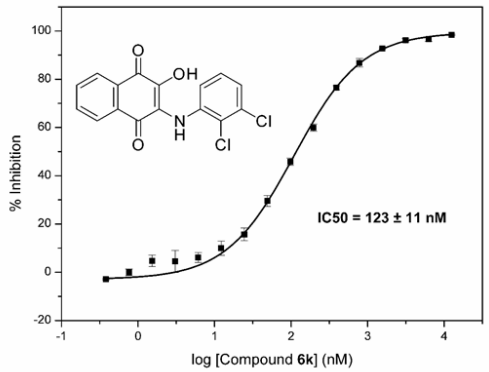
IC50 = 123 ± 11 nM
% Inhibition
log [Compound 6k] (nM)

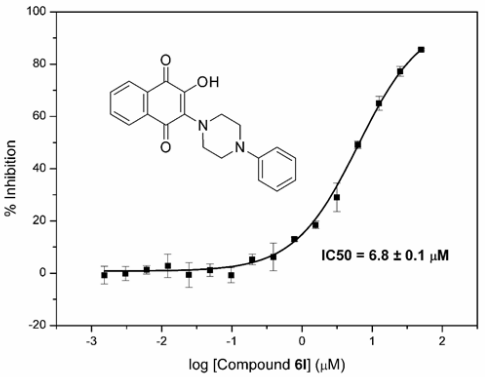
IC50 = 6.8 ± 0.1 μM
% Inhibition
log [Compound 6l] (μM)

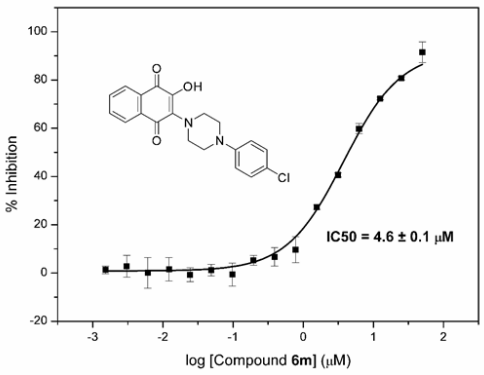
% Inhibition
log [Compound 6m] (μM)
IC50 = 4.6 ± 0.1 μM

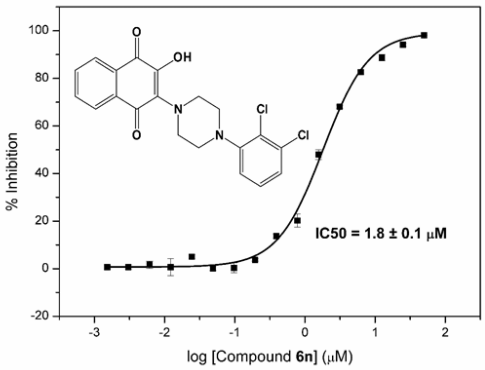
% Inhibition
log [Compound 6n] (μM)
IC50 = 1.8 ± 0.1 μM

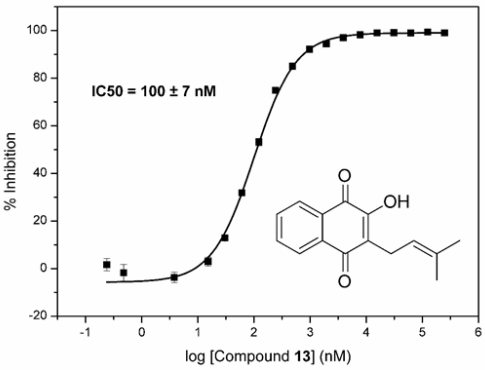
% Inhibition
log [Compound 13] (nM)
IC50 = 100 ± 7 nM

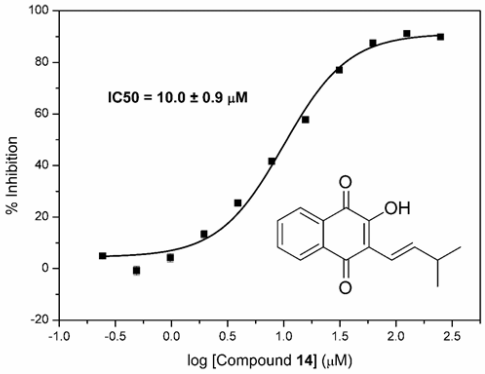
% Inhibition
log [Compound 14] (μM)
IC50 = 10.0 ± 0.9 μM

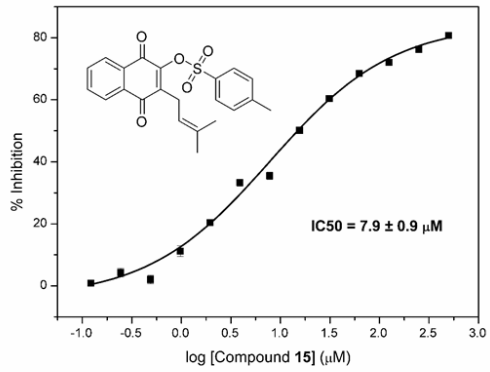
% Inhibition
log [Compound 15] (μM)
IC50 = 7.9 ± 0.9 μM

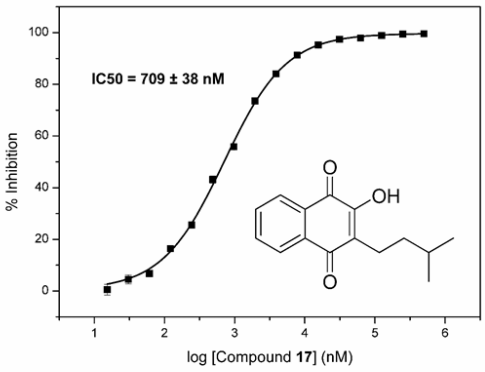
% Inhibition
log [Compound 17] (nM)
IC50 = 709 ± 38 nM

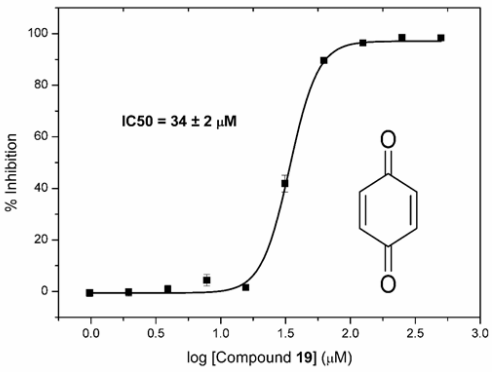
% Inhibition
log [Compound 19] (μM)
IC50 = 34 ± 2 μM

Figure S51. Graphs showing the mixed-type inhibition mechanism for Compound **2** against ***Sm*DHODH**. A) Michaelis-Menten hyperbolic fitting curve, B) Lineweaver-Burk linear fitting curve.

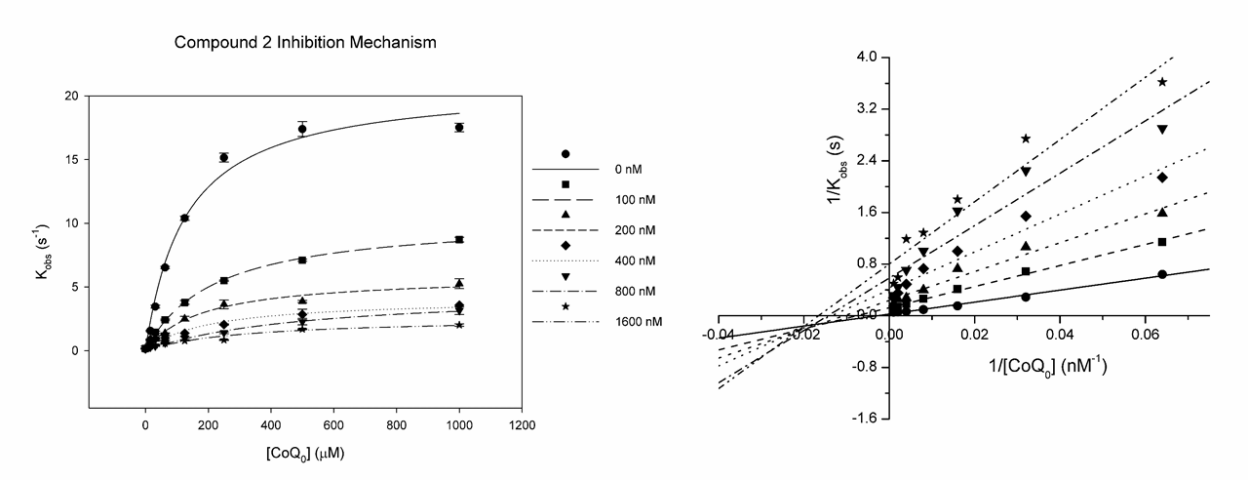

Figure S52. Graphs showing the noncompetitive inhibition mechanism for Compound **6c** against ***Sm*DHODH**. A) Michaelis-Menten hyperbolic fitting curve, B) Lineweaver-Burk linear fitting curve.

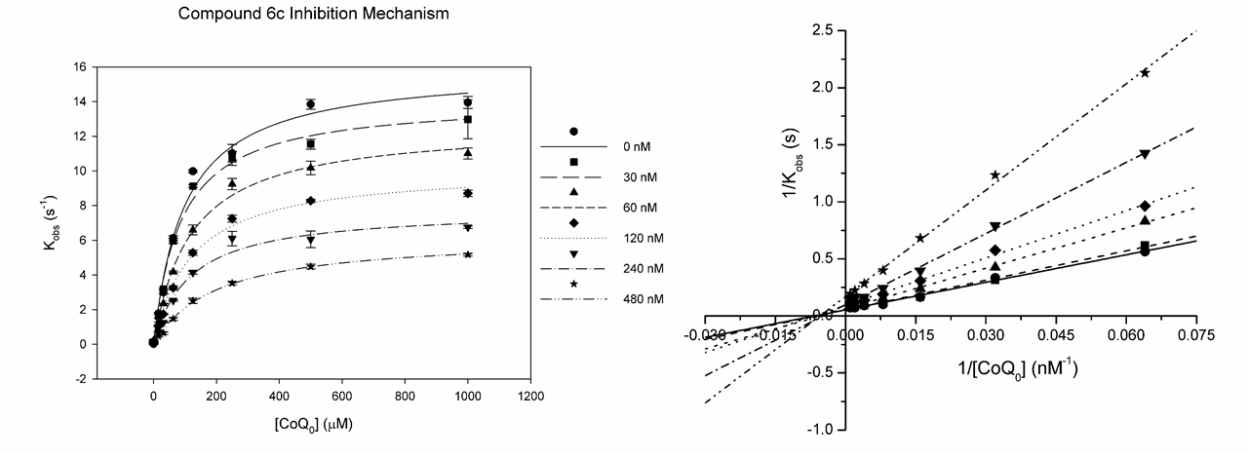

Figure S53. Graphs showing the noncompetitive inhibition mechanism for Compound **10** against ***Sm*DHODH**. A) Michaelis-Menten hyperbolic fitting curve, B) Lineweaver-Burk linear fitting curve.

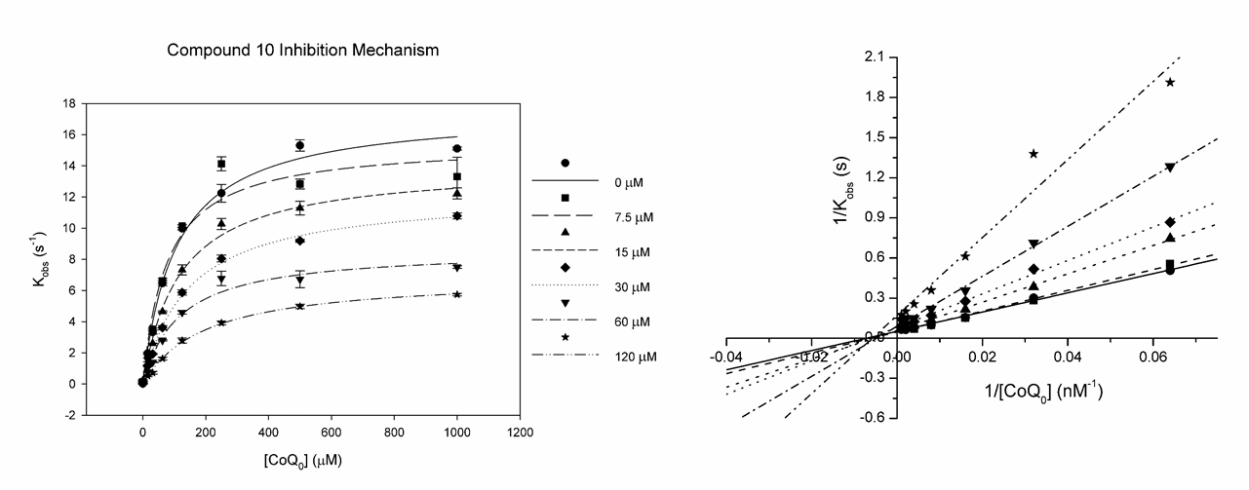

Figure S54. Graphs showing the noncompetitive inhibition mechanism for Compound **17** against ***Sm*DHODH**. A) Michaelis-Menten hyperbolic fitting curve, B) Lineweaver-Burk linear fitting curve.

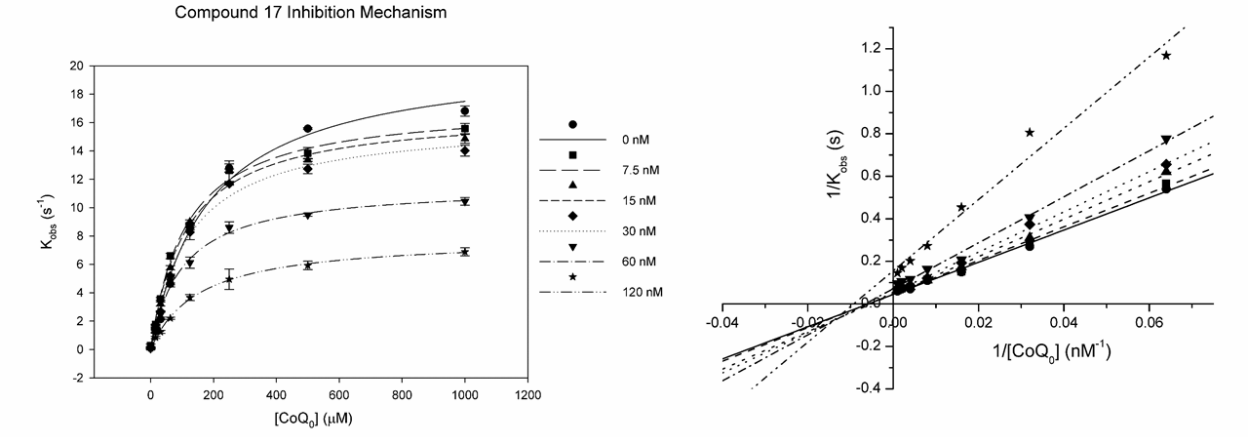

Figure S55. Graphs showing the competitive inhibition mechanism for Compound **19** against ***Sm*DHODH**. A) Michaelis-Menten hyperbolic fitting curve, B) Lineweaver-Burk linear fitting curve.

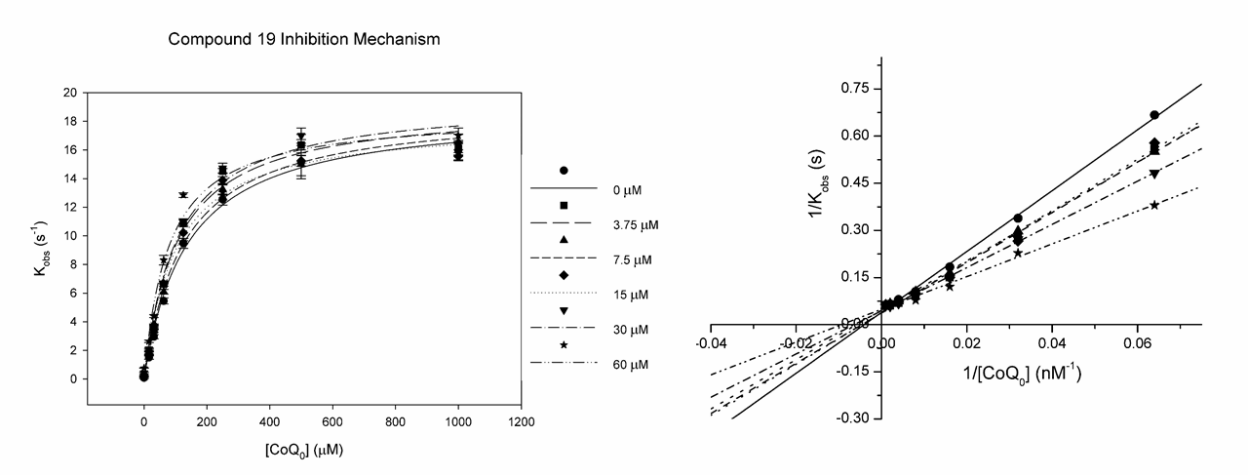

Figure S56. Graphs showing the noncompetitive inhibition mechanism for Compound **17** against ***Hs*DHODH**. A) Michaelis-Menten hyperbolic fitting curve, B) Lineweaver-Burk linear fitting curve.

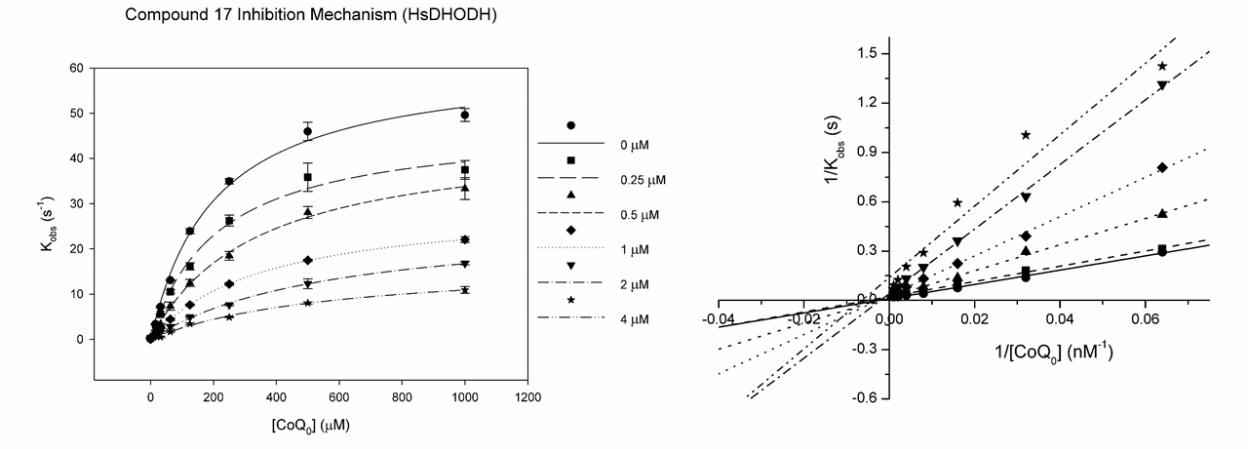

Table S1. Preliminary antischistosomicidal activity assay. Table shows each compound action against *Schistosoma mansoni* parasites incubated for 24, 48, 72 and 96 h. It was evaluated in the experiment: normal and altered motor activity, dead worms and with tegumental alterations.

Group	Sex	Incubation period (h)	Normal motor activity	Altered motor activity	Dead (no motor activity)	Tegument alterations
Control	♂	24h	2	1	0	1
	♀	24h	3	0	0	0
	♂	48h	2	1	0	1
	♀	48h	3	0	0	0
	♂	72h	2	0	1	1
	♀	72h	3	0	0	0
	♂	96h	3	0	0	0
	♀	96h	3	0	0	0
PZQ	♂	24h	0	3	0	3
	♀	24h	0	3	0	3
	♂	48h	0	3	0	3
	♀	48h	0	3	0	3
	♂	72h	0	2	1	3
	♀	72h	0	3	0	3
	♂	96h	0	2	1	3
	♀	96h	0	3	0	3
6c	♂	24h	2	1	0	1
	♀	24h	3	0	0	0
	♂	48h	2	1	0	1
	♀	48h	3	0	0	0
	♂	72h	2	0	1	2
	♀	72h	3	0	0	1
	♂	96h	2	0	1	3
	♀	96h	3	0	0	1
6i	♂	24h	3	0	0	0
	♀	24h	3	0	0	0
	♂	48h	3	0	0	3
	♀	48h	2	1	0	0
	♂	72h	2	1	0	3
	♀	72h	1	2	0	0
	♂	96h	2	1	0	3
	♀	96h	1	2	0	0

6j	♂	24h	1	1	1	1
	♀	24h	2	1	0	0
	♂	48h	1	1	1	1
	♀	48h	2	1	0	0
	♂	72h	2	0	1	1
	♀	72h	3	0	0	0
	♂	96h	2	0	1	1
	♀	96h	3	0	0	0
6k	♂	24h	3	0	0	2
	♀	24h	3	0	0	0
	♂	48h	0	3	0	2
	♀	48h	1	2	0	1
	♂	72h	0	3	0	3
	♀	72h	2	1	0	1
	♂	96h	0	3	0	3
	♀	96h	1	2	0	2
6l	♂	24h	2	1	0	1
	♀	24h	3	0	0	0
	♂	48h	0	2	1	2
	♀	48h	1	2	0	0
	♂	72h	1	1	1	2
	♀	72h	1	2	0	0
	♂	96h	1	1	1	2
	♀	96h	3	0	0	0
6m	♂	24h	2	1	0	2
	♀	24h	3	0	0	0
	♂	48h	1	2	0	2
	♀	48h	2	1	0	0
	♂	72h	0	3	0	3
	♀	72h	2	1	0	0
	♂	96h	2	1	0	3
	♀	96h	3	0	0	0
6n	♂	24h	1	2	0	1
	♀	24h	2	1	0	0
	♂	48h	1	2	0	2
	♀	48h	2	1	0	0
	♂	72h	0	3	0	3
	♀	72h	1	2	0	1
	♂	96h	0	3	0	3

	♀	96h	1	2	0	1
6o	♂	24h	2	1	0	0
	♀	24h	3	0	0	0
	♂	48h	2	1	0	2
	♀	48h	2	1	0	1
	♂	72h	0	3	0	3
	♀	72h	0	3	0	1
	♂	96h	0	3	0	3
	♀	96h	0	3	0	1
13	♂	24h	0	3	0	3
	♀	24h	1	2	0	1
	♂	48h	0	3	0	3
	♀	48h	2	1	0	1
	♂	72h	1	2	0	3
	♀	72h	1	2	0	1
	♂	96h	0	3	0	3
	♀	96h	1	2	0	1
14	♂	24h	3	0	0	1
	♀	24h	3	0	0	0
	♂	48h	3	0	0	3
	♀	48h	2	1	0	0
	♂	72h	3	0	0	3
	♀	72h	3	0	0	1
	♂	96h	2	1	0	3
	♀	96h	2	1	0	1
17	♂	24h	0	3	0	3
	♀	24h	2	1	0	3
	♂	48h	2	1	0	3
	♀	48h	1	2	0	3
	♂	72h	2	1	0	3
	♀	72h	0	3	0	3
	♂	96h	0	3	0	3
	♀	96h	0	3	0	3

The effects of the compounds on motor activity and tegumental alterations of adult *S. mansoni* were assessed qualitatively and were monitored under a microscope.

[a] Numbers relative to the 3 worms investigated.

[b] 0.5% DMSO.

[c] Tested at concentration of 5 µM.

Table S2. Antimalarial compounds tested in the screening against *Sm*DHODH and their respective codes, molecular weight (Da) and percent of activity. The tested concentration for all compounds was 10 µM. The compounds that presented inhibition higher than 80% are highlighted in bold.

Sample code	Molecular weight (Da)	Activity ± SD (%)
BRD-K58428023-001-01-0	407.50	88 ± 2
BRD-K09844503-001-01-7	375.44	100 ± 3
BRD-K22341231-001-01-6	361.41	90 ± 2
BRD-K39518306-001-01-0	396.46	51 ± 1
BRD-K16069580-001-01-8	385.41	25 ± 1
BRD-K07841005-001-01-8	433.48	95 ± 5
BRD-K97096726-001-01-8	416.45	92 ± 5
BRD-K45769386-001-01-4	391.40	108 ± 2
BRD-K23699180-001-01-7	355.43	89 ± 2
BRD-K00645693-001-01-7	357.41	105 ± 2
BRD-K08992380-001-01-3	415.41	95 ± 4
BRD-K36481331-001-01-3	401.38	82 ± 4
BRD-K37282083-001-01-4	415.49	22 ± 1
BRD-K83277066-001-01-8	409.48	27 ± 1
BRD-K39501364-001-01-5	398.46	46 ± 1
BRD-K33197954-001-01-4	**409.43**	**15 ± 1**
BRD-K45045373-001-01-4	388.46	101 ± 4
BRD-K69414340-001-01-3	441.52	20.4 ± 0.1
BRD-K37426825-001-01-0	329.23	98 ± 1
BRD-K38930348-001-01-8	403.37	98.9 ± 0.5
BRD-K43789185-001-01-7	485.42	30.6 ± 0.5
BRD-K02955208-001-01-6	**407.89**	**14 ± 1**

BRD-K27505055-001-01-4	**373.45**	**15.8 ± 0.4**
BRD-K32075950-001-01-7	**403.47**	**14.3 ± 0.4**
BRD-K14538269-001-01-2	352.23	27 ± 1
BRD-K20543508-001-01-5	377.48	35.9 ± 0.5
BRD-K02140483-001-01-1	416.45	49 ± 2
BRD-K04373483-001-01-6	485.42	92 ± 3
BRD-K36481331-001-03-9	401.38	70.2 ± 0.4
BRD-K31857539-001-04-3	**391.44**	**13.1 ± 0.2**
BRD-K92356992-001-01-8	390.40	94 ± 3
BRD-K86135968-001-01-4	388.43	94 ± 3
BRD-K81924091-001-01-6	384.38	86 ± 3
BRD-K36481331-001-04-7	401.38	77 ± 3
BRD-K20601732-001-01-9	415.41	59 ± 1
BRD-K32540946-001-01-7	380.44	92 ± 1
BRD-K79981216-001-01-0	402.37	78 ± 1
BRD-K76803377-001-01-4	446.55	95 ± 1
BRD-K48156091-001-01-7	397.47	59 ± 1
BRD-K60291101-001-02-1	401.38	99 ± 2
BRD-K80047413-001-01-8	332.33	95 ± 1
BRD-K09681131-001-01-3	**391.44**	**13.0 ± 0.1**
BRD-K82875726-001-01-2	377.41	39 ± 1
BRD-K56027141-001-01-9	425.45	89 ± 2
BRD-K27391543-001-01-9	306.33	86 ± 2
BRD-K84927643-001-01-9	374.44	50 ± 2
BRD-K69574760-001-01-5	415.41	92 ± 2
BRD-K80583645-001-01-2	415.41	90 ± 3
BRD-K52800818-001-01-5	444.41	91 ± 1

BRD-K31671068-001-01-3	390.40	93 ± 2
BRD-K07380319-001-01-8	459.42	93 ± 2
BRD-K36824271-001-01-6	420.39	94 ± 4
BRD-K46946874-001-01-6	397.35	92 ± 2
BRD-K93629400-001-01-3	389.42	54 ± 1
BRD-K31655302-001-01-2	**405.47**	**18 ± 1**
BRD-K05583481-001-01-1	379.45	36 ± 2
BRD-K18679386-001-01-8	417.42	31 ± 2
BRD-K52081736-001-01-1	415.37	87 ± 1
BRD-K18887044-001-01-1	**389.49**	**19 ± 2**
BRD-K61758114-001-01-5	427.52	77 ± 1
BRD-K37218351-001-01-3	**405.53**	**15 ± 1**
BRD-K02670184-001-01-9	392.45	67 ± 2
BRD-K33894856-001-01-5	391.44	82 ± 3
BRD-K36790284-001-01-4	390.45	92 ± 2
BRD-K54972754-001-01-6	439.48	87 ± 3
BRD-K84953102-001-01-9	**379.45**	**7.8 ± 0.2**
BRD-K81376467-001-01-5	426.44	82 ± 4
BRD-K48537292-001-01-5	420.39	51 ± 1
BRD-K67455691-001-01-3	391.44	87 ± 2
BRD-K21740674-001-01-4	391.44	79 ± 3
BRD-K77544773-001-01-3	404.36	88 ± 2
BRD-K76255944-001-01-1	366.43	53 ± 2
BRD-K28453247-001-01-5	374.44	53 ± 2
BRD-K55730697-001-01-7	350.41	94 ± 3
BRD-K24857125-001-01-8	296.32	98 ± 1
BRD-K85288470-001-01-3	350.21	79 ± 2

BRD-K75050824-001-02-0	393.43	96 ± 1
BRD-K62008130-001-01-4	349.39	103 ± 3
BRD-K56211110-001-01-6	449.52	94 ± 1
BRD-K51445792-001-01-0	356.42	102 ± 4
BRD-K77544773-001-03-9	404.36	99 ± 2
BRD-K86088205-001-01-8	436.45	101 ± 6
BRD-K22505729-001-01-5	**409.43**	**15 ± 1**
BRD-K46154184-001-01-2	404.36	97 ± 4
BRD-K39565060-001-01-7	352.23	74 ± 2
BRD-K37385611-001-01-6	392.43	22 ± 1
BRD-K02342544-001-01-0	367.42	29.3 ± 0.2
BRD-K79306370-001-02-0	402.37	91 ± 1
BRD-K13344820-001-02-6	349.43	24.1 ± 0.4
BRD-K67526605-001-01-6	417.42	29 ± 1
BRD-K15383271-001-01-8	417.48	88 ± 4
BRD-K61737057-001-01-8	433.50	83 ± 1
BRD-K19544663-001-01-7	425.83	97 ± 1
BRD-K55487747-001-01-4	424.47	35 ± 1
BRD-K77972610-001-02-1	391.44	93 ± 1
BRD-K80906650-001-01-7	379.45	95 ± 2
BRD-K28498951-001-01-6	367.42	26.1 ± 0.5
BRD-K47453320-001-01-2	392.42	95 ± 1
BRD-K66163481-001-01-8	403.40	29 ± 1
BRD-K11740130-001-01-4	376.37	94 ± 3
BRD-K04732608-001-01-3	414.46	83 ± 4
BRD-K48207974-001-01-0	348.40	85 ± 2
BRD-K25037558-001-01-2	404.39	53 ± 2

BRD-K12941885-001-01-4	445.39	96 ± 2
BRD-K96891346-001-01-3	383.37	94 ± 1
BRD-K25070337-001-01-1	402.46	100 ± 3
BRD-K45190645-001-02-8	391.44	92 ± 1
BRD-K94234276-001-01-2	**441.45**	**14 ± 1**
BRD-K98408199-001-02-0	379.45	29 ± 1
BRD-K83384185-001-01-8	374.44	34 ± 1
BRD-K41284582-001-01-0	442.43	36.4 ± 0.2
BRD-K08804415-001-01-9	440.42	83 ± 2
BRD-K31021301-001-01-8	**389.45**	**20 ± 2**
BRD-K88402291-001-01-4	**367.42**	**16 ± 1**
BRD-K08113597-001-01-5	419.45	85 ± 1
BRD-K56162277-001-01-0	403.45	79 ± 6
BRD-K60263288-001-01-7	**457.49**	**16 ± 1**
BRD-K15879709-001-01-7	**417.42**	**4 ± 1**
BRD-K09229186-001-02-3	429.44	96 ± 1
BRD-K82017078-001-01-5	374.41	95 ± 4
BRD-K76410202-001-01-9	428.45	80 ± 1
BRD-K05470326-001-01-0	384.42	101 ± 3
BRD-K10089781-004-02-1	391.44	86 ± 2
BRD-K18458688-001-01-2	385.38	96 ± 4
BRD-K60146127-001-02-7	273.33	33 ± 1
BRD-K51076979-001-01-8	370.45	91 ± 3
BRD-K02947110-001-01-0	475.48	29.1 ± 0.1
BRD-K16418033-001-01-0	344.41	91 ± 3
BRD-K24086213-001-01-7	385.41	27 ± 1
BRD-K36364251-001-01-7	416.40	79 ± 2

BRD-K03495176-001-01-0	416.40	76 ± 2
BRD-K70224802-001-01-4	391.44	91 ± 1
BRD-K75603460-001-01-7	412.48	88 ± 4
BRD-K13303013-001-01-1	353.46	34.8 ± 0.1
BRD-K21432362-001-01-5	354.45	87 ± 2
BRD-K08984836-001-01-0	391.44	95 ± 4
BRD-K59780270-001-01-3	295.34	80 ± 1
BRD-K49934164-001-01-8	348.40	73 ± 10
BRD-K94995437-001-01-4	390.45	83 ± 1
BRD-K45235328-001-01-7	**395.47**	**17 ± 1**
BRD-K99869451-001-01-7	**393.45**	**0.12 ± 0.05**
BRD-K53597648-001-01-2	405.47	100 ± 2
BRD-K08187511-001-01-2	**374.44**	**15 ± 2**
BRD-K86496683-001-01-4	**391.44**	**17 ± 2**
BRD-K60167980-001-01-1	426.44	79 ± 2
BRD-K11057231-001-01-1	406.36	91 ± 1
BRD-K44360164-001-01-1	270.33	88 ± 2
BRD-K36481331-001-05-4	401.38	70 ± 1
BRD-K57242473-001-01-1	426.34	80 ± 2
BRD-K07966893-001-01-8	418.37	92 ± 5
BRD-K04823598-001-01-2	339.31	87 ± 2

Figures S57 to S76. Graphs showing the log of the inhibitor concentration versus the percent of inhibition, for obtaining the compounds IC_{50} against ***Sm*DHODH**.

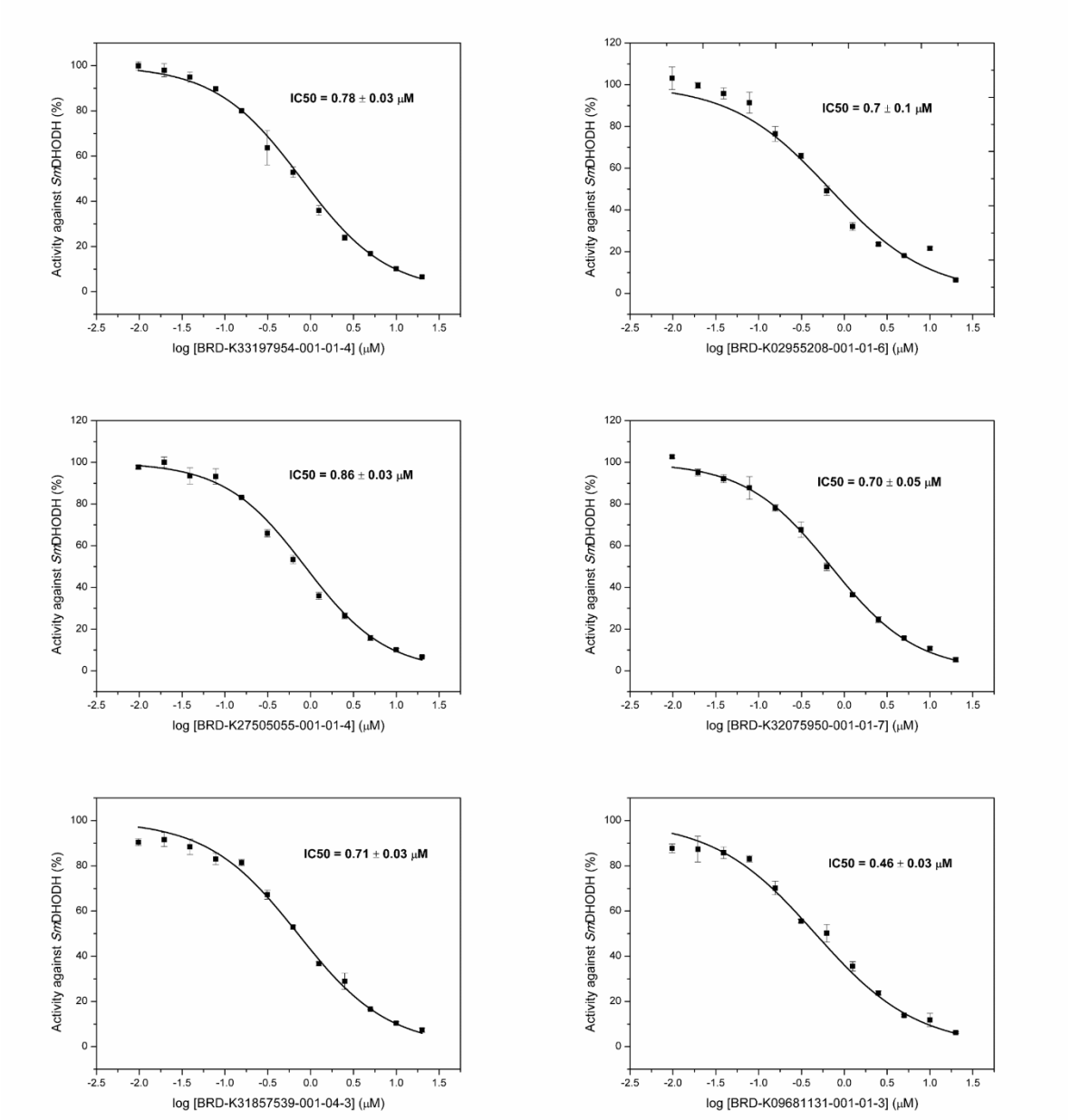

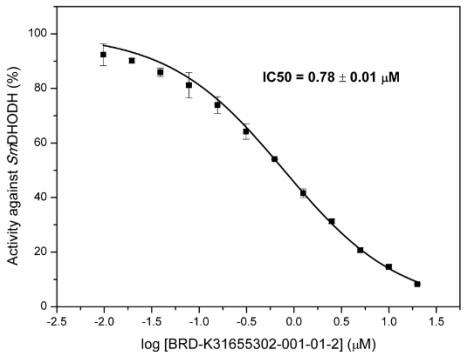
IC50 = 0.78 ± 0.01 μM
Activity against SmDHODH (%)
log [BRD-K31655302-001-01-2] (μM)

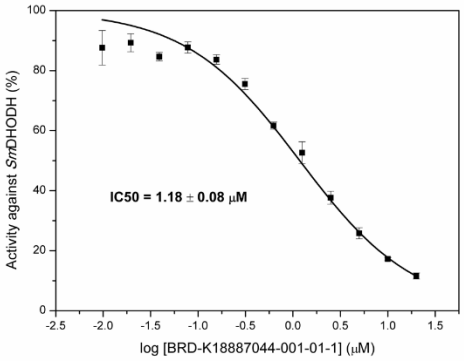
IC50 = 1.18 ± 0.08 μM
Activity against SmDHODH (%)
log [BRD-K18887044-001-01-1] (μM)

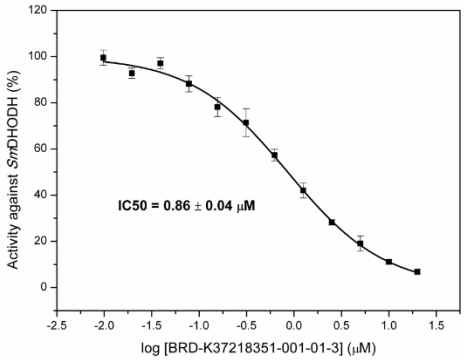
IC50 = 0.86 ± 0.04 μM
Activity against SmDHODH (%)
log [BRD-K37218351-001-01-3] (μM)

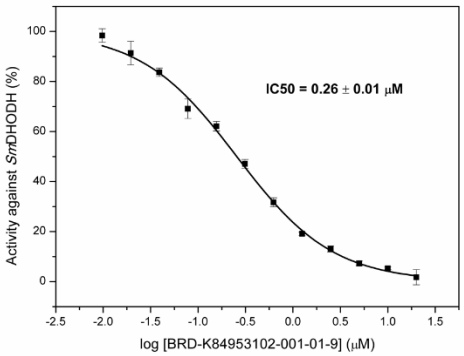
IC50 = 0.26 ± 0.01 μM
Activity against SmDHODH (%)
log [BRD-K84953102-001-01-9] (μM)

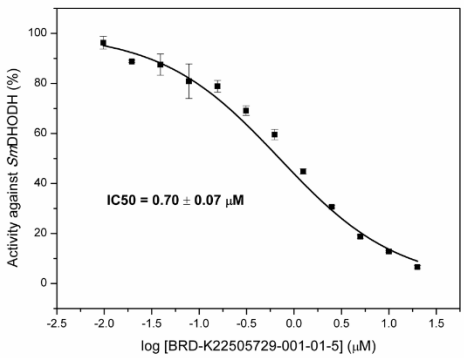
IC50 = 0.70 ± 0.07 μM
Activity against SmDHODH (%)
log [BRD-K22505729-001-01-5] (μM)

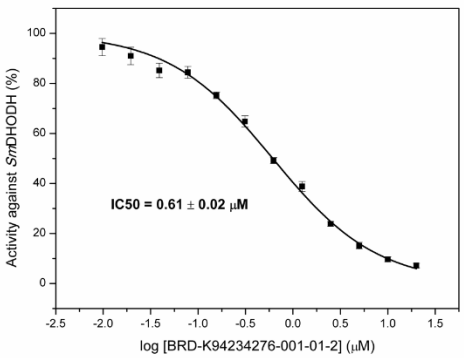
IC50 = 0.61 ± 0.02 μM
Activity against SmDHODH (%)
log [BRD-K94234276-001-01-2] (μM)

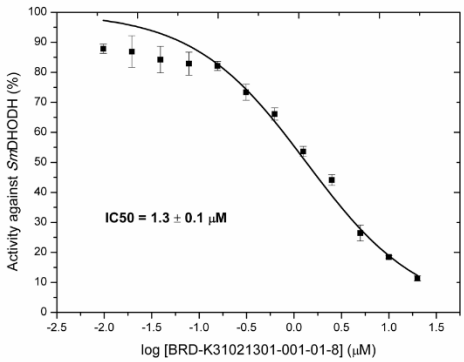
IC50 = 1.3 ± 0.1 μM
Activity against SmDHODH (%)
log [BRD-K31021301-001-01-8] (μM)

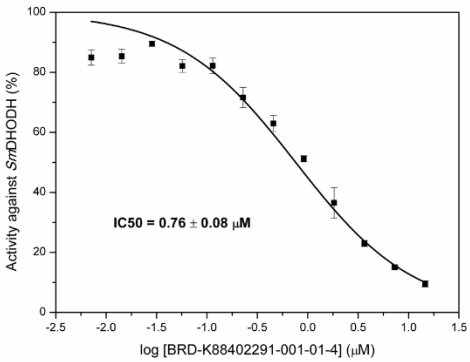
IC50 = 0.76 ± 0.08 μM
Activity against SmDHODH (%)
log [BRD-K88402291-001-01-4] (μM)

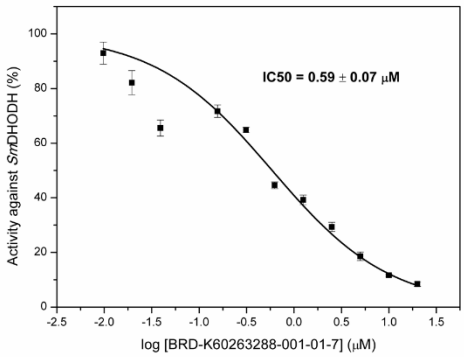
IC50 = 0.59 ± 0.07 μM
Activity against SmDHODH (%)
log [BRD-K60263288-001-01-7] (μM)

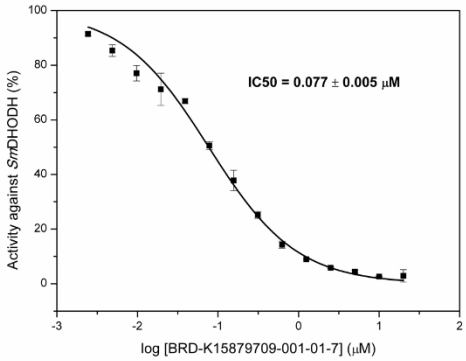
IC50 = 0.077 ± 0.005 μM
Activity against SmDHODH (%)
log [BRD-K15879709-001-01-7] (μM)

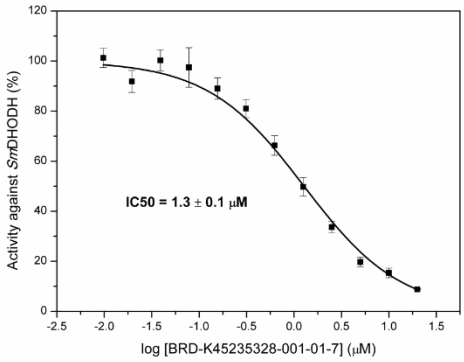
IC50 = 1.3 ± 0.1 μM
Activity against SmDHODH (%)
log [BRD-K45235328-001-01-7] (μM)

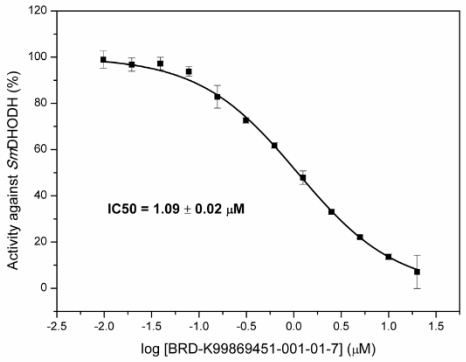
IC50 = 1.09 ± 0.02 μM
Activity against SmDHODH (%)
log [BRD-K99869451-001-01-7] (μM)

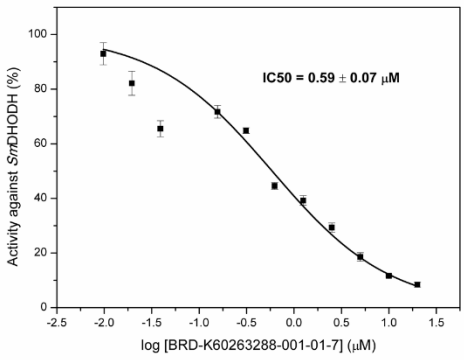
IC50 = 0.59 ± 0.07 μM
Activity against SmDHODH (%)
log [BRD-K60263288-001-01-7] (μM)

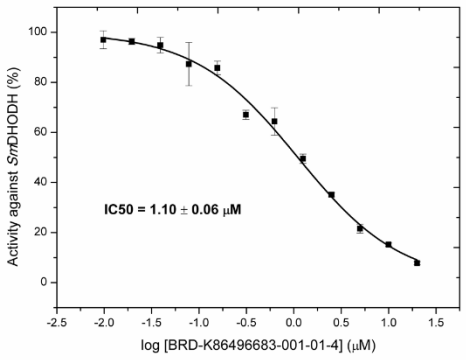
IC50 = 1.10 ± 0.06 μM
Activity against SmDHODH (%)
log [BRD-K86496683-001-01-4] (μM)

Table S3. Crystallographic and statistical data collected at SOLEIL synchrotron, PROXIMA-1 for *Pf*DHODHΔloop.

Spacegroup	P321
Cell parameters	172.663 172.663 73.215
	90.0 90.0 120.0
Wavelength [A]	0.97857
Resolution limits [A]	4.049 4.049 2.988
Eigenvector-1	1.000 0.000 0.000
Eigenvector-2	0.000 1.000 0.000
Eigenvector-3	0.000 0.000 1.000
Direction-1	0.894 _a_* - 0.447 _b_*
Direction-2	_b_*
Direction-3	_c_*

	Overall	**Inner Shell**	**Outer Shell**
Low resolution limit	86.331	86.331	3.488
High resolution limit	3.174	10.439	3.174
Rmerge (all I+ & I-)	0.215	0.065	1.327
Rmeas (all I+ & I-)	0.226	0.068	1.399
Rpim (all I+ & I-)	0.068	0.022	0.439
Total number of observations	142403	6040	6548
Total number unique	13165	656	655
Mean(I)/sd(I)	8.4	26.0	1.7
Completeness (spherical)	61.2	100.0	12.5
Completeness (ellipsoidal)	93.6	100.0	77.0
Multiplicity	10.8	9.2	10.0
CC(1/2)	0.998	0.998	0.711